



POLITECNICO DI MILANO

School of Industrial and Information Engineering
Department of Chemistry, Materials and Chemical Engineering
"Giulio Natta"
Master of Science in Materials Engineering and Nanotechnology

MASTER THESIS

IN - SITU CHARACTERIZATION OF THIN THERMOSET COATINGS OBTAINED BY PHOTO - INDUCED POLYMERIZATION

Supervisor: Prof. Gianmarco GRIFFINI
Co-supervisor: Prof. Mats JOHANSSON (KTH, Stockholm – Sweden)

Candidate:
Stefano MONTANI 873738

ACADEMIC YEAR 2017 - 2018

ABSTRACT

This essay will present the experimental results obtained by the *in-situ* characterization of the photo-polymerization process that involves two UV-curable resins with different chemical composition.

The effects of different curing parameters, such as the curing time and intensity of the UV lamp, are taken into consideration, with the aim to describe and follow the main physical and chemical transformations occurring during the polymerization.

Remarkable results showed that equivalent doses of radiation are able to produce the same degree of C=C conversion and density of crosslinking, which means that the network is insensitive to the use of higher intensities or times; however, when particularly high light intensities are involved, the activation of a large number of radicals pushes the process to very large extent, making the previous conclusion no more valid.

It has been found that viscosity and gelation point of the material, which are defined by its chemical composition, are responsible for the evolution of the structure, allowing molecular movements and chain rearrangements: this has a direct effect over the properties of the material, such as the roughness, thickness and glass transition temperature. The definition of a gelation point also allows to distinguish two regimes of reaction, which are characterized by different rates of polymerization.

For the first time in literature, by performing synchrotron *in-situ* characterization, it has been possible to detect the presence inside the material of scattering centres which increase their dimensions during the polymerization of the resin. Moreover, X-Ray scattering allowed to study the roughness of the materials by looking through the whole thickness of the coatings, thus demonstrating the presence of changes both at the coating-air and at the substrate-coating interface.

Key words

Photopolymerization, Characterization, In-situ, Acrylates, Crosslinking density, Coating, Scattering

ESTRATTO INTRODUTTIVO

In questo elaborato si presentano i risultati sperimentali ottenuti dalla caratterizzazione del processo di foto-polimerizzazione che coinvolge due resine foto-reticolanti con diversa composizione chimica.

Vengono presi in considerazione gli effetti derivanti dalla modifica dei parametri di reticolazione, come il tempo di esposizione e l'intensità della lampada UV, con l'obiettivo di descrivere e seguire le principali trasformazioni che avvengono durante la polimerizzazione.

Si è osservato che l'applicazione di dosi equivalenti di radiazione sono in grado di produrre lo stesso grado di conversione di C=C e la stessa densità di reticolazione: ciò significa che il network non è in grado di distinguere tra la applicazione di tempi o intensità più elevate. Ad ogni modo, l'utilizzo di intensità di radiazione particolarmente elevate comporta l'attivazione di una grande quantità di radicali e forza l'avanzamento del processo, rendendo non più valida la precedente conclusione.

Si è mostrato inoltre che la viscosità e il punto di "gelation" del materiale, che sono definiti dalla sua composizione chimica, sono responsabili dell'evoluzione della struttura consentendo movimenti molecolari e riorganizzazione delle catene polimeriche: questo ha un effetto sulle proprietà del materiale, come la sua rugosità, spessore e temperatura di transizione vetrosa. La definizione di un punto di "gelation" consente anche di distinguere due regimi di reazione, che sono caratterizzati da diverse velocità di polimerizzazione.

Per la prima volta in letteratura è stato possibile, attraverso una caratterizzazione *in-situ* al sincrotrone, individuare nel materiale la presenza di centri di scattering, le cui dimensioni aumentano nel corso della polimerizzazione della resina. Inoltre, lo scattering a raggi X ha consentito di studiare la rugosità dei materiali esaminando l'intero spessore dei rivestimenti e dimostrando così l'esistenza di modifiche sia all'interfaccia rivestimento-aria sia a quella substrato-rivestimento.

Parole chiave

Foto-polimerizzazione, Caratterizzazione, In-situ, Acrilati, Densità di reticolazione, Rivestimento, Scattering

TABLE OF CONTENTS

1. PURPOSE OF THE STUDY	1
2. INTRODUCTION	2
2.1. PHOTO-POLYMERIZATION	2
1.1.1 Photo-polymerization of acrylates	4
1.1.2 Effects of the chemical reaction	7
1.1.3 Kinetic aspects and regimes of reaction	10
2.2. NETWORK FORMATION	12
3. EXPERIMENTAL	19
3.1. MATERIALS AND SETUP	19
3.1.1. Substrates	19
3.1.2. Monomers and oligomers	19
3.1.3. Photo-initiator	22
3.1.4. Setup	23
3.2. SYSTEM PREPARATION	23
3.3. PHOTO-CHEMISTRY AND LIGHT SOURCE	25
3.4. SET CONDITIONS AND PARAMETERS	27
3.5. CHARACTERIZATION TECHNIQUES	28
3.5.1. Fourier Transformed-Infrared Spectroscopy (FT-IR)	28
3.5.2. Dynamic Mechanical Analysis (DMA)	29
3.5.3. Differential Scanning Calorimetry (DSC)	30
3.5.4. Atomic Force Microscopy (AFM)	31
3.6. X-RAY SCATTERING AND SYNCHROTRON RADIATION	32
3.6.1. Small-Angle X-Ray Scattering (SAXS)	34
3.6.2. Grazing incidence Small-Angle X-Ray Scattering (GISAXS)	35
3.6.3. X-Ray Reflectometry (XRR)	40
3.6.4. Beamline setup	41

4.	RESULTS	43
4.1.	PRELIMINARY ANALYSIS	43
4.1.1	Resins stability	43
4.1.2	Thickness analysis	43
4.2.	KINETIC ANALYSIS	46
4.2.1	IR spectra investigation	46
4.2.2	Conversion evaluation	50
4.2.3	Rate of polymerization	52
4.3.	MORPHOLOGY	54
4.3.1	AFM measurements	54
4.4.	DYNAMIC MECHANICAL ANALYSIS	58
4.4.1	General overview	59
4.4.2	Density of crosslinking	59
4.5.	THERMAL ANALYSIS	62
4.5.1	Glass transition temperature	62
4.6.	SCATTERING EXPERIMENTS	66
4.6.1	Radius of gyration	66
4.6.2	XRR images	68
4.6.3	<i>In-situ</i> photo-polymerization	74
4.6.4	Surface differential reflectance spectroscopy	78
5.	DISCUSSION AND CORRELATIONS	79
5.1.	GENERAL FEATURES	79
5.2.	POLYMER CONVERSION AND GELATION	80
5.3.	DEVELOPMENT AND STRUCTURE OF THE NETWORK	85
6.	CONCLUSIONS AND FUTURE WORKS	89
6.1.	CONCLUSIONS	89
6.2.	FUTURE WORKS	92
7.	ACKNOWLEDGMENT	93
8.	REFERENCES	95

1. PURPOSE OF THE STUDY

Photo-induced polymerization of thermoset films is nowadays a widely used industrial technique, since it offers the possibility to polymerize the monomer *in-situ*, by using UV light as a trigger to activate the process. However, the associated reaction is affected by the concurrent action of a large number of parameters that contribute to the obtainment of the final structure and properties of the material.

Although this field has been largely investigated for what concerns the pristine and polymerized conditions, there is not full understanding regarding the way in which the network develops during the photo-polymerization of thermosets as thin film on a substrate. This is particularly interesting because, by having a deeper theoretical knowledge of the process, it is possible to steer the properties of the material in order to make it suitable for a given application.

The present paper will thus focus on the study of the properties of two thermoset polymers deposited in form of thin coatings, before and after the polymerization, trying to correlate the deposition and curing parameters to the obtained structure. This will allow to figure out the effects of some of the parameters involved in the network formation with the aim of being able to tune the properties of the material for future applications.

Moreover, photo-polymerization will be studied *in-situ* and real time, so as to achieve a deeper comprehension of the liquid-solid phase transformation by collecting data directly during the reaction. The *in-situ* characterization offers the clear advantage of maintaining some of the variables completely unchanged, so that the correlation among causes and effects becomes straightforward.

2. INTRODUCTION

2.1. Photo-polymerization

Photo-polymerization of thermoset polymers is a technique which allows the rapid conversion of a mixture of liquid oligomers into a solid semi-crystalline or amorphous product: this occurs due to the transformation of the C=C double bonds of the monomers into single bonds, that connect the different building blocks. The polymerization reaction starts immediately after the absorption of a photon with suitable wavelength, which triggers the generation of radicals or cationic species that are capable of starting a chain process; more precisely the process should be distinguished into photo-crosslinking, when it leads to the connection of polymer chains to form a network, and crosslinking polymerization, which consists on the simultaneous formation of both the polymer and the network¹.

It is also possible to distinguish between two types of photo-polymerization, which are called respectively free radical and cationic. Even if cationic polymerization has had a strong development in the last years, practical industrial applications in this field are nowadays mostly based on free radical polymerization, because of the easiness of realization of the reaction. Cationic photo-polymerization requires in fact the use of salts bearing anions of low nucleophilic character (SbF_6^- or PF_6^-), which constitute latent photochemical sources of strong protonic acids: once the generation of the correspondent acid has occurred, they will behave as cationic polymerization initiators². The main advantage given by this technique is the possibility to broaden the range of monomers which can be polymerized, together with the opportunity to work in presence of oxygen without having the inhibition of the reaction, as it occurs instead in radical polymerization².

Differently from the cationic reaction, in free radical photo-polymerization the required initiator should be sensitive to specific wavelengths of light in order to start the radical polymerization. Chain-radical crosslinking photo-polymerization can be described as a series of steps:

- Dissociation, in which the initiator is cleaved to create two reactive radicals: $I \rightarrow 2I^{\bullet}$.
- Initiation, in which the reactive radical attacks a monomeric unit (or an oligomer), thus creating a carbon-centre radical: $I^{\bullet} + M_n \rightarrow M_n^{\bullet}$.
- Propagation, which implies the collision between an unreacted monomer and a macro-radical: $M_n + M_n^{\bullet} \rightarrow M_{n+1}^{\bullet}$.
- Termination, that can occur by either combination (reaction of two macro-radicals to give rise to a unique chain) or disproportionation (annihilation of the two radicals with the formation of two separated chains): it implies the end of the polymerization process.

Under the assumptions of a steady state total free-radical concentration and of size-independent reactivities of the growing radicals, it is possible to obtain an expression to calculate the rate of photo-polymerization:

$$R_p = k_p [M] \left\{ \frac{\varphi I_0 (1 - 10^{-\varepsilon d [I_n]})}{k_t} \right\}^{1/2} \quad [1]$$

The expression highlights the dependence of the photo-polymerization rate on the propagation and termination constants (k_p and k_t), on the intensity of the incident light (I_0), on the path travelled by light in the material (d), on the quantum efficiency for photo-dissociation and initiation (φ), on the coefficient of molar extinction (ε), on the concentration of the monomer (or oligomer) ($[M]$) and of the initiator ($[I_n]$). The relation also takes into consideration the possible variation of I_0 with thickness in strongly absorbing systems: this may lead to considerable change in the rate of polymerization across the sample thickness. Indeed, the empirical Lambert-Beer law reveals the linear dependence of the absorbance on the path length travelled by light inside a material: $A = \varepsilon \cdot l \cdot C$. Hence, the absorbance turns out to depend on the molar extinction coefficient ε , on the molar concentration C and on the travelled path l .

When a very thin coating (in the range of μm) is considered, the change in polymerization rate across the thickness could be in first analysis neglected; nevertheless it is not clear if the formation path of the polymeric network and the presence of a density gradient generated through the thickness could affect the physical properties of the obtained film and to which extent¹. Furthermore, the obtainment of a target set of physical properties requires a full description of the

formed network at a microstructural level and this can be done by means of both experimental measurements and statistical approaches.

The chemical reaction of photo-polymerization offers therefore the significant advantage of having one-part materials that can be cured on demand with the possibility to manipulate the reaction rate by changing the process parameters so that a control over the final achieved properties is conceivable³.

Accordingly, the possible applications of UV-curable organic materials are diverse, and they include dental applications, contact lenses, coatings, photolithography, microfluidic device fabrication, tissue engineering matrices and 3D prototyping⁴.

The present study will mostly concentrate on thin acrylate films, whose photo-polymerization is expected to take advantage by the use of a reflecting substrate, that, in principle, should be able to level the intensity gradient across the sample, thus obtaining a more uniform crosslinking.

2.1.1. Photo-polymerization of acrylates

Free-radical polymerization is a chemical reaction which offers either advantages or disadvantages. The main advantage is the easiness in realization of the reaction that only requires light to be supplied; at the same time, the control over the process is complicated by the multitude of events which are entailed in the polymerization. In first place, when densely crosslinked networks are prepared at relatively low temperature, vitrification (or gelation) can occur. This phenomenon involves the progressive reduction in the chains mobility caused by the increase in viscosity with crosslinking. This is initially followed by the suppression of the termination process, with a consequent auto-acceleration of the polymerization (Trommsdorff-Norrish effect); lately, however, also the mobility of the free monomer can be suppressed, so that the rate of polymerization becomes limited by diffusion^{1,4}. The decrease in diffusion coefficient, upon further crosslinking, is accompanied by a reduction in the polymerization rate, thus giving rise to an auto-deceleration: an incomplete conversion of the double bonds will result, with the presence of a residual amount of radicals and monomer reactants^{1,4}.

The final extent of reaction increases with temperature and so does the crosslink density of the polymer^{1,5}; furthermore, J.G. Kloosterboer and G.F.C.M. Lijten discovered, by looking at the shift towards higher temperature of the $\tan \delta$ peak in DMA measurements, that the ultimate conversion also depends on light intensity

and that this effect is independent on the self-heating that occurs during irradiation. However it was proved that the intensity dependence vanishes when equal doses of radiation are applied⁵; it must be noticed that this consideration does not imply the obtainment of an identical network structure.

Differently from bulk polymerization, in which the Trommsdorff effect of auto-acceleration starts at about 15-20% of conversion, in the case of acrylates, the gelation sets in near zero conversion, especially when undiluted monomers are considered: this may lead to considerable difficulties in the obtainment of high yield of conversion¹.

The use of reactive diluents (mostly monomers containing one or more acrylic double bonds) is therefore a common industrial solution to contrast the described event, since this reduces the crosslink density; moreover, the reactive diluents are also added with the aim of reducing the viscosity of the mixture, which is generally very high. Depending on the characteristics of the selected monomer, it is also possible to attribute specific properties to the polymer. In the case of monofunctional acrylic monomers, the result is an increase in the flexibility of the network and in the total double bond conversion during the curing process, with a decrease in the curing rate; moreover the obtained films often show low surface properties, low hardness and scratch resistance⁶. Monomers having two or more acrylic functions are generally preferred to monofunctional ones, since they show very high curing rates and high surface properties. On the other hand, the mobility of the reactive species is lower because of the very dense three-dimensional network that is formed; the polymerization reaction thus could be inhibited before obtaining a complete polymerization of the acrylic double bond. The final materials will be very rigid, hard and brittle⁶. Multifunctional monomers are also interesting for toxicological reasons, as they are less prone to migrate out of the coating and thus offer minor health concerns⁷.

Other possibilities to reach higher conversion are an increase in the reaction temperature, an increase in the flexibility and length of the moieties between functional groups or an increase in the rate of polymerization. Gelation can also be retarded by the presence of pendant functional groups: even if their conversion into microgels is pushed to high extents during the first stages of polymerization, they do not contribute to a significant network development⁴. These “wasted” crosslinks are thus able to delay the gel-point significantly with respect to the classical predictions⁴.

Another aspect to be considered is the possible trapping of radicals in the network that can be produced by high-energy irradiation of glassy polymers, by mechanical destruction or by trapping during free-radical polymerization of monomers¹. The radicals result to be trapped because they are isolated from unreacted double bonds and cannot continue the propagation reaction. Since they can remain inside the structure even for months or years, it is important to determine their concentration, that can be measured by Electron Spin Resonance (ESR) during and after the reaction, even if this measurement is generally unpractical for most photo-polymerizations⁴.

Nevertheless, trapped radicals show a quite fast decay in case of acrylates, which can be further accelerated by a heat treatment performed after curing. Their decay can also be favoured by the presence of oxygen in the atmosphere, that induces an enhanced mobility of the radical sites in the network and a consequent enhanced termination and reduced rate of polymerization¹. This effect is more pronounced at the lowest light intensities, where oxidation can compete effectively with the polymerization process; at the highest intensities, instead, the rate of initiation is so high that the oxygen cannot be replenished at a sufficient rate¹. Oxygen can thus be considered as an efficient inhibitor of the photo-polymerization, which affects the top surface layer (over 1-10 μm) by favouring the formation of a peroxy-based radical that is quite unreactive towards propagation and terminates the reaction⁴; for this reason, photo-polymerization requires a proper atmosphere to be performed.

In addition, the inhibition reaction with oxygen can cause concentration gradients in the film (Fig. 1) and therefore diffusional effects should be taken into account when we are modelling the network formation in presence of oxygen^{4,8}.

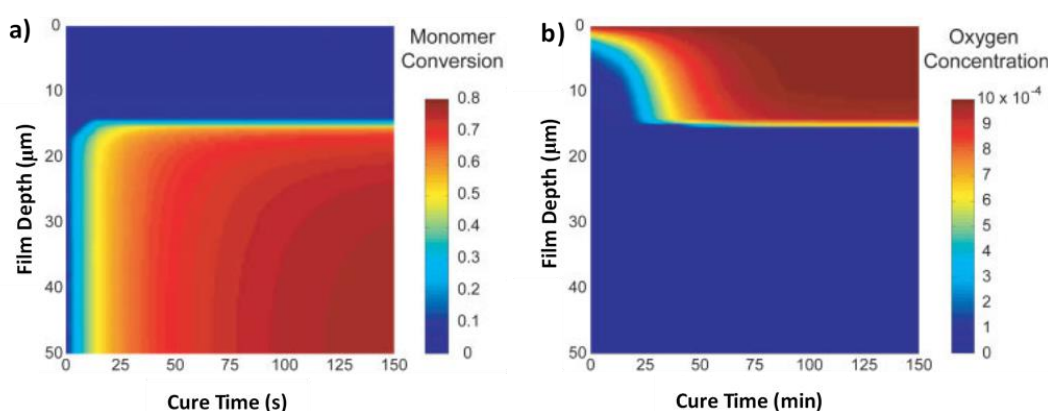


Figure 1. Theoretical predictions of (a) the double bond conversion and (b) oxygen concentration as a function of film depth and time.⁴

A reaction-diffusion model has been prepared by P.D. Iedema *et al.*⁸ which considered the photopolymerization of diacrylates films with a thickness of 10 μm in a nitrogen atmosphere: for high light intensities the experimental results follow the classical theory of initiation, propagation and termination, according to which $R_p \propto \sqrt{I_0}$ (Eq. 1), while at lower intensities a deviation is present, which can be explained by considering the presence of a tiny quantity of oxygen left after the purging procedure performed with nitrogen. It has been estimated an equilibrium oxygen concentration of $3.3 \pm 0.79 \cdot 10^{-6}$ mol/l, that is much lower than the atmospheric one, but still influential (Fig. 2). According to the model, the oxygen inhibition effect only becomes tangible for light intensities below 3 mW/cm^2 .

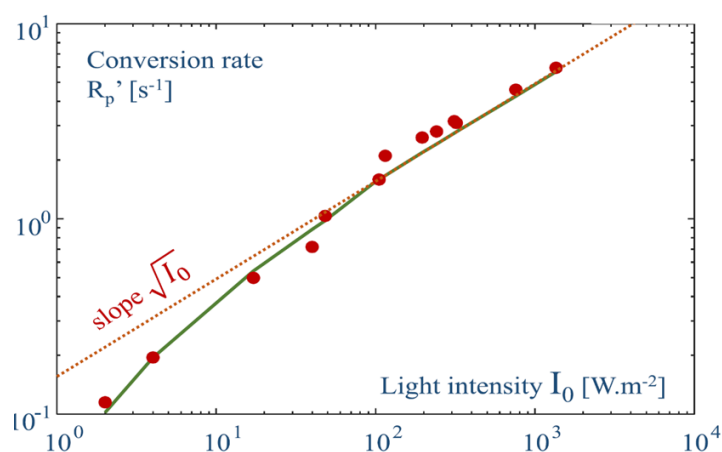


Figure 2. Conversion rate vs light intensity. The ideal slope, the real data and the model with oxygen are plotted.⁸

2.1.2. Effects of the chemical reaction

One of the most important and evident effect of the photo-polymerization of a resin is shrinkage, which is connected to the conversion of Van der Waals bonds into shorter covalent bonds; the accompanying reduction of the entropy also favours a closer packing. Since polymerization shrinkage is based on the initial monomeric reactive group concentration and on the attained degree of conversion, monomers with higher molar mass and lower degrees of functionality will produce a lower absolute shrinkage results³.

The volume shrinkage does not occur only during the irradiation time, but also after switching off the light (Fig. 3a): this can be explained by considering the occurrence of a slow post-reaction, called “dark polymerization”, together with a shrinkage retardation with respect to the chemical conversion¹.

Retardation can be explained by considering the low conversion gelation of acrylates, that makes the polymerization to proceed in the gelled phase; under these conditions, to convert the free volume generated by the chemical reaction into overall shrinkage, the gel has to move in a cooperative way and this requires longer time than the diffusional motion of free monomer molecules. It follows a retardation in the shrinkage (Fig. 3b), in which the time lag allows the generation of a temporary excess of free volume that in turn favours an increase in the mobility of unreacted double bonds¹. This theory constitutes an evidence of the possibility to increase the conversion by an increase in light intensity, that occurs because of the stronger action supplied in the period in which the mobility is still high.

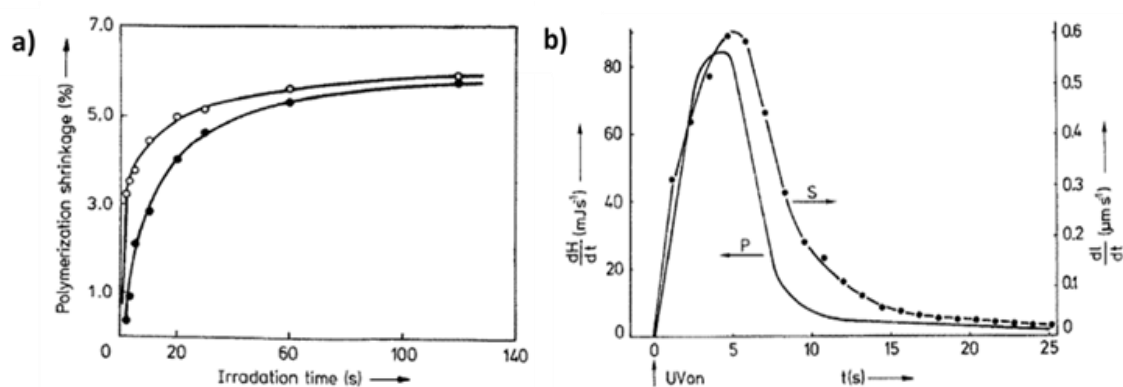


Figure 3. (a) Polymerization shrinkage for a coating. Filled dots: immediately after shutter closure. Empty dots: 10 minutes after shutter closure. (b) Rate of polymerization (P) and of shrinkage (S) for the photopolymerization of HDDA at 20°C.¹

Shrinkage can be reduced by increasing the length of the moiety between the acrylate groups, but this implies a reduction in the crosslink density and in the final hardness of the material¹. Therefore it is possible to conclude that the rate of chemical reaction, the extent of reaction and the extent of volume shrinkage are interconnected: the chemical reaction drives the shrinkage process, but a high extent of reaction reduces the rate of shrinkage; at the same time a high extent of volume shrinkage reduces the rate of the chemical reaction¹.

The main consequence of shrinkage is the development and accumulation of stresses inside the polymeric network structure, which may cause the detachment or bending of the deposited film from the substrate.

Another important effect of the chemical reaction is the change in E' and $\tan \delta$ values, which is due to the growing crosslink density of the network, according to the rubber elasticity theory.

The change in the $\tan \delta$ profile also shows a progressive increase in the glass transition temperature of the polymer as the proportion of free monomer is reduced with respect to the growing polymer phase: this explains why the final material is solid and rubbery. A demonstration of the progression in glass transition temperature profiles as a function of conversion can be seen in Fig. 4, whose curves have been obtained by DMA measurements on the same polymer at various extent of network formation³. It should also be noticed the broadening of the $\tan \delta$ curves, that is caused by the increasing heterogeneity of the structure⁴.

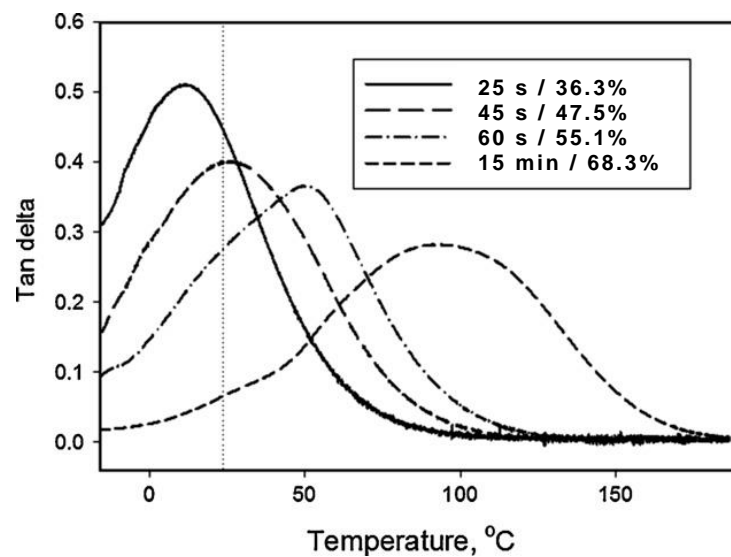


Figure 4. DMA measurements of the same resin mixture whose photo-polymerization is interrupted at different extent of reaction.³

Additionally, the final conversion of the polymer and thus its properties are influenced by the photo-polymerization conditions and by the initiator concentration, which control the initiation rate and the initial active radical concentration: higher radical concentration leads to shorter chain length of the macro-radicals at the point of termination and higher achievable conversion, since they would have lower probability to undergo gelation³. According to this argument, the use of higher curing intensities causes the activation of a larger number of radicals that are expected to delay the conversion at which gelation occurs; differently, the lower intensities will produce gelation at an earlier stage of conversion³ (Fig. 5). However, as previously underlined, the variation of the degree of conversion with the light intensity completely disappears by applying equivalent dose of illumination, since during the early stage of polymerization, the short propagating chains will display higher termination rates due to disparities in the diffusion rate³.

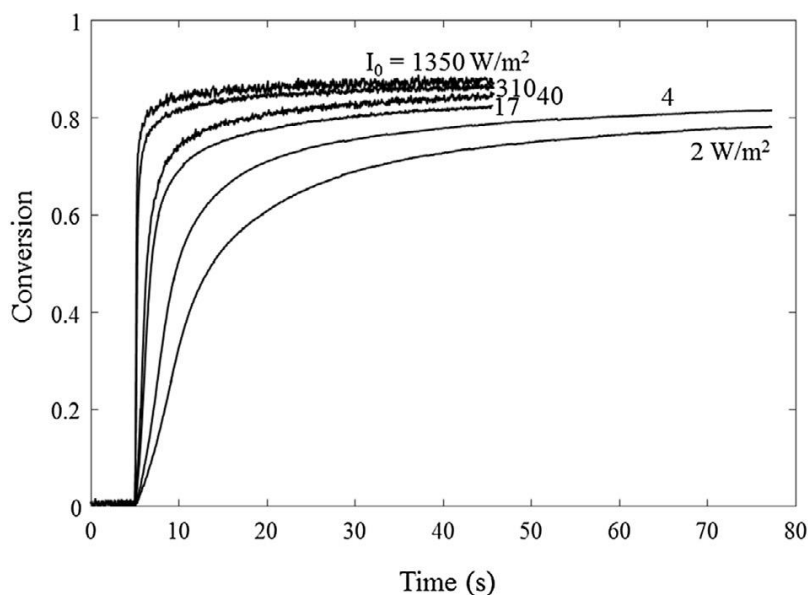


Figure 5. Curves obtained by FTIR data which describe the variation of the conversion as a function of time for different light intensities.⁸

2.1.3. Kinetic aspects and regimes of reaction

One of the most important phases of photo-polymerization reactions is the propagation, which proceeds ideally at low conversion in a reaction-rate controlled regime. Progressively, however, the rate of diffusion of the monomer towards the radical becomes slower with the increase of conversion, such that the diffusion of the monomers is hindered by the crosslinks network: this phase will be controlled by the diffusion rate of the monomer. The transition between the two regimes corresponds to the onset of the formation of the crosslinking network⁹.

It has been demonstrated that the conversion degree at which the maximum rate of conversion is observed, remains always around 33% even by changing the intensity of irradiation (Fig. 6). It follows that the transition of the polymerization from reaction to diffusion control occurs always at the same conversion and therefore is not affected by the change in radical concentration⁸. However, the transition is affected by the viscosity of the monomers or of the resins: when they present higher initial viscosities before polymerization, they enter this transition at an earlier stage of conversion³.

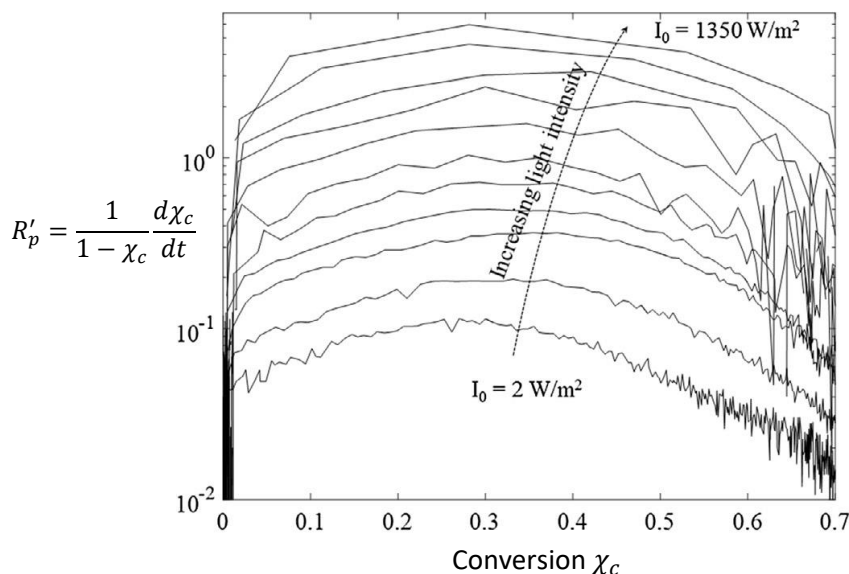


Figure 6. Curves obtained by FTIR data which show the change in the modified polymerization rate as a function of the conversion degree for different light intensities.⁸

Other experimental proof of the passage from a regime to the other can be supplied by determining the variation in diffusion coefficient of the monomer or in the propagation and termination kinetic constants with the conversion of double bonds: all these changes can be explained by oxygen inhibition or by the network formation⁹.

The studies carried out by Kentaro Taki *et al.*⁹ about the kinetic constants variation demonstrated the existence of a plateau for the propagation kinetic constant at low conversion degree, which prove the existence of a reaction-controlled regime; at high conversion, instead, the constant decays and this indicates the starting of a diffusion-controlled regime⁹. The authors showed also that the transition occurs before in case of oligomers with a shorter chain length⁹, thus leading to a lower conversion; the conversion of longer oligomers is instead faster and proceeds toward higher extents⁹.

Finally the kinetic chain is proved to increase its length during reaction-controlled polymerization, while it is not able to propagate during the second step because of the limited diffusivity of the monomer: it is thus possible to conclude that the kinetic chain length reaches a maximum in correspondence of the transition from one regime to the other⁹.

2.2. Network formation

The network structure, that is formed during photo-polymerization, outlines a specific distribution of the crosslink density and this directly affects some of the properties of the obtained film, such as the relaxation time and the frequency dependent modulus¹⁰. Both globally averaged material parameters and spatial heterogeneity contribute to the resulting physical and mechanical properties; for instance, since the network microstructure determines the degree of disorder, it can in turn affect the collective mode properties, such as the phonon density of states and the mean free path¹⁰.

The network structure is mostly determined by the processing parameters, such as light intensity, mode of polymerization, temperature, initiator concentration and conversion degree for gelation. During any instant of polymerization, the spatial distribution of a crosslinked network is the result of a competition between chemical reaction and fluctuation events, which is affected by all the previously mentioned parameters, interacting in complex ways¹⁰.

Different models have been suggested to describe the formation of the network structure. The most classical treatment has been proposed by Flory and Stockmayer and it is based on a combinatorial model that provides an adequate description for the formation of networks via step reactions and for crosslinking of linear chains¹. The model is based on the assumptions of having equal and independent reactivity of chemical groups of the same type and no ring formation. Cyclization entails the reaction between a propagating chain radical and a pendant reactive group either already attached to the same chain (primary cycle) or attached to another chain that has previously been connected to the first by a crosslink (secondary cycle)^{1,3}; cyclization produces therefore ineffective crosslinks and delays the gel point conversion³.

Even if it is possible to extend the treatment to take into account unequal reactivity and substitution effect within monomer units or restricted cyclization, the obtained models are generally only limited to systems which can be described by Markovian statistics without any long-range correlation affecting the reactivity of a functional group^{1,4}.

In case of chain crosslinking copolymerization, the Flory and Stockmayer' assumptions are not fulfilled, since strong cyclization and intermolecular crosslinking can easily occur and they cause the formation of inhomogeneities, consisting of densely crosslinked regions surrounded by less densely crosslinked

ones¹. Moreover, in the vicinity of the reactive end of a growing chain, the concentration of pendent group is much higher than average and this results in an apparently enhanced chemical reactivity of the pendent group with respect to the free monomer and this is difficult to be accounted for adequately¹.

The formation of densely crosslinked network obtained by chain polymerization can however be described by using a percolation model, in which the monomers are considered to be points on a cubic lattice. Initially, an arbitrary site is changed into a free radical and every unit of time a neighbour is chosen: if the neighbour has not fully reacted, a chemical bond is formed, and the radical function is transferred to the neighbouring site. Thus, the radical moves randomly on the lattice and connects a series of monomers until the radical is trapped between fully reacted sites; then a new radical is formed in another arbitrary position. If the radical concentration is increased, it is possible to simulate also a termination by combination¹. The same modelling can be applied to step reactions by considering the possibility of forming bonds between neighbouring sites which have not yet fully reacted¹.

The results can be visualized by making snapshots of simulations on a two-dimensional lattice (Fig. 7a-d). It can be noticed that a shorter chain length implies a lower inhomogeneity.

At low conversions, the percolation model give the chance to satisfyingly predict the sudden increase in crosslink density; at high conversions, instead, it underestimates the shielding of pendent double bonds¹. This deviation can be explained by considering the reorientations and small displacements that are required for the reaction to occur, which become particularly important at high conversions¹.

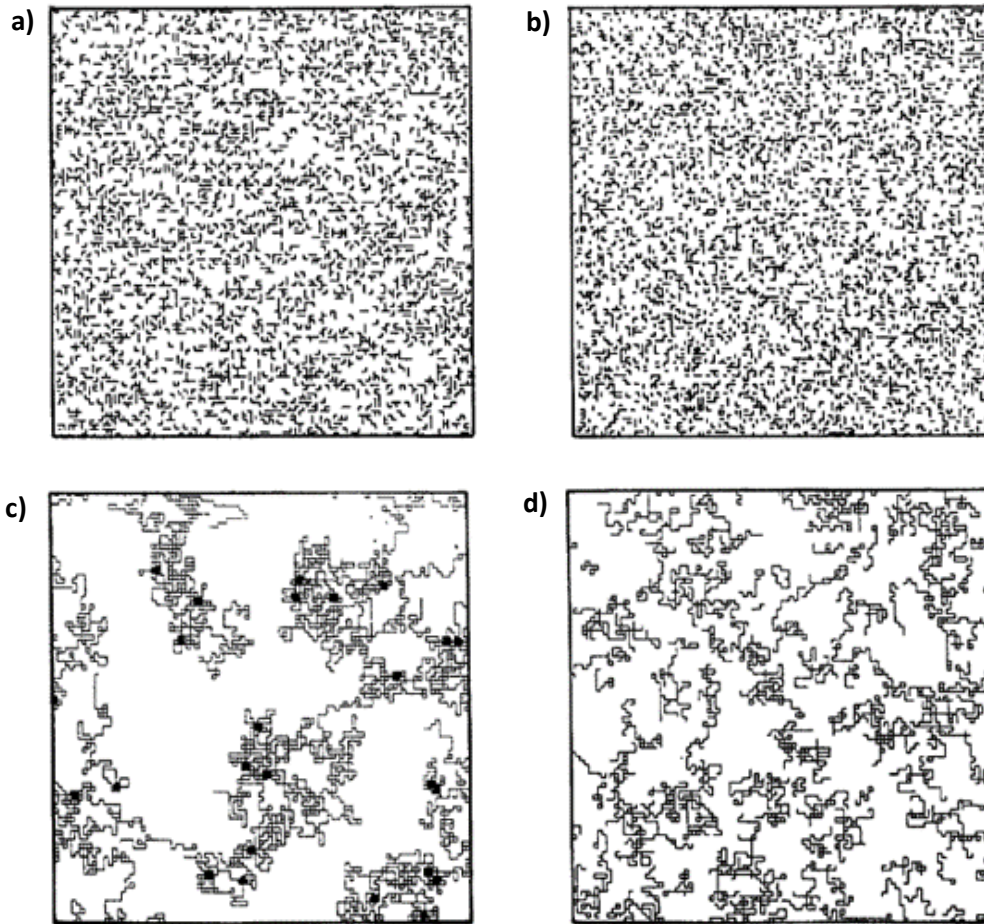


Figure 7. Snapshots of polymerization of tetrafunctional monomer in two dimensions at a bond conversion of 25%. Bonds are indicated, units themselves are not. (a) is obtained by a chain reaction of one “living” radical at a time, while (d) is for a step polymerization. To show the decrease of inhomogeneity on decreasing the kinetic chain length, it is possible to compare (b), where the chain length is limited to 20 steps, and (c), where it is limited to 2 steps.¹

Another way of describing the crosslinks network is proposed by S. Sarkar *et al.*¹⁰, that considered a constitutive model to reproduce the system before and after curing (Fig. 8a,b).

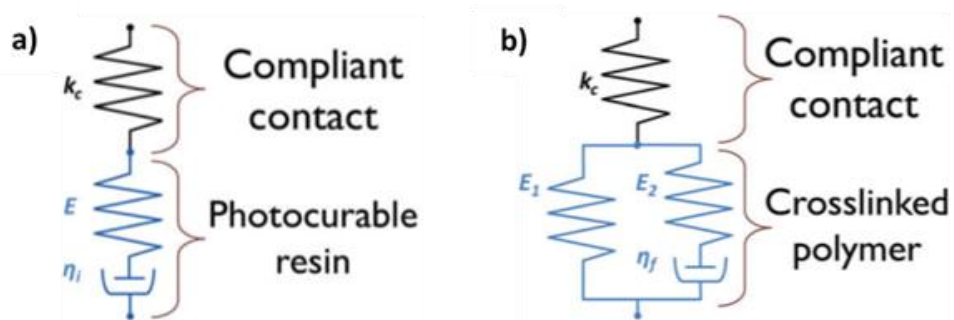


Figure 8. Material models for a crosslinking resin before and after curing: (a) Maxwell model (before curing) and (b) standard linear solid model (after curing).¹⁰

By using this model, it is possible to derive an expression for the low frequency ($\omega \ll \omega_f = \frac{2\pi E_2}{\eta}$) modulus of the crosslinked polymer network: $E_1 = 3\rho_c k_B T$, where ρ_c is the crosslink density, k_B is the Boltzmann constant, T is the temperature. The crosslink density can be calculated as $\rho_c = DC^2 \rho_0$, where DC is the degree of conversion, while ρ_0 is the initial molar density of the monomers before curing. Experimental results by S. Sarkar *et al.*¹⁰ on a model binary dimethacrylate system, showed that by increasing the light intensity, the growth in relaxation time is progressively delayed (Fig. 9a). A similar trend can also be observed when considering the temperature change against the degree of conversion (Fig. 9b): the temperature drop, which corresponds to the slowing down of polymerization due to the decrease in the diffusivity of radicals and monomers through the network, is shown to occur at different DC values when the light intensity is changed. The differences in the produced heat can be connected to the rate of polymerization, which in turn depends on the molecular diffusivity, which turns out to be a crucial parameter to define the level of network clustering.

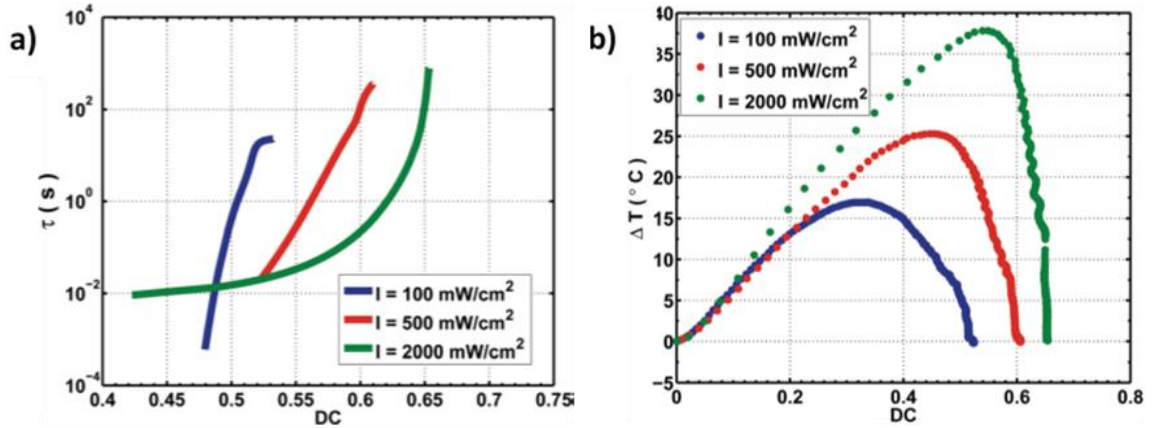


Figure 9. (a) Growth of the relaxation constant against DC for the three light intensities. (b) Shift of the temperature peak with increasing light intensities.¹⁰

Numerical studies on a polymer network on a simple cubic lattice have been performed to describe the change in diffusivity of a small molecule as a function of the network size, crosslink density and network heterogeneity: this permits to explain the trends presented previously¹⁰.

Specifically, a trend for the decrease in the diffusivity coefficient (D_{em}) with an increase in conversion degree has been derived: both the effect of a change in the interaction energy and of the clustering have been taken into consideration (Fig. 10a,b).

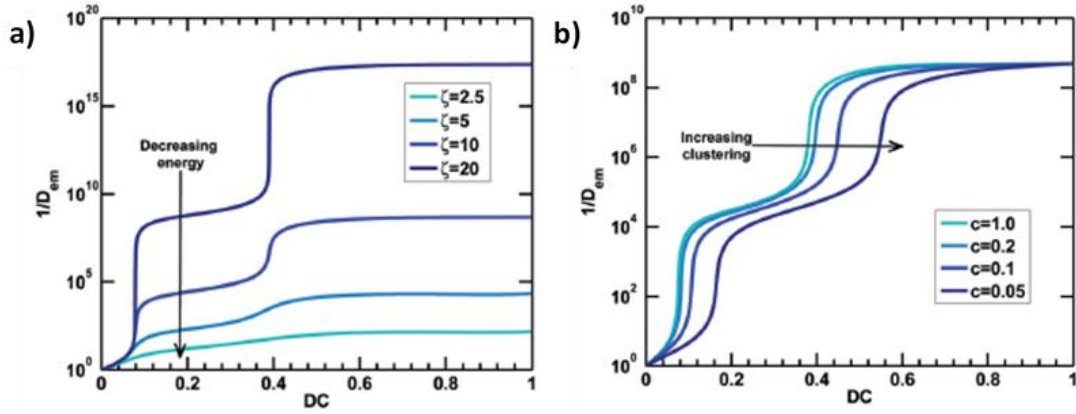


Figure 10. Theoretical values of D_{em} obtained by using effective medium calculation: (a) influence of interaction energy ζ and (b) effect of cluster formation on the location of the sharp transition of the (a) curves.¹⁰

The coefficient D_{em} is reduced by increasing the energy cost for the occupation of a lattice site; moreover, two regions of sharp transition can be observed in correspondence of which clustering is delaying the degree of conversion. The location of the sharp transitions is related to the site fractions reaching certain threshold values. The decrease in diffusivity is $\propto \exp\left(-\frac{\zeta}{k_B T}\right)$ at the first transition, while it is $\propto \exp\left(-\frac{2\zeta}{k_B T}\right)$ at the second transition. From experimental measurement it is shown that the second transition region is close to the DC at which the growth in relaxation time and the exothermic peak are observed, so that it is possible to use the shift in the τ -DC curves (Fig. 7¹⁰) to assess the spatial distribution of crosslinks for networks cured under different processing parameters. Indeed, since a combination of the change in local network stiffness (ζ) and in clustering modifies the shape of the τ -DC curves, these parameters can be derived and used to calculate the probability of having two occupied neighbouring sites.

Finally, by using the fraction of monomers forming crosslinks and the probability values, it is possible to compute sample crosslink distributions for the photocured network at different light intensities (Fig. 11a,b).

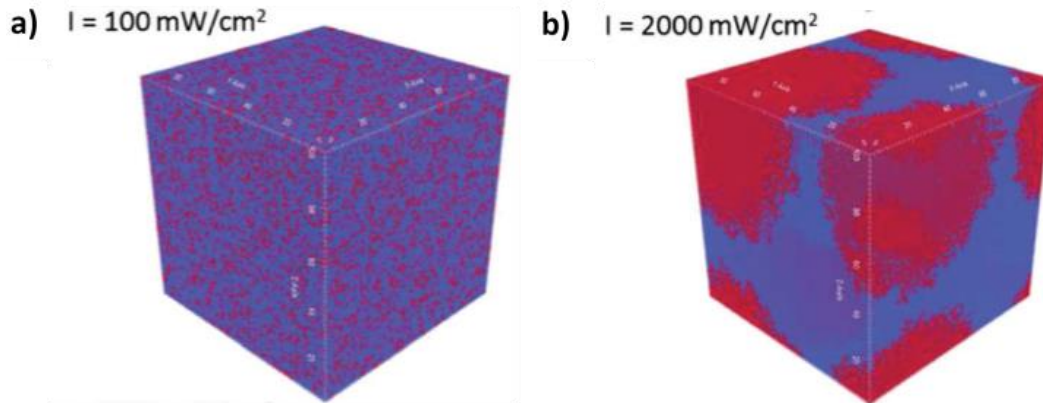


Figure 11. Simulation of crosslink distribution for light intensities (a) 100 mW/cm² and (b) 2000 mW/cm² on a simple cubic lattice with $z=6$. Red sites denote the crosslink.¹⁰

It can be noticed that a higher intensity of the incident light is able to produce a higher density of crosslinking, but the crosslinks are more clustered. This method supplies a way to characterize the spatial distribution of crosslinks¹⁰.

A lot of efforts have also been done to perform a real time monitoring of the photopolymerization process, with the aim to correlate directly the conversion of the resin to the development of its physical properties.

Example of this attempt is the NIR/MIR Photo-rheology measurement performed by C. Gorsche *et al.*⁷ Firstly it was shown that a larger quantity of reactive diluent in the resin mixture implies a faster reaction speed and an higher normal force (F_N) arising in the film (Fig. 12a), which is an indication of the polymerization induced shrinkage stress that is produced during the conversion after gelation; the value for the maximum storage modulus also showed an increase (Fig. 12b).

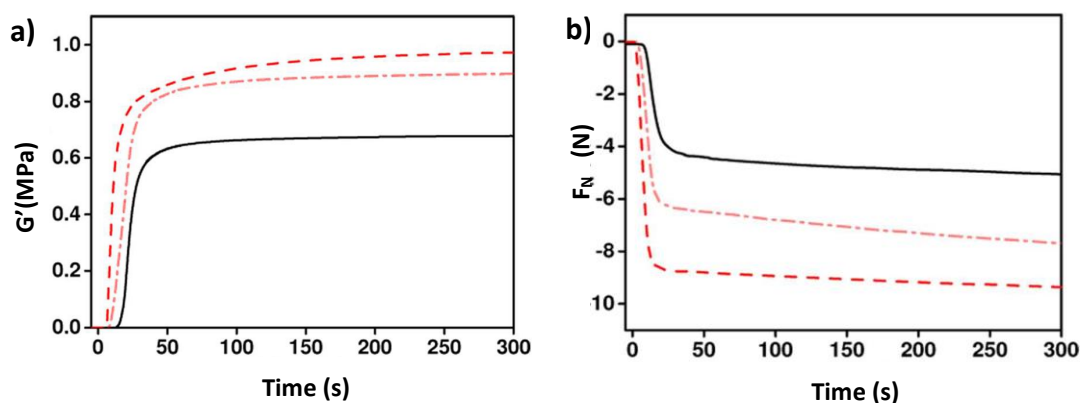


Figure 12. RT-NIR Photo-rheology study of a pure photo-polymer (solid line) and of its mixtures with a reactive diluent 10wt% (dot-line) and 50wt% (dashed line): (a) storage modulus G' ; (b) normal force F_N .⁷

Successively, it has been shown that the final conversion of the cured resins, which describes the extent of polymerization, did not vary considerably even though the gel point conversion decreased with increase in concentration of diluent (Fig. 13).

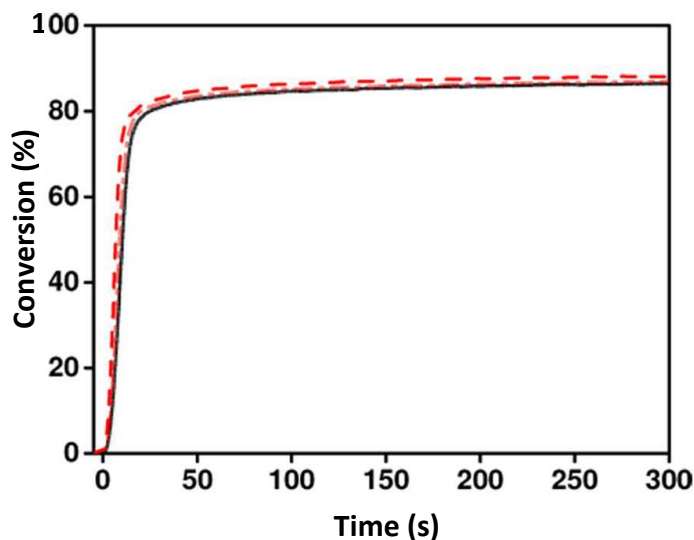


Figure 13. RT-NIR Photo-rheology measurements of conversion vs time for a pure photo-polymer (solid line) and its mixtures with a reactive diluent 10wt% (dot-line) and 50wt% (dashed line).⁷

The obtained results can be explained by considering that a faster conversion and increased modulus cause an enhanced shrinkage stress towards the final stages of photo-polymerization. Hence, the faster systems will be subjected to faster mobility restrictions, that result in a similar extent of the final double bond conversion.

Therefore, the values of G'_{\max} can be directly correlated to the mobility restriction.

3. EXPERIMENTAL

3.1. Materials and setup

In this work, the analysed system is composed by two different monomeric mixtures to which a photo-initiator is added so as to induce the polymerization reaction. Subsequently the polymers are deposited on substrates and polymerized by UV exposure in a proper experimental chamber.

3.1.1. Substrates

The selection of the substrate to be used for the deposition of the resin is crucial, since it can have specific influences on the cure speed, on the crosslink density distribution and on the development of internal stresses inside the coating, thus resulting in a completely different network structure. Also the adhesion to the substrate is an important parameter which depends on the performed surface treatment and on the nature of the deposited coating¹¹.

Specifically, Silicon and Silica will be used for the following study, because they constitute well-known systems, whose needed properties are tabulated and characterized¹². The surfaces are cleaned with a specific sequential treatment, which includes the exposure to an acetone ultrasonic bath for 15 minutes, subsequently flushing with acetone, ethanol and a final rinsing with deionised water. The substrates are kept hydrated till usage, when they are finally dried with gaseous nitrogen (N₂)¹³.

3.1.2. Monomers and oligomers

Two different resins will be considered for this analysis which are composed by three components mixed in different ratios: an oligomer (polyether urethane diacrylate) and two monomeric acrylic diluents (2-Ethylexyl acrylate and Bisphenol A diglycidyl ether diacrylate) (Tab. 1).

	LT	HT
Polyether urethane diacrylate (oligomer)	71.4%	40.8%
2-Ethylhexyl acrylate	28.6%	18.4%
Bisphenol A diglycidyl ether diacrylate	0.0%	40.8%
Total	100%	100%

Table 1. Composition of the two monomer mixtures considered in the study.

Since the components are present in different ratios, the resulting glass transition temperature (T_g) will be different: in case of comonomer mixtures, the monomeric T_g is linearly additive, since most monomer combinations yields homogeneous amorphous glasses upon cooling³.

Considering the different glass transition temperatures, from now on the two mixtures will be respectively called LT (low T_g) and HT (high T_g) for simplicity.

- The main component in both the formulations is an oligomer (polyether urethane, PU) which is a diacrylate, whose theoretical molecular weight is 2850g/mol, so that its viscosity results to be very high. The PU is composed by three building blocks assembled as sketched in Fig. 14: 2-Hydroxyethyl Acrylate (HEA), Toluene Diisocyanate (TDI) and Polypropylene Glycol (PPG). The estimated number of monomeric units which forms the PPG blocks is around 25.

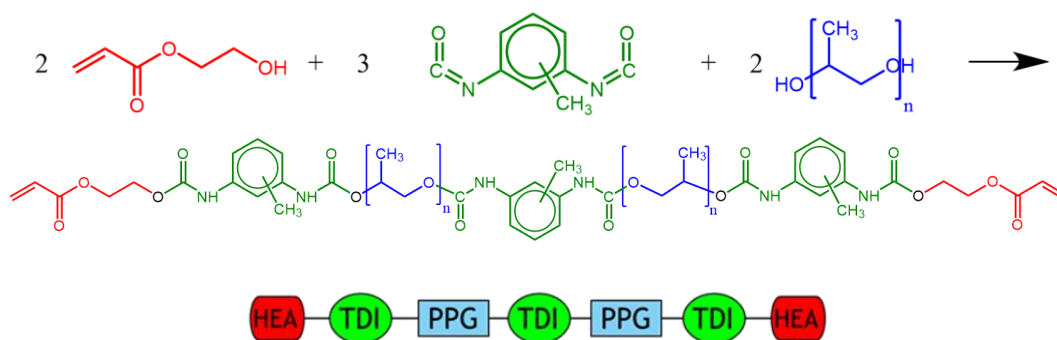


Figure 14. Oligomer structure and composition: 2-Hydroxyethyl Acrylate (HEA, red), Toluene Diisocyanate (TDI, green), Polypropylene Glycol (PPG, blue).

PU acrylate are usually characterized by inferior mechanical properties than thermoplastic PUs, in fact they show a low ultimate extension due to the high crosslink density that can be achieved¹⁴. Nevertheless, PU acrylates have the potential to combine the high abrasion resistance, toughness, tear strength and good low temperature properties of PU with the optical properties and weatherability of polyacrylates^{14,15}. PU acrylates are composed by soft segments (polyol chains, such as PPG), hard segments (diisocyanates, such as TDI) and acrylic structure units

(HEA)¹⁴. Due to the presence of both soft and hard phases, a two-phase system is created and micro-phase separation occurs: this phenomenon, which is governed by the segment length and type, is a key parameter to control the mechanical properties of the material¹⁴. The soft segment in PU contributes to the high extension and elastic recovery, while hard segments attributes high modulus and strength to the composition. The polar nature of the hard urethane segments causes a strong mutual attraction leading to hard domain formation; on the other hand, soft domains can be formed by interaction between the soft segments, which give flexibility and elastomeric properties to the polyurethane acrylates¹⁴.

The oligomer is photopolymerized in different amounts with two reactive diluents, which are used to reduce volatility, toxicity, odour, polymerization shrinkage and to improve the properties of the cured material¹:

- 2-Ethylhexyl acrylate, which is an alkylic mono-acrylate used as a chain extender (Fig. 15).

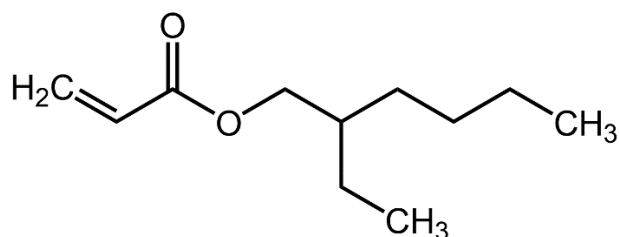


Figure 15. Chemical structure for 2-Ethylhexyl acrylate.

- Bisphenol A diglycidyl ether diacrylate (DGEBA) (epoxy acrylate): it is a liquid of low viscosity, which combines to the acrylate units by opening of the ether ring (Fig. 16).

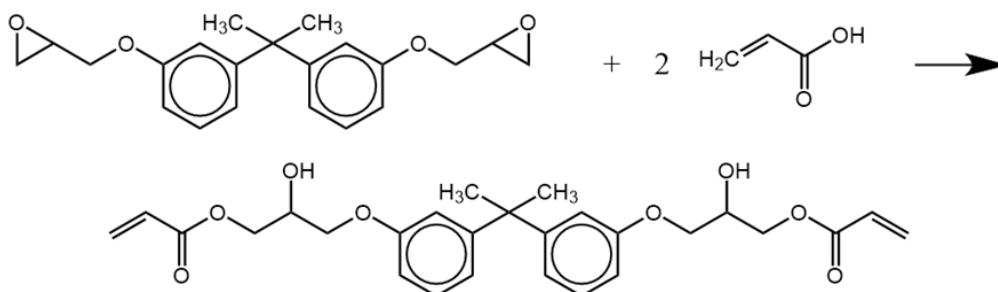


Figure 16. Chemical structure for Bisphenol A diglycidyl ether diacrylate (DGEBA) and reaction mechanism for its combination with acrylate units.

The two monomeric mixtures, with the above described formulations, have been supplied by *Royal DSM N.V.*, Geleen (the Netherlands).

3.1.3. Photo-initiator

As it has been previously underlined, photo-polymerization requires the presence of an initiator, which should be able to start the chemical process: important properties are the absorption in the appropriate wavelength region, the quantum yield for dissociation, the reactivity of the radicals towards monomers, stability in the dark, solubility and absence of yellowing in the photopolymer¹.

The radical formation can occur mostly by direct photo-fragmentation (homolytic cleavage of the single bond), as it occurs in phosphinoyl (TPO), by sensitization (hydrogen abstraction), as in the case of benzophenone, or by cationic polymerization^{1,4}.

In the present study Irgacure[®] 651¹⁶ was used as initiator (Fig. 17).

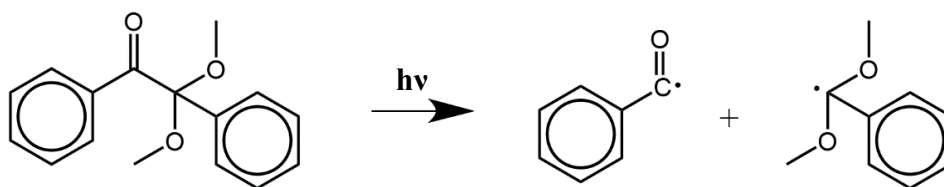


Figure 17. Reaction mechanism of Irgacure[®] 651: a photon causes the homolytic cleavage of the single bond.

The initiator selection is mostly based on two parameters, which are the solubility in the considered resin mixture and the matching between its absorption spectrum and the emission spectrum of the lamp used for photo-polymerization.

As a matter of fact, the polar nature of the carbonyl group in the initiator well combines to the polar nature of the urethanes groups of the oligomer. At the same time, the selected initiator shows appreciable absorption in the UV and no absorption in the visible range (Fig. 18), so that the system would be more stable and it will not require to operate always in the dark.

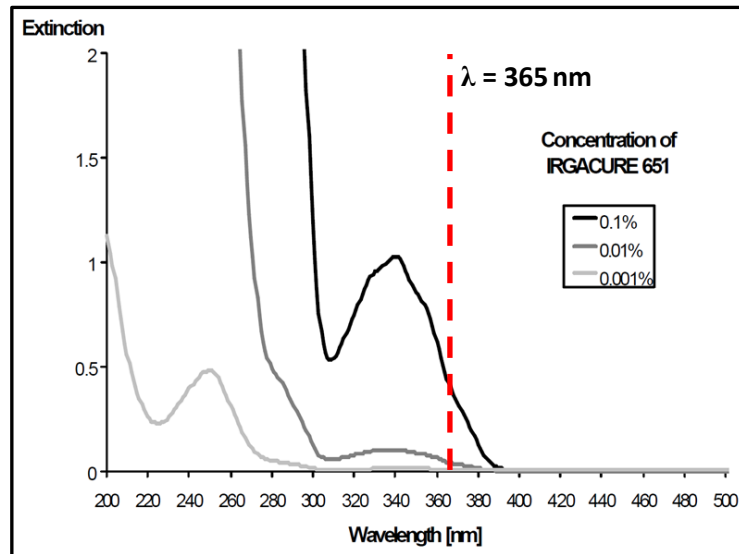


Figure 18. Absorption spectrum for the initiator Irgacure® 651 at different concentrations; the red line indicates the emission wavelength of the UV lamp that has been used.¹⁶

3.1.4. Setup

The experimental setup consists of a sealed polymerization chamber, covered by a UV-transparent glass. A valve permits to control the flow of nitrogen gas which is injected in the chamber and that allows to purge the oxygen contained inside, which would otherwise hinder the photo-polymerization. At the centre of the chamber a support is present, which sustains the sample at a fixed distance from the UV lamp. A remote control of the lamp is used in order to regulate the UV exposure period.

3.2. System preparation

The analysed system is constituted by a substrate on top of which a polymeric coating is deposited, after performing a careful cleaning of the substrate itself, as specified in section 3.1.1.

The polymer is firstly mixed with the initiator and magnetically stirred for 6h at 300 rpm at room temperature before performing the deposition.

The deposition process is performed by spin coating, which is a well-known deposition technique to obtain uniform films, ranging from a few nanometres to a few microns in thickness.

The substrate is placed on the spin-coater (*Chemat Technology INC, KW-4A*) and sucked by vacuum; immediately after depositing some liquid polymer droplets on the surface, the substrate is rotated at high speed with a specific time ramp. The

action of the centrifugal force, combined with the surface tension of the solution, yields a highly uniform thin film. The airflow generated during rotation can also help the eventual solvent evaporation (Fig. 19).

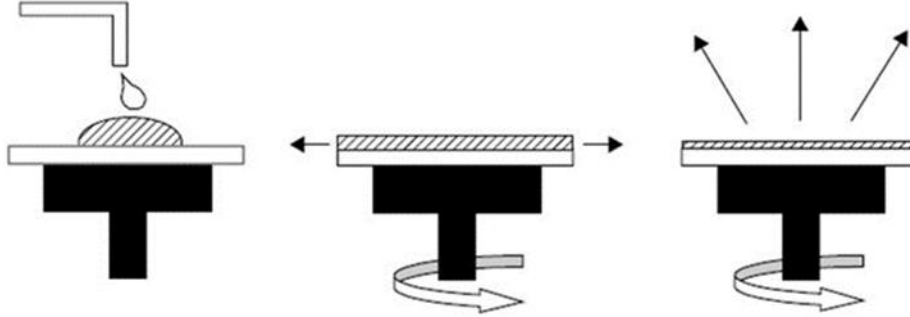


Figure 19. Scheme for spin coating deposition: drop casting, spinning and solvent evaporation.

For the purpose of the present analysis, it is useful to have a straightforward quantitative correlation among the thickness of the obtained film, the angular velocity and the rotating time; such a relation was studied by many authors, trying to describe also the effect of evaporation and of the shear stresses created by air on the deposited film^{17,18}. According to N. Sahu *et al.*¹⁷, it is possible to express the final thickness of the coating h_t as a function of the density ρ , viscosity η , angular velocity ω , rotating time t and initial thickness h_0 :

$$h_t = \frac{h_0}{\left[1 + \frac{4h_0^2 \rho \omega^2 t}{3\eta}\right]^{1/2}} \quad [2]$$

It can thus be concluded that, in a dimensionless sense, $H \sim \tau^{-1/2}$, where $H = \frac{h_t}{h_0}$, while $\tau = \frac{2h_0^2 \rho \omega^2}{3\eta} t$.

The equation 2 has been derived by neglecting the evaporation of the solvent during the final rotation steps, but also by neglecting the effect of the shear stress at the polymer-air interface during the initial stage. Whereas the first can be correctly neglected in the present case, since the considered oligomeric mixture does not contain any solvent (unless differently indicated for specific analysis), the latter approximation can be unrealistic: the air shear stress is found in fact to significantly increase the rate of thinning, to the extent $H \sim \tau^{-1}$ for small H , rather than $H \sim \tau^{-1/2}$. After the film deposition, a UV lamp is used to induce the photo-polymerization of the material in an inert nitrogen atmosphere.

3.3. Photo-chemistry and light source

Any photo-reaction that involves the absorption of light requires strong matching between the absorption spectrum of the absorber and the emission spectrum of the lamp which is used to generate the radiation.

As a matter of fact, the absorption of a photon is only possible if its energy is exactly equal to the energy difference between two electronic levels of the absorber: if this occurs, then an electron can jump from a lower to a higher energy level, leading the absorber to the excited state.

This process is typical of photo-polymerization initiators, which are generally characterized by absorption peaks in the UV range. Their excitation requires therefore the use of UV light with peaks at suitable wavelength, which can be generated by several different lamps and methodologies.

A simple and widespread technique to generate UV light consists on the use of a Hg-vapor-lamp, which is a gas discharge lamp that uses an electric arc to produce the excitation of vaporised mercury, so that the subsequently released energy can be exploited to generate light. Sometimes Hg lamp are implemented by addition of Xenon, which allows to enhance the obtained output and to focus the light with higher precision. The emission line spectrum is then characterized by well-defined peaks at different wavelength, one of which is at 365 nm (Fig. 20a): it follows that a filter is required to perform an excitation in correspondence of a precise wavelength (Fig. 20a).

A similar method implies the use of deuterium as a low-pressure gas to be excited by plasma arc; the consequent emissions will be constituted by a continuous spectrum in the ultraviolet region, which is generally exploited in spectroscopy (Fig. 20b).

An interesting alternative, which will also be exploited for the curing procedure, is the use of a LED lamp, that produces light by using light emitting diodes, which allow an improvement in efficiency, directionality and monochromaticity of the emission. The basic principle that allows the light production is the recombination of electrons and holes within the light emitting diode, which is constituted by a p-n junction of two-lead semiconductors: as soon as the recombination occurs, according to the principle of electroluminescence, a photon is emitted, and it will have a wavelength that corresponds to the energy band gap of the semiconductors. The use of a LED lamp allows therefore to obtain an emission exactly at 365 nm (Fig. 20a).

In the case in which light in the visible range is needed, halogen lamps can be used (Fig. 20b): they are constituted by a tungsten filament which is heated by Joule effect at high temperature, in order to achieve emission of visible white light. The lamp bulb also contains an inert gas and a small amount of halogen which helps the re-deposition of the evaporated tungsten atoms on the filament, thus increasing the life of the lamp.

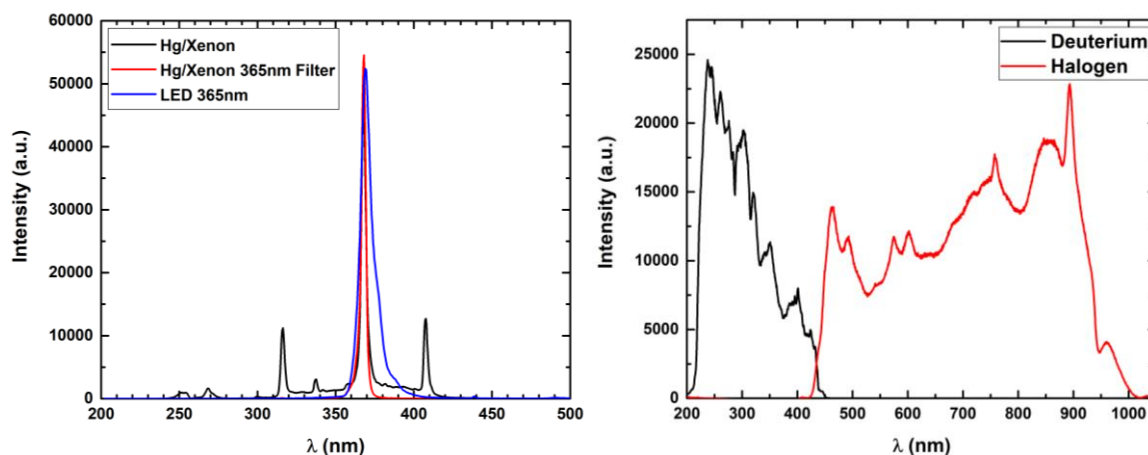


Figure 20. Emission spectra from different lamp sources. (a) shows a comparison among a LED lamp (blue), a Hg/Xenon lamp (black) and the same lamp with a filter (red); (b) shows a comparison among the spectra of a deuterium lamp (black) and of a halogen one (red).

The UV lamp which is used for the present work (*Phoseon Technology*, FireJet FJ800) is characterized by a control over powering time and a control over the percentage of intensity which is supplied. A study over the change in the lamp intensity with the lamp-sample distance and with the intensity percentage indicated on the lamp controller has been carried out, so that a straightforward correlation among them is possible (Fig. 21). The study is performed by means of a light power meter by *Hamamatsu* (C6080-03).

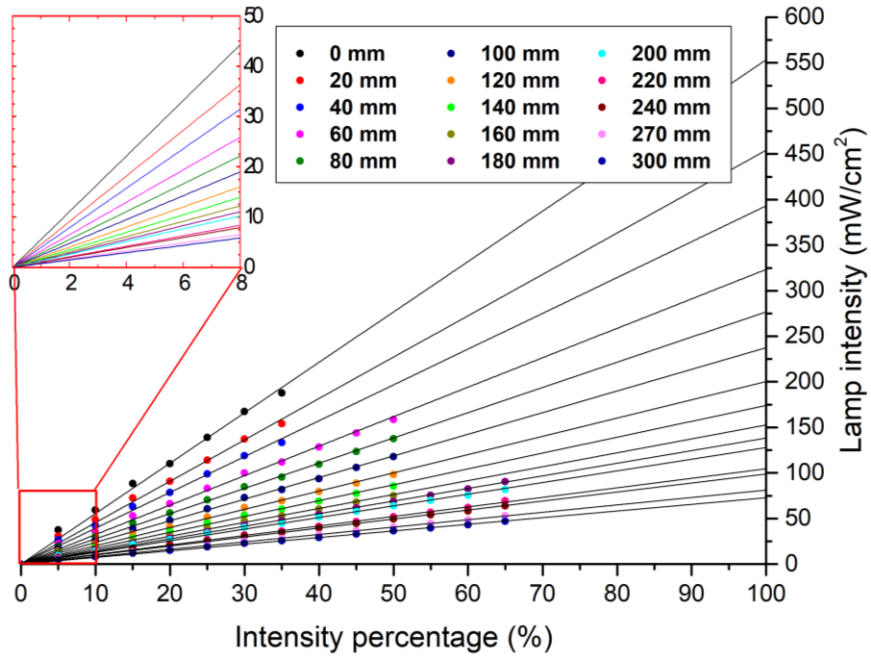


Figure 21. Summary graph that shows the correlation among the lamp intensity, lamp-sample distance and intensity percentage of the lamp controller.

3.4. Set conditions and parameters

The investigation over the network structure formed after polymerization is carried out by keeping some parameters constant, while others have been modified to understand what the effect on the material is and how this can be used to tailor a specific property.

Set conditions are the polymerization temperature ($T=25^{\circ}\text{C}$), the atmosphere inside the chamber (N_2) and its pressure, the initiator concentration (except for some preliminary analysis), the substrate over which the resin is deposited (unless differently indicated) and its preparation, in term of cleaning and deposition procedure.

The varying parameters are the dose and intensity of the radiation, the thickness of the deposited coating (maintained constant within the same technique of analysis) and the curing time.

3.5. Characterization techniques

The characterization of the two polymeric systems requires the use of various techniques in order to obtain a full description of their thermal, mechanical, kinetic and morphological properties. The more common techniques supply data that can later be used for a better interpretation and evaluation of the X-Ray diffraction/scattering results.

3.5.1. Fourier Transformed-Infrared Spectroscopy (FT-IR)

FT-IR is a spectroscopic technique that supplies information about the chemical composition of a material on the base of the amount of electromagnetic radiation that is absorbed by the sample. According to the Lambert-Beer law ($A = \varepsilon \cdot C \cdot L$) the absorbance A is in fact directly proportional to the absorption coefficient ε , to the concentration of a certain species C and to the length L travelled by the beam inside the material.

The light absorption induces atomic vibrations, which are characterized by different frequencies depending on the bond strength and on the mass of the atoms involved in it:

$$\omega \propto \sqrt{\frac{k}{\mu}} \quad [3]$$

where ω is the wavenumber associated to the vibration, k is the bond strength constant and μ is the reduced mass. The final spectrum is obtained by applying the Fourier transform to the raw data collected by the instrument: depending on the detected wavenumber, it is then possible to derive quantitatively the chemical composition of the analysed material.

The used instrument is a *PerkinElmer FT-IR spectrometer* (Spectrum 100): it collects the data by means of an ATR (Attenuated Total Reflectance) quartz crystal and send them to the software *PerkinElmer Spectrum* (vs. 10.5). The spectra have been collected in air with 16 accumulation scans in the range 4000-600 cm^{-1} .

FT-IR has been used in the present study to investigate the chemical structure and the polymerization kinetics of the two considered monomeric mixtures. The resin conversion is measured by observing the change in intensity of the absorption peak at 1636 cm^{-1} , which is associated to the C=C vibrations along the alkylic chain.

The analysis has been carried out by depositing the liquid polymers over glass substrates (10x10 mm) by spin coating with a fixed procedure (3 s ramp at 1500 rpm followed by 60 s spinning at 2000 rpm). Before curing the samples, a time of 5 minutes has been waited to obtain a proper levelling of the deposited material. No solvent has been used to obtain these samples.

The data have been normalised to the absorption peak at 1601 cm^{-1} (for LT) and at 1607 cm^{-1} (for HT) which are associated to the C=C vibrations in the aromatic group of the polymers. The degree of conversion has been calculated as the ratio between the cured and uncured absorption at 1636 cm^{-1} .

The varying parameters have been the curing time and dose of supplied radiation. As a confirmation of the obtained outcomes, an *in-situ* real-time FT-IR has been carried out on both polymers. In this case, for practical reasons, the polymerization has been performed by using a different lamp together with a band-pass filter ($365 \pm 10\text{ nm}$), which allows to maintain consistency with the previous results; moreover, the experiment is not carried out in a sealed chamber, but by blowing nitrogen towards the polymerizing resins. Due to the high viscosity of the resin, no control over the deposited volume and thickness is possible: in fact the resin is dropped directly on top of the ATR crystal and there is no possibility to spread it adequately.

3.5.2. Dynamic Mechanical Analysis (DMA)

DMA is an investigation technique that supplies information about the viscoelastic properties of polymers by applying to the samples a sinusoidal stress and measuring the consequent sinusoidal strain. This allows to estimate the complex modulus of the material at varying temperatures or frequencies.

The complex modulus of the material is given by a real part (Storage Modulus, E') and by an imaginary part (Loss Modulus, E''): $\tilde{E} = E' + iE''$; the ratio between the two moduli is defined as the loss factor ($\tan \delta$). From the examination of such properties, it is possible to derive information about phase transitions occurring in the polymer or about the crosslink density distribution inside the material.

The used instrument is a *TA Instruments DMA* (Q800); data are evaluated by using the software *Universal Analysis 2000* (vs. 4.5).

DMA has been performed with the aim to evaluate the viscoelastic properties of the two fully cured polymers as a function of the different light intensities applied

during curing. Moreover, also the changes occurring at different curing time have been investigated.

The samples, with an area of 10x5 mm and a thickness in the range of 50-80 μm , have been obtained by depositing the polymers over Silicon substrates and by successively detaching them just before the analysis. The deposition by spin coating has been performed with a fixed procedure: 3 s ramp at 1000 rpm followed by 60 s spinning at 1500 rpm in the case of HT and 60 s spinning at 800 rpm in case of LT. Before curing the samples, a time of 20 minutes has been waited to obtain a proper levelling of the deposited material. No solvent has been used to obtain these samples.

The measurements have been performed in Temperature sweep (frequency 1 Hz) with a ramp rate of 3°C/min and the following temperature range has been analysed for the two polymers:

LT: - 60°C \rightarrow 50°C

HT: - 50°C \rightarrow 120°C

3.5.3. Differential Scanning Calorimetry (DSC)

DSC analysis offers the possibility to register the temperature differences which correspond to the heat flux difference between the sample and the reference exposed to the same temperature cycle. It is possible to derive information relative to the phase transitions associated to the thermal content, such as crystallization, melting and glass transition. The obtained curve also allows to define if a transition is endothermic or exothermic (Fig. 22).

In the present study, the analysis has the aim to supply the glass transition temperature (T_g) of the two polymers at different levels of conversion during the photo-polymerization. This kind of study allows to obtain a validation of some of the results obtained by DMA for what concerns the thermal properties; moreover, it allows to measure the T_g of the polymer in case of films which are not self-standing, because of the low conversion degree: this would not be possible by using DMA.

The DSC samples have been prepared by depositing the polymers over Silicon substrates (10x10 mm) and by successively detaching them: a maximum of two layers of the same coating has been placed in the same crucible. The temperature range of analysis was defined between -80°C and 120°C by including a first heating cycle to remove the thermal history, followed by one cooling and one heating cycle.

The calorimetry measurements have been performed with *Mettler Toledo* (DSC1 Star system) and the data have been analysed with the software package *Mettler STARe* (vs. 10.10). The selected scan rate has been 10°C/min.

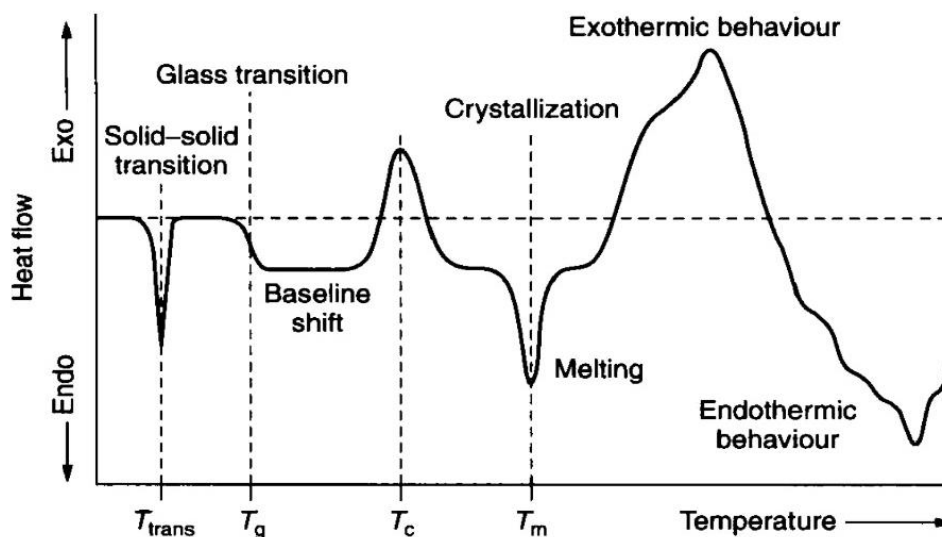


Figure 22. DSC diagram depicting the main transitions that can be detected with this technique and how to recognize them.

3.5.4. Atomic Force Microscopy (AFM)

AFM is a scanning probe microscopy which allows to detect the surface morphology. The instrument is composed by an oscillating cantilever attached to a tip with a small curvature radius (Fig. 23).

The surface mapping is performed by evaluating the cantilever deflection due to the physical interactions between the tip and the sample: such interactions generally have an electrostatic nature and can be described by the potential-well trend shown by Van der Waals forces as a function of the distance between the two objects.

The cantilever deflection can be measured either by sending a laser beam that is reflected and detected by an optical system or by using a piezoelectric probe. In this case the deflection creates a potential difference at the two ends of the probe and this turns to be an indication of the bending to which the cantilever is subjected.

Atomic force microscopy has been exploited to evaluate the surface morphology (roughness) and thickness of the two cured polymeric films. The thickness is determined by creating a cut in the coating and analysing the height difference between the substrate beneath and the surface of the coating itself.

The used instrument (*Bruker*, MultiMode 8) makes use of the software *Nanoscope* (vs. 8.15); the used Silicon tips are produced by *Bruker* (ScanAsyst-air, $r_{\text{tip}} = 2 \text{ nm}$, $f_0 = 70 \text{ kHz}$, $k = 0.4 \text{ N/m}$). The data have been elaborated by using the software *Gwyddion SPM data analysis* (vs. 2.50).

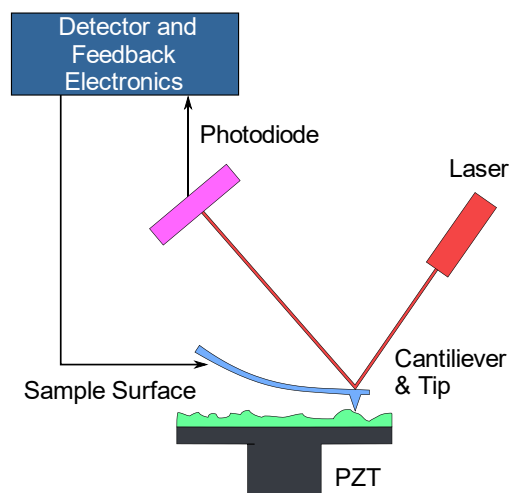


Figure 23. Scheme of the working mechanism and laser detection of an AFM.

3.6. X-Ray scattering and synchrotron radiation

One of the most powerful possibilities to analyse and understand the atomic and molecular organization inside a material consists on the use of a diffraction or scattering experiment, which supplies comprehensive information about the periodicity of the analysed material.

From a theoretical point of view, it is vital to operate a distinction between scattering and diffraction. The term “scattering” refers to a wide family of events occurring in a material that produce images in which the intensity of the scattered signal is changing from point to point; the term “diffraction” applies instead only to the elastic scattering events which are created when crystalline materials are investigated. Both the phenomena can imply the generation of periodic patterns because of the interaction between energetic photons, such as X-Rays, and the electronic structure of the material. The electric field associated to the X-Rays is in fact able to induce vibrations of the electrons inside the material with consequent emission of spherical waves, which sum up to give constructive and destructive interference¹⁹. If the scattering intensity is weak with respect to the energy of the incident photons, the overall scattered wave can be considered as a plane wave, according to the Born Approximation (also called kinematical approximation)¹⁹.

Since the condition for the Born Approximation is often verified in practical applications, the interpretation of diffraction patterns results to be simplified, even if a lower obtained signal is implied when weaker interaction is present.

With the aim of implementing the strength and resolution of the obtained signal, synchrotron radiation can be exploited, since highly energetic and focused X-Rays can be produced. The generation of such strong photons requires the acceleration, at relativistic speeds, of charged particles along curved paths, called storage rings, through the application of a magnetic field¹⁹. The obtained light is highly collimated, linearly polarized and has a defined time structure, with short pulses separated by longer intervals; moreover, it is characterized by a continuous spectrum from infrared up to hard X-Rays and by spatial and temporal coherency^{19,20}.

The intensity of the scattered wave is directly related to a crystal form factor, which can be expressed as:

$$F^{crystal}(\vec{q}) = \sum_j f_j(\vec{q}) e^{i\vec{q} \cdot \vec{r}_j} \sum_n e^{i\vec{q} \cdot \vec{r}_n} \quad [4]$$

where f_j is the atomic form factor, $\vec{q} = \vec{k}_i - \vec{k}_s$ is the wavevector transfer (difference between the incident and scattered wavevector), $\sum_j f_j(\vec{q}) e^{i\vec{q} \cdot \vec{r}_j}$ is the unit cell structure factor, $\sum_n e^{i\vec{q} \cdot \vec{r}_n}$ constitutes the sum over all the lattice sites.

According to Bragg's law for diffraction ($n\lambda = 2d \sin \vartheta$), also applicable to more general scattering events, only certain values of the incident angle give rise to a diffraction peak; accordingly, Von Laue offered a more theoretical treatment about diffraction and set up as a condition to observe a non-vanishing scattering intensity that $\vec{q} = \vec{k}_i - \vec{k}_s = \vec{G}$, which means that the wavevector transfer needs to be a reciprocal lattice vector \vec{G} . The main consequence of the Von Laue derivation is the obtainment of images which have to be represented on a reciprocal lattice.

Nevertheless, when scattering from amorphous materials, such as polymers or glasses, is considered, a statistical approach has to be adopted; the defining structural characteristic will be in this case a degree of randomness in the position of the atoms¹⁹. Indeed, if the structure of a crystal is mathematically described by a discrete and periodical structure, the nanostructure of soft matter is a continuous function with short range of order²⁰.

A statistical description of the structure frozen in time, which is detected by X-Ray scattering, can be given by the radial distribution function: $g(r) = \frac{\rho(r)}{\rho_{at}}$, where $\rho(r)$ is the radial density, while ρ_{at} is the average areal number density¹⁹. Both in case of

crystalline and amorphous materials, the radial distribution function is oscillating and shows some peaks, but in the second case it dampens and broadens out, tending rapidly to 1 when the radius is increased¹⁹. It can be shown that the scattering intensity is directly connected with the radial distribution function, which in turn depends on a liquid structure factor that contains the information about the wavevector transfer¹⁹.

3.6.1. Small-Angle X-Ray Scattering (SAXS)

Small-angle X-Ray scattering experiments are normally carried out with a transmission setup, in which the primary beam penetrates the sample and is scattered towards the detector, so that a circular pattern is recorded around the position of the attenuated central beam²⁰ (Fig. 24).

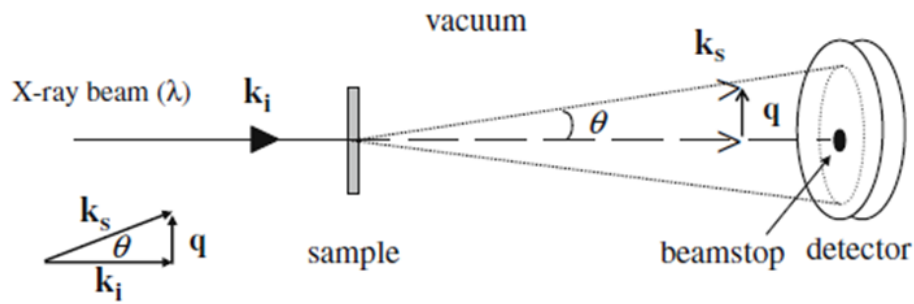


Figure 24. Schematic layout of a SAXS setup depicting the incident, scattered and transmitted X-Ray beams, the two-dimensional detector and the definition of the scattering vector \vec{q} ²⁰.

Within the Born approximation, the variation in intensity of the detected signal can be correlated to the fluctuation of electron density inside the sample by means of the Fourier transform, which connects real and reciprocal space²⁰.

The scattering intensity can thus be expressed by the following proportionality:

$$I^{SAXS}(q) \propto |\mathcal{F}(\vec{q})|^2 \mathcal{S}(q) \quad [5]$$

where $\mathcal{F}(\vec{q})$ is the form factor, that depends on the morphology of the particle, in term of shape and size, while $\mathcal{S}(q)$ is a structure factor that is introduced to keep into account the inter-particle correlations¹⁹.

The analysis of the signal is based on the representation of the form factor as a function of the wavevector transfer: this is possible by azimuthally averaging the scattering signal that is obtained by the sample. The study of the obtained maps

permits to find correlations between the dimension of the particles and the frequency of oscillation of the signal, which is seen to increase with a decrease in the dimension, according to Guinier analysis¹⁹. Moreover, the scattering intensity at the long-wavelength limit (or the low wavevector transfer limit) gives the possibility to perform an exact calculation of the dimension of the particle:

$$I^{SAXS}(q) \xrightarrow{qR \ll 1} \exp\left(-\frac{q^2 \bar{R}^2}{3}\right) \quad [6]$$

where \bar{R} corresponds to the radius, in case of spherical particles, or to the gyration radius, in case of particles with different shapes¹⁹. It should be anyway reminded that the obtained dimension is averaged over a large area in case of polydisperse systems¹⁹.

Instead, by considering the short-wavelength limit and according to Porod analysis, it is possible to obtain information about the morphology and shape of the particles: this can be done by looking at the Porod power-law exponent, which will be different for spheres ($n=4$), disks ($n=2$) or rods ($n=1$). This would be particularly interesting in the case of polymers, which will be seen as rigid rod at long wavevector transfer, but they will assume different morphology at shorter scale of observation, depending on the conformation of the macromolecular chain¹⁹.

During the following analysis, SAXS is used to investigate the two considered monomeric mixture before curing, with the aim to determine the two gyration radii, that constitute estimations of the dimensions of the random coil of the oligomers.

3.6.2. Grazing Incidence Small-Angle X-Ray Scattering (GISAXS)

Despite the existence of numerous techniques that can be exploited for the analysis of the polymer structure and of the crosslink density distribution, GISAXS results to be of particular interest when thin polymeric films are involved²¹: it permits in fact to obtain micro and nano-scale correlations and shape analysis of objects at surfaces or at buried interfaces²⁰, thus allowing the determination of the internal morphology of a film.

This technique is particularly advantageous because it is macroscopically non-destructive, supplies accurately averaged information about a large sample area (in the range of square centimetres)²¹, requires few seconds to record a scattering pattern and can be performed at ambient conditions: this characteristics make it

suitable to realise *in-situ* real-time investigations of dynamic structural changes in physical and chemical processes at surfaces and in thin films.

Moreover a grazing incidence geometry offers advantages over a transmission experiment: in transmission a weak scattering would derive from thin films and this can be easily obscured by the scattering from the substrate, whereas in grazing-incidence a much longer path is travelled through the film and the penetration into the substrate results to be limited²¹. Furthermore, it is also possible to obtain a depth-dependent structural information by using different incident angles²⁰.

On the other side GISAXS is very sensitive to small thickness variations: even if the sample preparation is not as demanding as the one required by TEM analysis, big efforts can be required to obtain homogeneous films with a thickness in the range of hundreds of nm.

As it can be noticed from Fig. 25, GISAXS supplies both the normal density profile and the lateral film structure. The specular scattering probes in fact a depth-sensitive information only, while the off-specular scattering probes the in-plane structure of the sample and appears when any type of surface roughness, scattering entity or lateral contrast variation is present on the surface or inside the film²⁰.

When GISAXS is performed, the direct beam and the specular reflected beam are often suppressed by a beam stop to avoid the detector saturation, as several order of magnitude in intensity separate the diffuse scattering from the specular reflectivity²⁰.

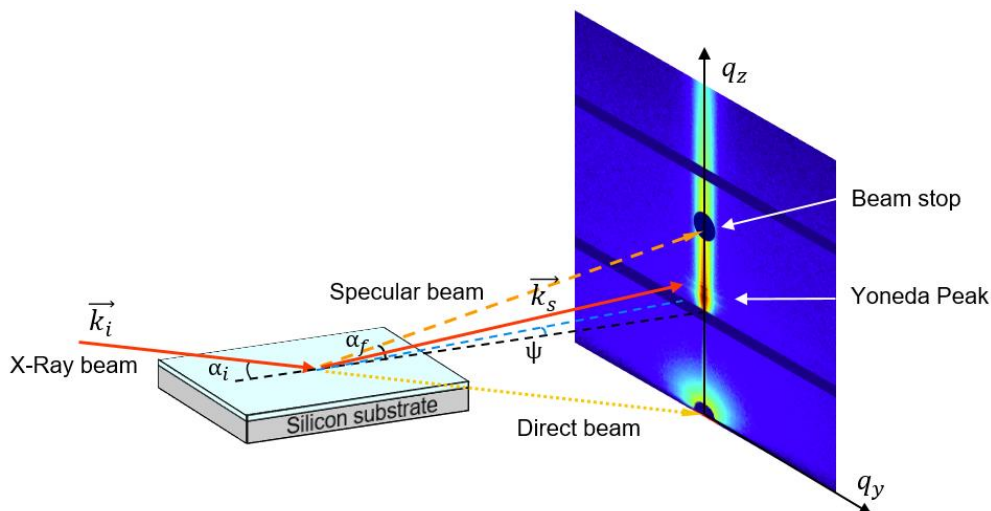


Figure 25. Schematic pictures of the GISAXS scattering geometry. The incident angle is denoted α_i , the exit angle α_f and the out-of-plane angle ψ . The colour coding indicates differences in the scattering intensity on the two-dimensional detector. Main characteristic features are the specular beam (orange arrow), the scattered beam (red arrow), the direct beam (yellow arrow) and the Yoneda peak (visible on the detector).

GISAXS measurements are performed with an incident angle which is slightly above the critical angle ($\alpha_c \sim 0.15^\circ$ in case of polymers); in correspondence of these quasi-total reflection conditions, an evanescent wave is formed at the surface of the material: this wave propagates along the boundary and exponentially decays by going inside the inspected material. The fast decay in intensity allows to achieve a strong surface sensitivity, which permits the analysis of surfaces and near surface regions.

The occurrence of total external reflection can be explained by a refractive index which is slightly lower than 1 when X-Rays are involved¹⁹ (Fig. 26):

$$n = 1 - \delta + i\beta < 1 \quad [7]$$

where $\delta = \frac{2\pi\rho r_0}{k^2} \sim 10^{-5}$ in solids and the imaginary part $\beta \ll \delta$. The expression for δ contains the electron density ρ , the scattering amplitude per electron r_0 and the wavevector k . The parameter δ is also called dispersion, while β corresponds to the absorption.

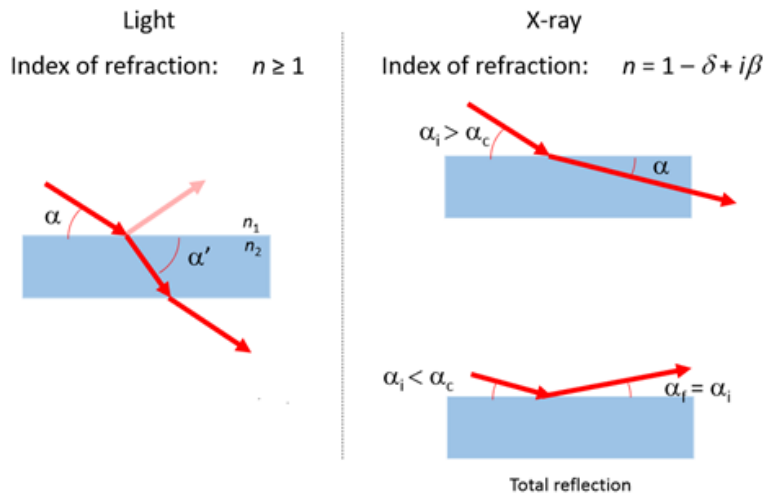


Figure 26. Comparison between the interaction of light and X-Rays with matter. The refractive index for X-Rays is slightly less than 1, so that total external reflection occur when the incidence angle is smaller than the critical angle¹⁹.

The major implication of a real part of the refractive index smaller than 1, is that the phase velocity inside the material, c/n , is larger than the velocity of light; this does not violate the law of relativity which requires that only signal carrying “information” does not travel faster than c . Such signals move indeed with the group velocity, which is smaller than c , and not with the phase velocity, so that the relativity law is respected¹⁹.

Considering now the Snell's law ($\cos \alpha = n \cdot \cos \alpha'$), neglecting β and imposing $\alpha' = 0$, it is possible to obtain $\alpha_c \sim \sqrt{2\delta}$, so that the critical angle below which total reflection occurs results to be in the order of milli-radian or below $1^{\circ 19}$.

This can be verified by exploiting the expressions suggested by H. Dosch *et al.*²³, which give the possibility to calculate the penetration depth of X-Rays inside the material and consequently the critical angle:

$$z = \frac{\lambda}{2\pi(l_i+l_f)} \quad [8]$$

$$l_{i,f} = \frac{\sqrt{2}}{2} \sqrt{(2\delta - \sin^2 \alpha_{i,f})} + \sqrt{(\sin^2 \alpha_{i,f} - 2\delta)^2 + (2\beta)^2} \quad [9]$$

where λ is the wavelength of the radiation, z is the penetration depth, while α_i and α_f are respectively the incidence and exit angles.

According to these expressions and by knowing the chemical composition of the components of the two monomeric mixtures, it is possible to estimate the penetration depth that is obtained in the following study (Fig. 27, Tab. 2).

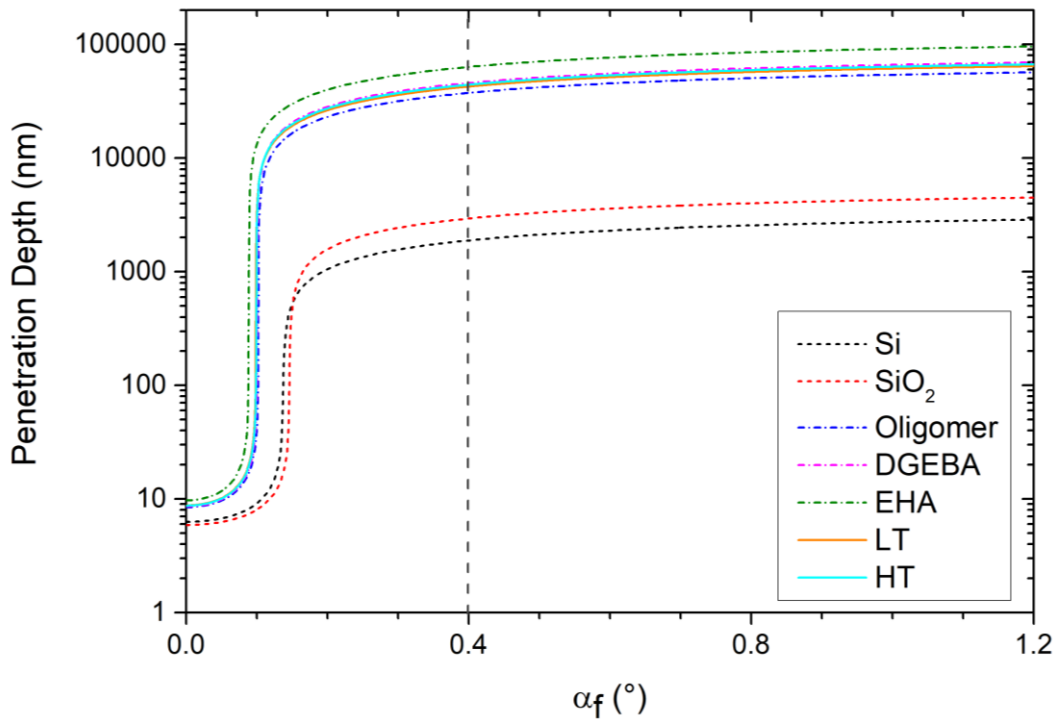


Figure 27. Plot showing the dependence of the X-Rays penetration depth on the value of the exit angle α_f for Silicon/Silica, for the oligomer and for the two reactive diluents. The computation is performed by using the Dosch's equations and by fixing $\alpha_i = 0.4^\circ$ and $\lambda = 0.095 \text{ nm}$.

Material	Formula	ρ (g/cm ³)	δ ($\times 10^{-6}$)	β ($\times 10^{-8}$)	α_c (°)
Silicon	Si	2.33*	2.88	2.62	0.137
Silica	SiO ₂	2.65*	3.27	1.66	0.146
Oligomer	C ₁₃₃ O ₆₁ N ₆ H ₂₃₃	1.20**	1.59	0.14	0.102
DGEBA	C ₂₁ O ₄ H ₂₄	1.17*	1.54	0.11	0.100
EHA	C ₁₁ O ₂ H ₂₀	0.88*	1.20	0.08	0.088
LT			1.48	0.12	0.098
HT			1.50	0.12	0.099

Table 2. Parameters used for the computation of the penetration depth and resulting critical angle for all the considered materials. The dispersion and absorption coefficient for the two monomeric mixtures has been calculated by exploiting the percentage of each component. [* refers to tabulated values; ** refers to approximated values]

When this range of critical angles is considered, the kinematical simple Born approximation used in SAXS, cannot be adopted anymore, and it should be extended with the distorted-wave Born approximation (DWBA), so as to keep into consideration the dynamical effect of reflection-refraction that takes place in correspondence of interfaces. The presence of an interface, in fact, makes it possible to have, in addition to a normal scattering event, also other phenomena (Fig. 28).

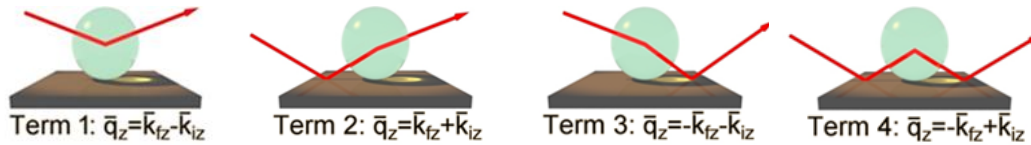


Figure 28. The four terms involved in grazing-incident scattering are represented. The first term corresponds to the simple Born approximation²².

The four scattered waves interfere coherently and are summed up by weighing each term by the corresponding reflection coefficient which is defined through the Fresnel formulae²⁰. The resulting scattering intensity for a lateral electron density fluctuation on the surface will be given by:

$$I(\vec{q}) \propto \langle |F_{DWBA}|^2 \rangle \cdot S(q_{||}) \quad [10]$$

where F_{DWBA} is an effective form factor, which carries information about the shape of the scattering centres, while $S(q)$ is a structure factor (or interference function), which tells about the 2D spatial distribution of the scattering centres²². Table 3 reports examples for the form factor of cylindrical particles and for the structure factor of a 1D para-crystal, which can be used to model the polymeric chains inside the analysed film.

<p>Form factor for randomly oriented cylinder of radius R_c and height H</p>	$\int_0^{\pi/2} \left\{ \left[\frac{2J_1(qR_c \sin \varphi)}{qR_c \sin \varphi} \right] \cdot \left[\frac{\sin\left(\frac{qH}{2} \cos \varphi\right)}{\frac{qH}{2} \cos \varphi} \right] \right\}^2 \sin \varphi d\varphi$ <p>J_1 – first-order Bessel function φ – orientation angle</p>
<p>Structure factor for a 1D/2D para-crystal model</p>	$\frac{1 - e^{-q_{\parallel} \sigma_d^2}}{1 + e^{-q_{\parallel}^2 \sigma_d^2} - 2e^{-q_{\parallel}^2 \sigma_d^2 / 2} \cos(q_{\parallel} d)}$ <p>σ_d – root-means-square deviation d – nearest-neighbour distance</p>

Table 3. Expressions to calculate the form factor and the structure factor valid in common situations in case of polymeric films²⁰.

The use of GISAXS in the following study is aimed at verifying the possibility to monitor *in-situ* changes in the crosslink density distribution during the photo-polymerization of the two different monomeric mixtures. In case these changes are observable, a correlation with the results obtained by well-known characterization techniques will be proposed.

3.6.3. X-Ray Reflectometry (XRR)

XRR is a surface-sensitive technique that exploits the reflection of an X-Ray beam at the surface of a material to evaluate the density profile of the interface normal to the surface itself. As a matter of fact, if the material presents small variations in the electron density profile, the reflected intensity will deviate from the value predicted by the Fresnel's law. Moreover, the technique also offers information about the roughness and the thickness of the analysed material (Fig. 29).

The data can be collected by moving the beam from 0.085° to 1°, so that both the critical angle of the substrate and of the coating are reached during the movement. The technique has been applied to the present investigation with the aim of detecting thickness and roughness of the coating at different step of the photo-polymerization; furthermore, this analysis may also offer the possibility to observe changes in crosslinking density.

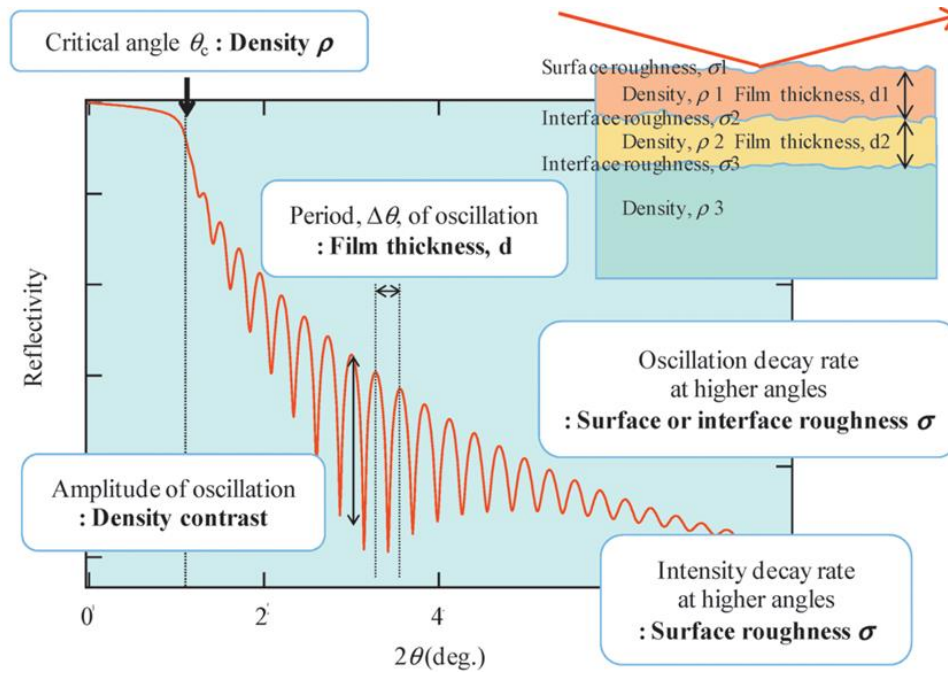


Figure 29. Information provided by X-Ray reflectivity profile.²⁴

3.6.4. Beamline setup

The setup for the *in-situ* measurements of photo-polymerization is shown in Fig. 30a,b: together with the setup used for the measurements *ex-situ* and described in paragraph 3.1.4, it also includes a light source, together with a UV/Vis spectrometer (*Ocean Optics*, Ocean-FX-XRI-ES) and a microscope camera. The first two devices permit to detect the changes in the reflectance spectrum of the material in the wavelength range 200-1100 nm (by surface differential reflectance spectroscopy), while the camera allows to correlate directly the application of the UV light to the scattering image obtained.

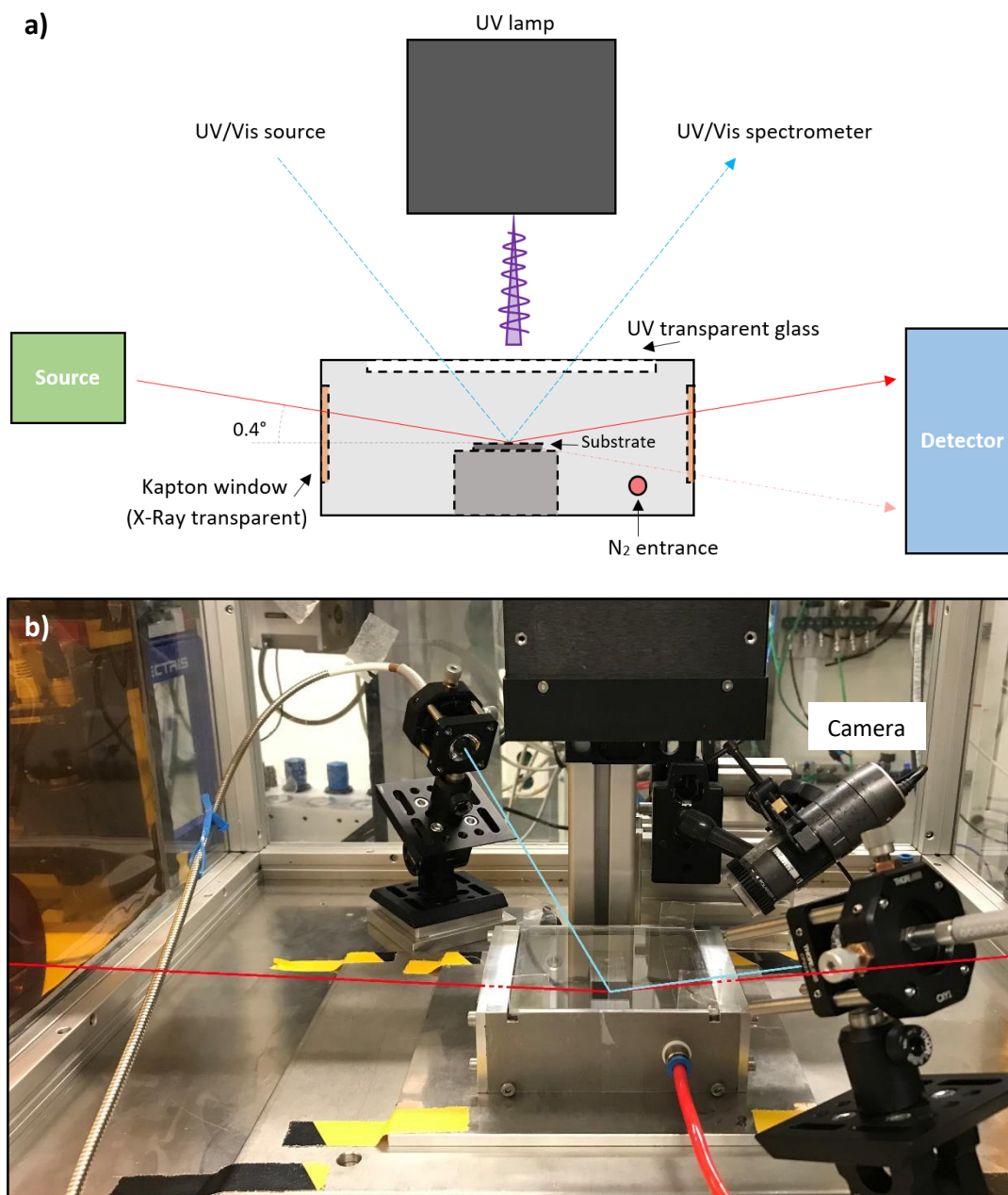


Figure 30. Setup used for GISAXS/XRR measurements: (a) scheme and (b) real image of the various components.

SAXS/GISAXS/XRR measurements have been performed at *P03 Beamline Petra III* at DESY (*Deutsches Elektronen-Synchrotron*) in Hamburg.

The data have been analysed with the software package *DPDAK* (vs. 1.3). The beam calibration has been performed by using collagen and silver behenate; the sample-to-detector distance was 3403 ± 1 mm; the energy of the beam was about 13KeV.

4. RESULTS

4.1. Preliminary analysis

In order to perform an in-depth characterization of the two analysed polymeric systems it is essential to carry out some preliminary analysis, such as a stability test to verify that the monomers are stable and do not evaporate with time after the deposition and a thickness study to understand quantitatively the effect of solvent addition or of rotation speed for the spin coating deposition.

4.1.1. Resins stability

The resins stability has been verified for both the monomers by dropping 100 mg over a glass substrate and by following the changes in weight with time (Tab. 4). The used balance is *Mettler Toledo* (AB54-S).

Resin composition	Loss percentage in 1h (%)
LT + 651 (1%)	0.9 ± 0.1
HT + 651 (1%)	0.5 ± 0.1

Table 4. Loss percentage after 1h from the deposition of the resin.

4.1.2. Thickness analysis

Each of the characterization techniques which has been performed and reported in the present work is characterized by a different required film thickness, which is ideal for the obtainment of reliable results. As a matter of fact, even if only thin films have been analysed, the quantitative definition of “thin” is strictly dependent on the specific application.

For instance, to perform DMA measurements, a thickness of tens of μm is essential to obtain a stable output signal from the material, especially when high temperatures are considered. GISAXS and XRR are also strongly influenced by the thickness and homogeneity of the obtained film, but, in this occasion, thinner coatings are always

preferred to thicker ones. Due to the high viscosity of the two monomeric mixtures, the obtainment of very low thicknesses requires the addition of a solvent (e.g. Butyl-acetate, BA), that evaporates rapidly during the first stages of the deposition process. The effect of solvent addition over thickness in the case of HT resin has been investigated and the results are reported in Table 5. The following analysis has been carried out only on HT because of its higher viscosity, which makes more complicated the obtainment of low thicknesses.

ID	Resin composition	Solvent amount (%)	Deposition		Curing		Thickness (μm)
			Ramp	Spinning	Time	Intensity	
HT_0%	HT + 651 (1%)	0	3 s, 2500 rpm	60 s, 8000 rpm	30 s	380 mW/cm ²	11 \pm 1
HT_23%		23					7 \pm 1
HT_43%		43					4 \pm 1
HT_50%		50					3 \pm 2
HT_83%		83					n.a.
HT_90%		90					n.a.

Table 5. Effect of the solvent addition on the thickness of the obtained film. N.a. indicates measurements which were below the limit of resolution of the instrument used.

According to the values of the obtained thickness and by using Eq. 2, it is possible to calculate the corresponding viscosities (Fig. 31).

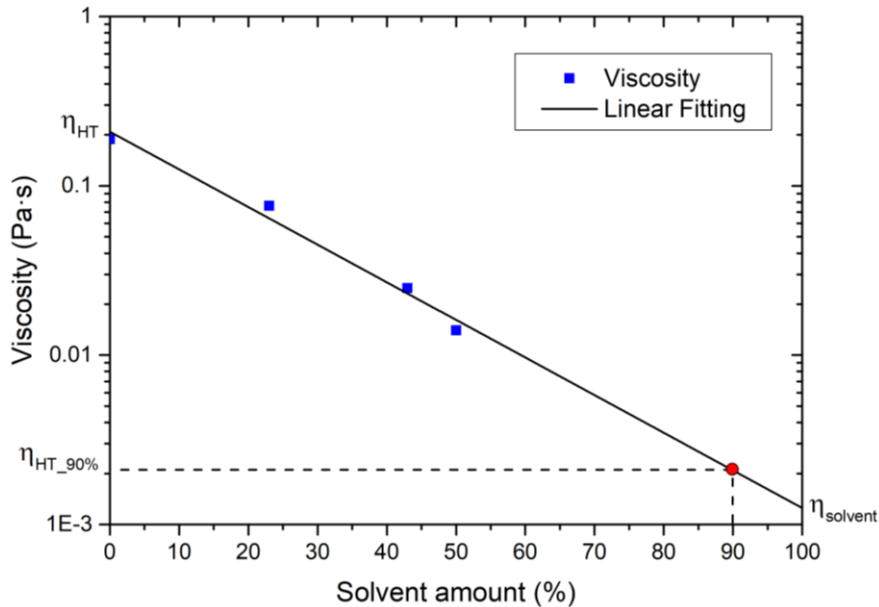


Figure 31. Plot showing the change in viscosity as a function of the solvent amount for the HT monomer mixture. The value of the viscosity of the solution with 90% of solvent is also indicated. The calculation required to fix an approximated density value $\rho = 1.1 \text{ g/cm}^3$.

From the obtained value of viscosity $\eta_{HT_90\%}$ and by using again Eq. 2, it is possible to determine the expected film thickness corresponding to this solvent amount and deposition parameters, which is in the range of 1 μm .

As a consequence, the analysis has proceeded by using this solvent amount to study the effect of the rotation velocity over the obtained thickness (Table 6). The ramp has been removed to have a further decrease in thickness.

For a first evaluation, the thickness has been assigned roughly by using the Michel-Lévy interference colour chart²⁵.

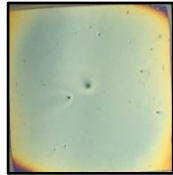
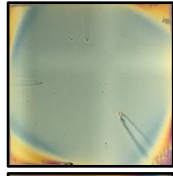
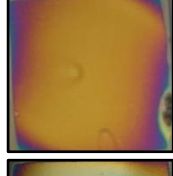
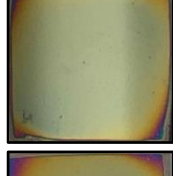
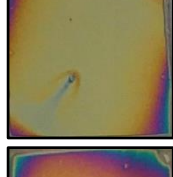
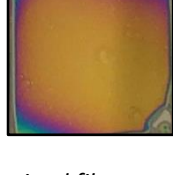
ID	Resin composition	Deposition			Curing		Thickness (μm)	
		Ramp	Spinning		Time	Intensity		
			Time	Speed				
LT_8000	LT + 651 (1%) + BA (90%)	-	60 s	8000 rpm	30 s	160 mW/cm ²	$\sim 0.25 \pm 0.05$	
LT_6000				6000 rpm			$\sim 0.30 \pm 0.05$	
LT_4000				4000 rpm			$\sim 0.45 \pm 0.05$	
HT_8000	HT + 651 (1%) + BA (90%)			8000 rpm			$\sim 0.30 \pm 0.05$	
HT_6000				6000 rpm			$\sim 0.40 \pm 0.05$	
HT_4000				4000 rpm			$\sim 0.55 \pm 0.05$	

Table 6. Effect of the spin coating rotation velocity on the thickness of the obtained film.

By applying again Eq. 2 to both the systems and considering average values of the two viscosities, it is possible to plot the thickness dependence on the rotation speed of the spin coater during the deposition (Fig. 32).

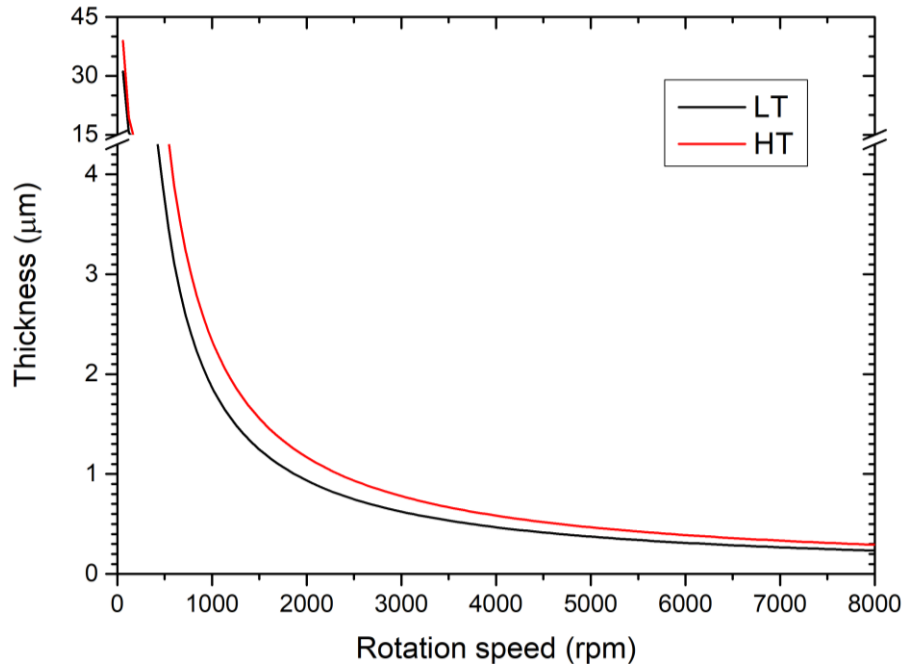


Figure 32. Plot showing the dependence of the obtained thickness on the rotation speed selected for the deposition in case of both LT (black) and HT (red) resin mixture. The calculation was possible by exploiting Eq. 2. The values for the viscosity have been determined by considering the thicknesses assigned by using the Michel-Levy interference colour chart; the density has been kept ideally fixed for both resins and approximated to a value $\rho = 1.1 \text{ g/cm}^3$.

4.2. Kinetic analysis

In order to study the photo-polymerization kinetics of the two polymeric systems, a FT-IR analysis has been performed: the varying parameters have been the curing time and the light intensity. Moreover, the spectra have been studied in order to assign the most important peaks to the corresponding functional group.

As a confirmation of the obtained results, Real-Time Infrared Spectroscopy (RT-IR) has been performed.

4.2.1. IR spectra investigation

As a first comparison, the spectra of the cured and uncured polymers are presented in Fig. 33a,b.

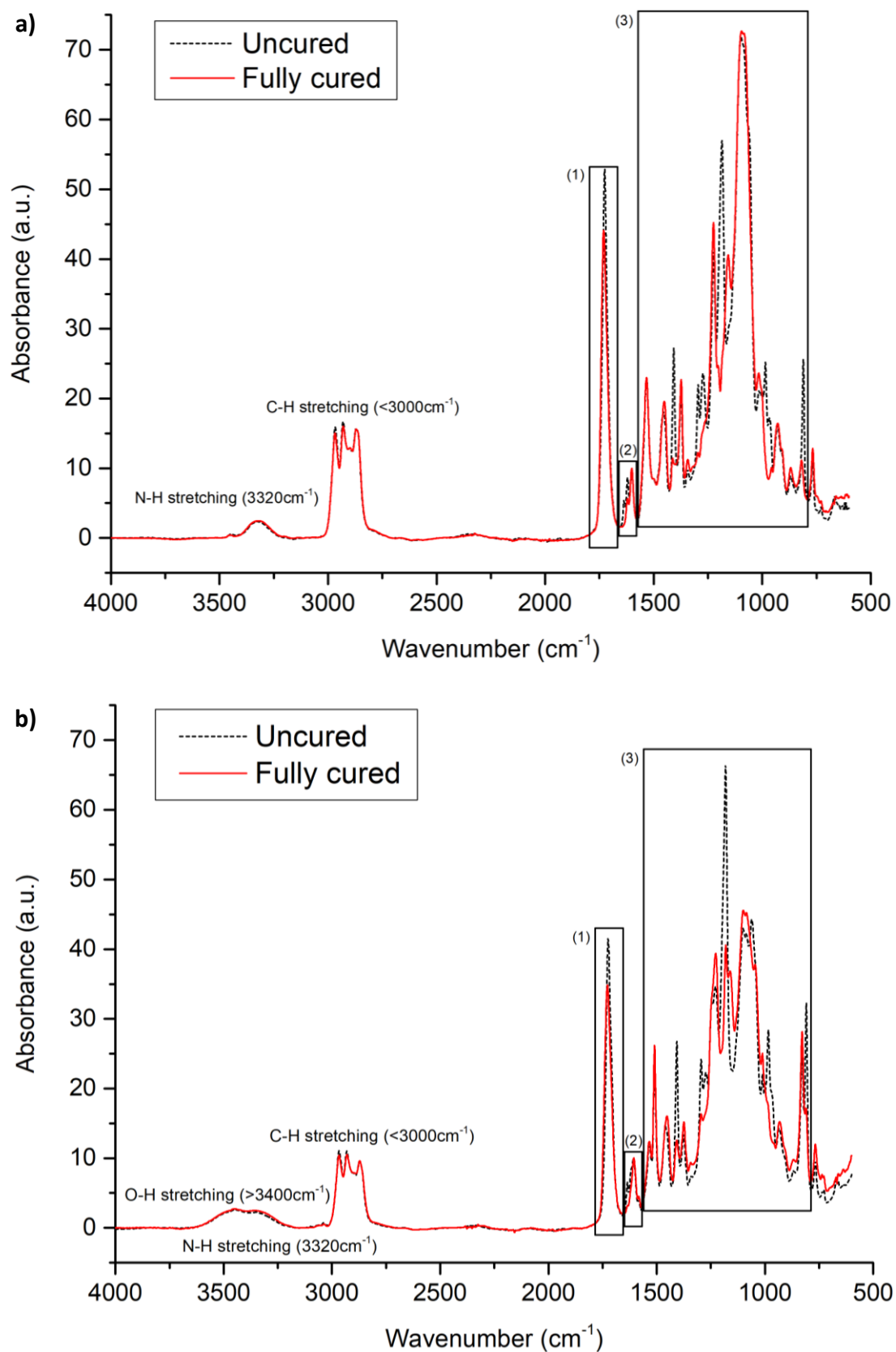


Figure 33. FT-IR spectra for the uncured and fully cured LT (a) and HT (b) monomer mixture.

The spectra have been divided into three regions to perform a deeper analysis: for both polymer the IR spectra are reported for different conversion time at the same light intensity (9 mW/cm^2).

Zone 1 (Fig. 34a,b) shows the decrease, shift and following increase in the peak associated to the C=O stretching. Zone 2 (Fig. 34c,d) shows the progressive decrease in the quantity of double bonds with conversion, indicated by the absorption peak located at 1636 cm^{-1} . The peaks at 1620 cm^{-1} (for LT) and at 1618 cm^{-1} (for HT) have not been assigned clearly: since they decrease with conversion, they should be related to a structural change which occurs during the polymerization; however, since they do not disappear completely, the possible presence of an underlying peak which is not changing with conversion has to be considered. Nevertheless, the kinetic analysis that is currently carried out does not require a complete understanding of the nature of such peak. Finally, zone 3 (Fig. 35a,b) has been reported for completeness: the full peak assignment in this region is much more complex and also not interesting for the present purpose.

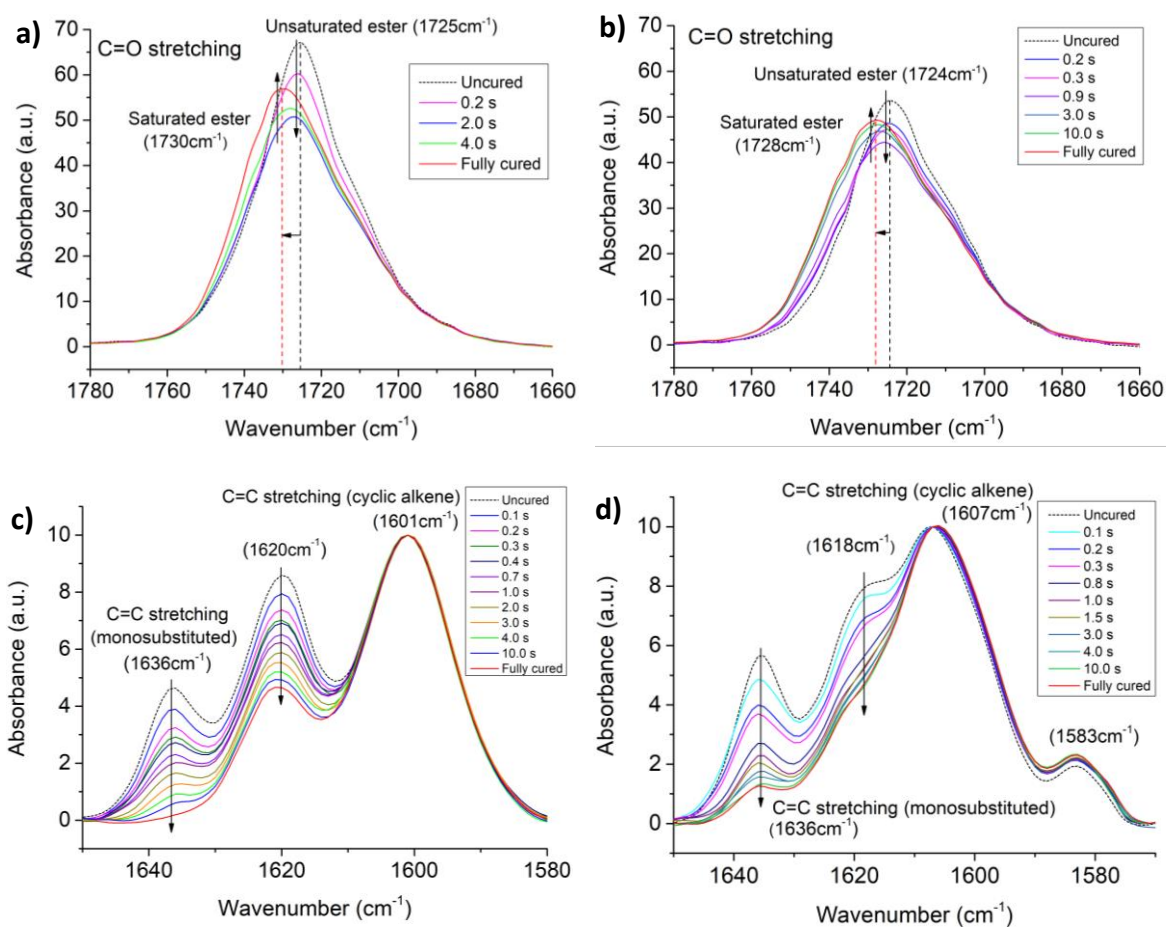


Figure 34. FT-IR spectra at different conversion time and for the same light intensity (9 mW/cm^2): (a) zone 1 in LT, (b) zone 1 in HT, (c) zone 2 in LT, (d) zone 2 in HT.

Results

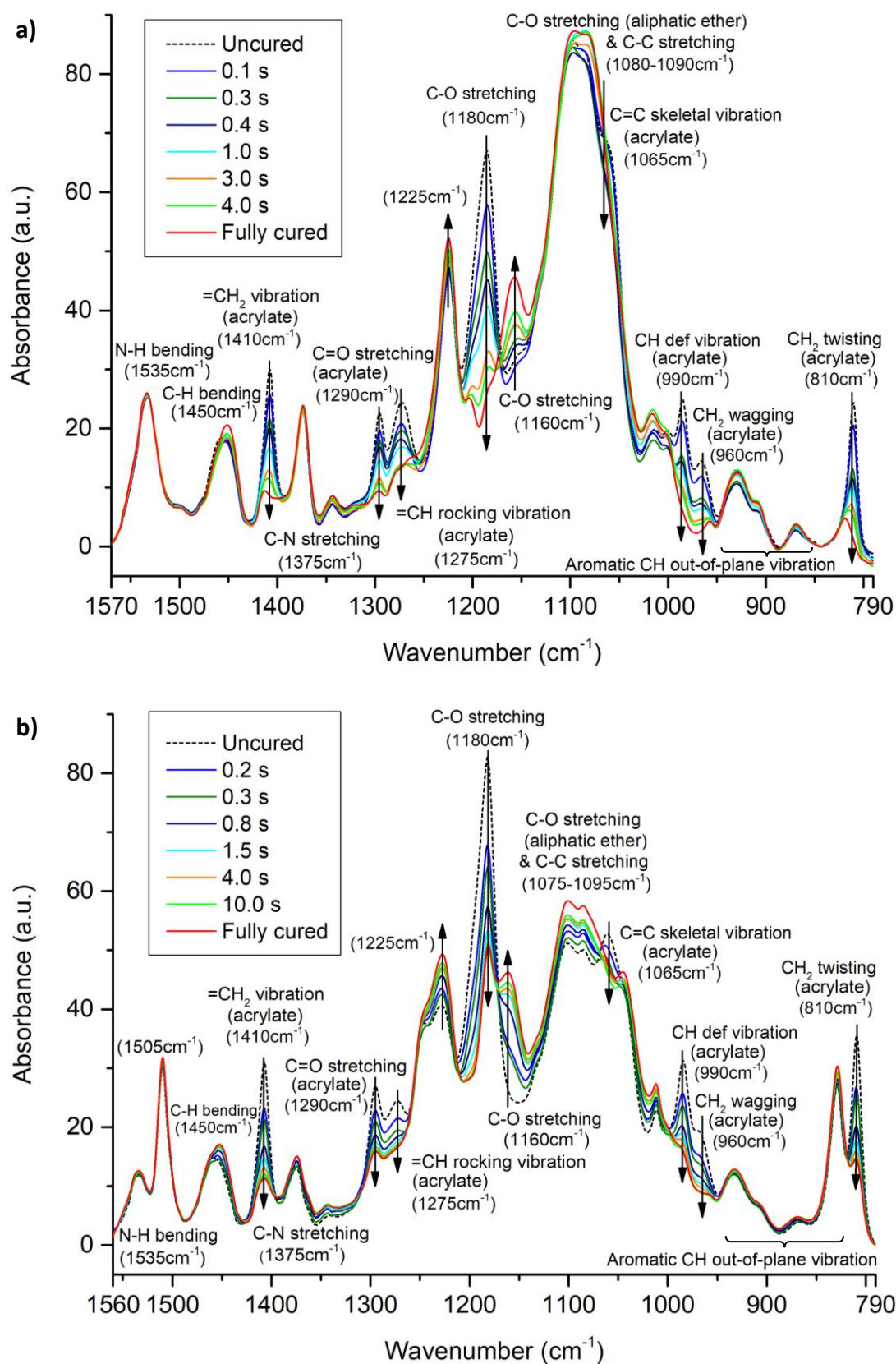


Figure 35. FT-IR spectra at different conversion time and for the same light intensity (9 mW/cm²): (a) zone 3 in LT and (b) zone 3 in HT. The peak assignment has been possible by using the text "Infrared and Raman Characteristic Group Frequencies" by George Socrates²⁶.

4.2.2. Conversion evaluation

The evaluation of conversion is possible by firstly performing a peak deconvolution in zone 2, so that a clear evaluation of the height of the peak of interest can be done. The peaks position have been initially denoted visually and, thanks to the multiple peak fitting performed with *Origin 8*, it has been possible to refine the deconvolution: a series of Gaussian functions have been chosen to reproduce the shape of the peaks.

As an example, the results of the deconvolution and fitting are reported for one of the analysed times (Fig. 36a,b).

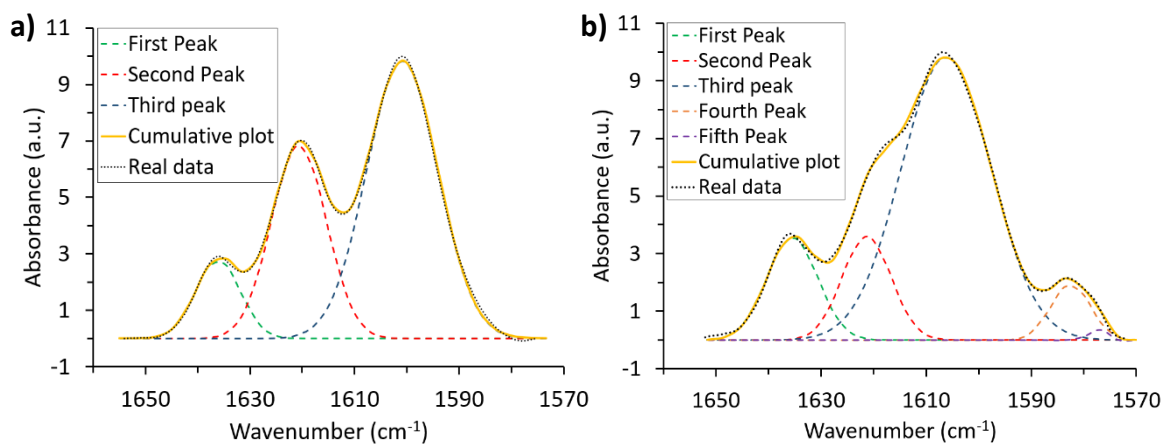


Figure 36. Results of the peak deconvolution and fitting performed for both polymers: (a) LT after 0.3ms of irradiation at 9 mW/cm², (b) HT after 0.3ms of irradiation at 9 mW/cm².

The degree of conversion has been calculated as the ratio between the absorption at 1636 cm⁻¹ of the cured resin over the uncured one. The results have been plotted as a function of time and then a data fitting have been performed (Fig. 37a,b).

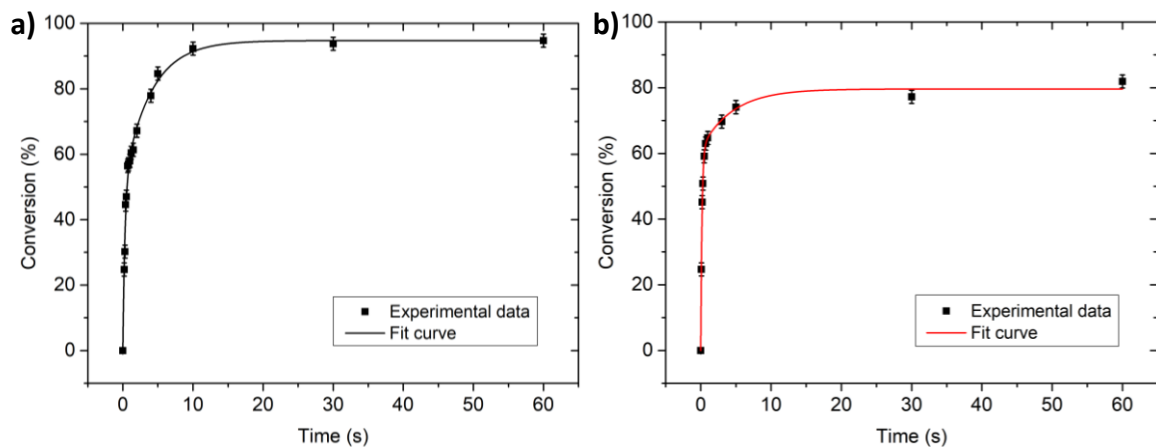


Figure 37. Percentage of conversion as a function of time for the same light intensity (11.4 mW/cm²) in case of (a) LT and (b) HT.

The fitting has been performed according to the equation and parameter which are reported in Table 7.

	Fitting Equation							
	$y = A_1 \exp\left(\frac{x}{t_1}\right) + A_2 \exp\left(\frac{x}{t_2}\right) + A_3 \exp\left(\frac{x}{t_3}\right) + y_0$							
Resin	A ₁	A ₂	A ₃	t ₁	t ₂	t ₃	y ₀	Adj. R-Square
LT	-26.3	-24.2	-44.3	-0.3	-0.3	-3.9	94.7	0.99811
HT	-30.6	-30.6	-18.3	-0.17	-0.17	-4.5	79.6	0.99842

Table 7. Equation and parameters used for the fitting of conversion data of the two polymers for the same light intensity (11.4 mW/cm²).

Finally, a comparison among the fitted curves of the two polymers at different light intensities is presented in Fig. 38.

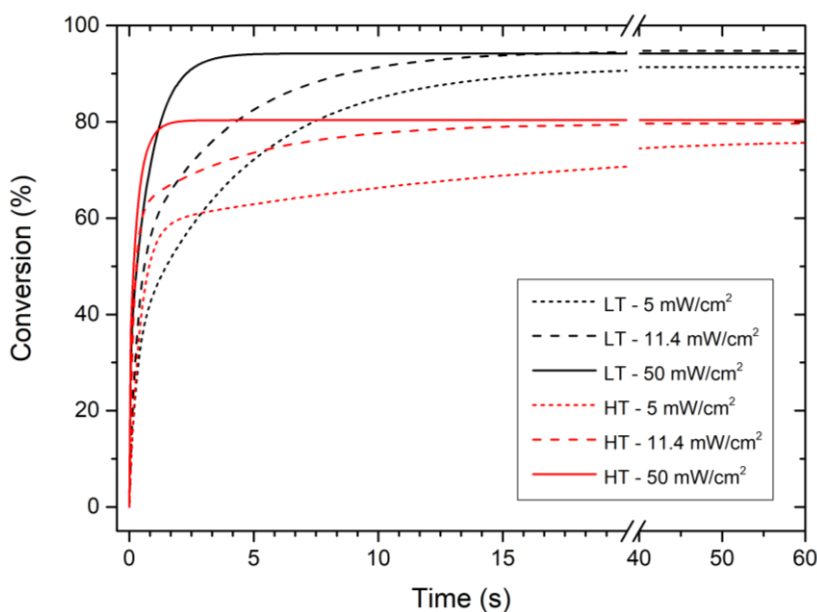


Figure 38. Graph reporting the fitted curves for the 2 monomer mixtures at different light intensities.

As a confirmation of the obtained results, *in-situ* real-time IR experiments have also been performed for both polymers. They have given the possibility to confirm the previous analysis in term of spectrum evolution during time and also offer a simple and direct way to appreciate the molecular and chemical changes occurring during the photo-polymerization. Due to the time resolution of the used spectrometer (~ 5 s), a light intensity of 2 mW/cm² has been exploited in this occasion, so as to obtain observable changes in the spectra: the resulting time-scale to have full conversion of double bonds is demonstrated to be coherent with the results obtained *ex-situ* (~ 90 s) (Fig. 39a,b).

Nevertheless, the initiation of conversion appears to be retarded in time of around 30 s: this delay, which is shown by both materials, can be correlated with the different polymerization conditions which are adopted during the RT-IR tests (see 3.5.1).

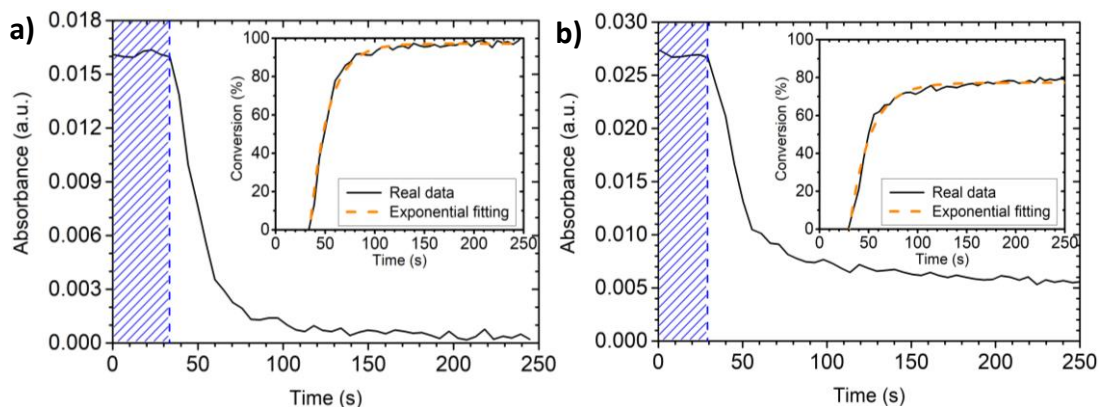


Figure 39. Graphs reporting the change in absorbance with time in correspondence of the C=C peak monitored by RTIR for (a) LT and (b) HT polymer. The insets show the conversion progression in time, together with an exponential fitting of the real data.

4.2.3. Rate of polymerization

The obtained data for the conversion of the two polymers at different lamp intensity can also be represented as a function of the polymerization rate (R_p), calculated by using the expression derived by Iedema *et al.*⁸, where χ_c indicates the conversion degree obtained from FT-IR:

$$R_p = \frac{1}{1-\chi_c} \frac{d\chi_c}{dt} \quad [11]$$

The modified rate of polymerization defined above is independent on the residual concentration of acrylic groups. The results obtained are reported in Fig. 40.

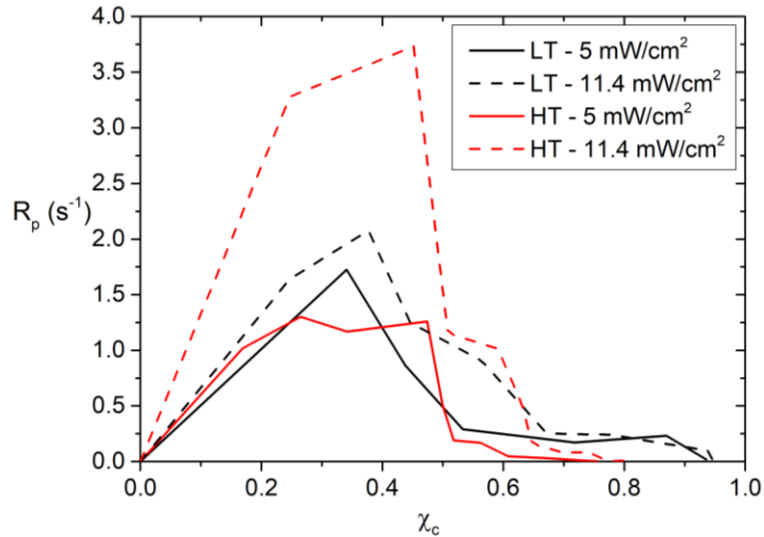


Figure 40. Graph showing the variation of the rate of polymerization as a function of the conversion degree for both LT (black) and HT (red) at different light intensity: 5 mW/cm² (solid line) and 11.4 mW/cm² (dashed line).

The plot shows that the rate of polymerization grows by increasing the light intensity, but the maximum rate is always achieved in correspondence of the same degree of conversion for each of the two materials. It is also possible to notice that the maximum rate of polymerization is shifted towards higher conversion level in case of HT.

By considering the values for the rates of polymerization of the two polymers in the first stages of the process, which means before the gelation, it is also possible to verify that $R_p \propto \sqrt{I_0}$ (Fig. 41).

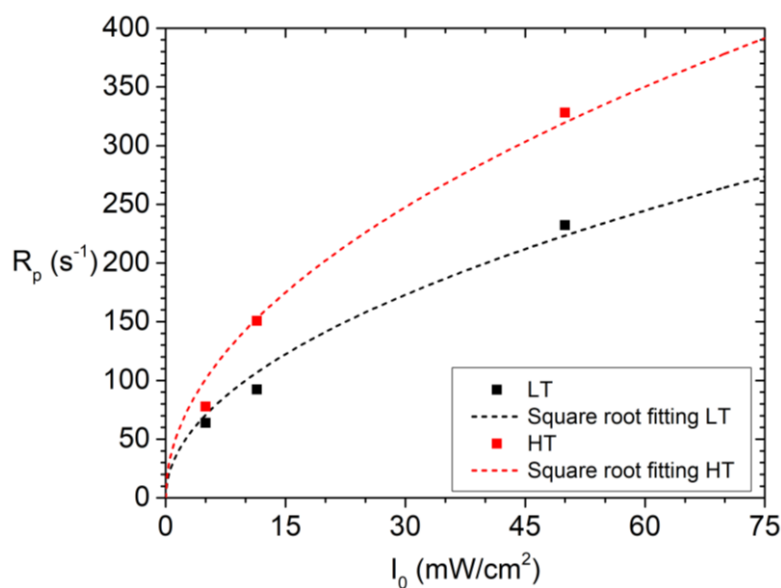


Figure 41. Graph showing the relation among the rates of polymerization and the corresponding lamp intensities together with a square root fitting for both the polymers.

4.3. Morphology

The surface morphology of a coating is a property of vital importance for any practical application, since it may determine a change in wettability, optical properties, friction behaviour or resistance to abrasion. Moreover, the possibility to perform some advanced characterization techniques, such as GISAXS, requires the verification of the average surface roughness and a rough estimation of the thickness of the analysed film. The obtainment of these information is made possible by the use of AFM.

4.3.1. AFM measurements

A preliminary measurement of the roughness of the two polymeric systems deposited and cured with the same parameters has been carried out; also coatings with different thicknesses have been analysed, but they don't show any significant difference. The parameters (Tab. 8) and the obtained images (Fig. 42a,b; Fig. 43a,b) are reported.

ID	Resin composition	Deposition		Curing		Roughness (RMS) (nm)
		Ramp	Spinning	Time	Intensity	
si_ref						0.22 ± 0.10
LT_thick	LT + 651 (1%)	-	60 s, 3000 rpm	50 s	380 mW/cm ²	0.27 ± 0.10
LT_thin			60 s, 4500 rpm			0.28 ± 0.10
HT_thick	HT + 651 (1%)		60 s, 3000 rpm			0.35 ± 0.10

Table 8. Parameters used and resulting roughness values for a pure silicon substrate and for the coatings obtained with the two polymers.

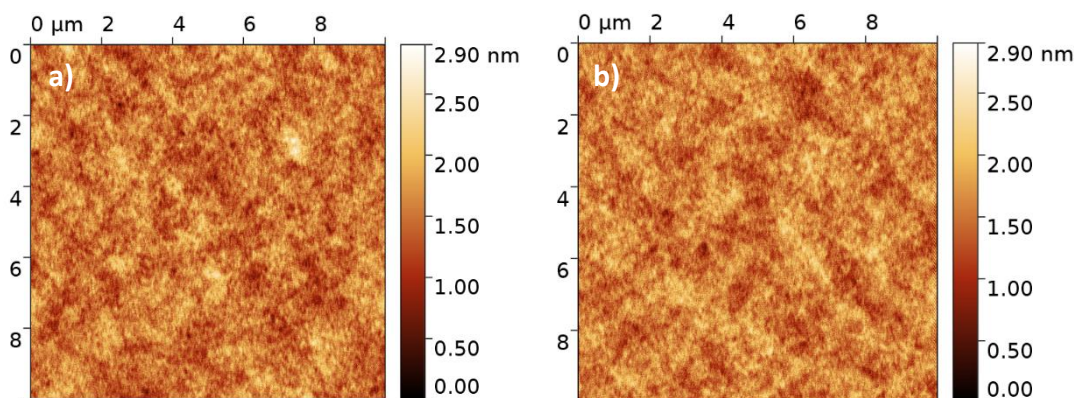


Figure 42. AFM images (10x10 μ m) obtained for (a) LT_thin and (b) LT_thick.

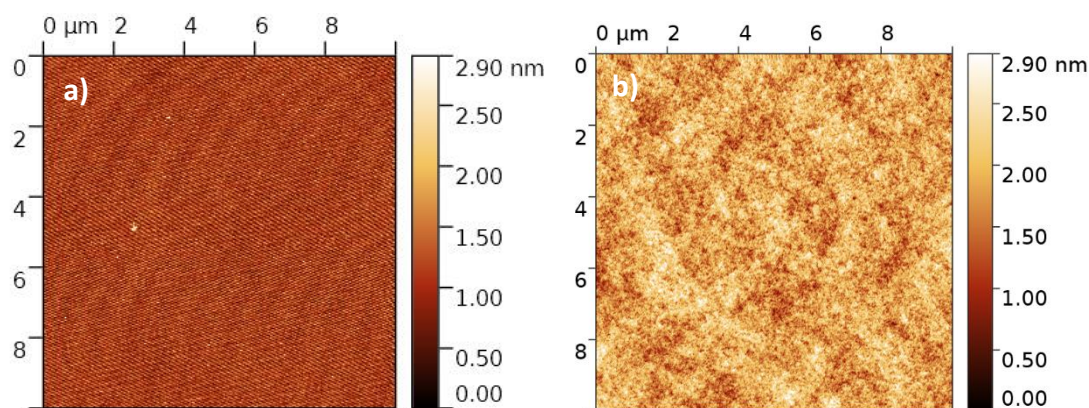


Figure 43. AFM images ($10 \times 10 \mu\text{m}$) obtained for (a) cleaned silicon substrate and (b) HT_thick.

The resulting roughness values appear to be in the correct range to perform GISAXS/XRR, but the thickness (in the range of tens of μm) is too high: for this reason, a solvent (Butyl Acetate, BA) is added according to the results obtained in paragraph 4.1.2.

After the addition of BA, AFM was used to determine the values for the thickness and roughness at different stage of conversion (Tab. 9): the varying parameter has been the curing time, while the intensity has been kept fixed. All the samples have been obtained with the same procedure, which is by rotating the substrate at 6000 rpm for 60 s with no ramp.

ID	Resin composition	Curing		Roughness (RMS) (nm)	Thickness (nm)
		Time	Intensity		
si_ref				0.25 ± 0.05	
LT_6000_0	LT + 651 (0.25%) + BA (90%)	0 s	11.4 mW/cm ²	0.59 ± 0.01	291 ± 20
LT_6000_0.1		0.1 s		1.49 ± 0.06	n.m.
LT_6000_0.3		0.3 s		1.17 ± 0.09	135 ± 20
LT_6000_0.6		0.6 s		0.92 ± 0.01	146 ± 20
LT_6000_1		1 s		0.49 ± 0.02	112 ± 20
LT_6000_6		6 s		0.55 ± 0.01	139 ± 20
LT_6000_28		28 s		0.71 ± 0.02	123 ± 20
HT_6000_0		HT + 651 (0.25%) + BA (90%)		0 s	0.47 ± 0.01
HT_6000_0.1	0.1 s			0.47 ± 0.02	214 ± 20
HT_6000_0.2	0.2 s			0.80 ± 0.05	n.m.
HT_6000_0.5	0.5 s			1.06 ± 0.05	177 ± 20
HT_6000_1	1 s			1.35 ± 0.07	134 ± 20
HT_6000_6	6 s			0.59 ± 0.03	160 ± 20
HT_6000_28	28 s			0.56 ± 0.02	152 ± 20

Table 9. Values obtained for roughness (RMS) and thickness of the two polymeric coatings measured by AFM at different curing time. [n.m. indicates the impossibility to perform the measurements due to practical reasons]

The roughness and thickness variations are also plotted versus time, with the aim to determine interesting trends for the two polymers (Fig. 44a-d).

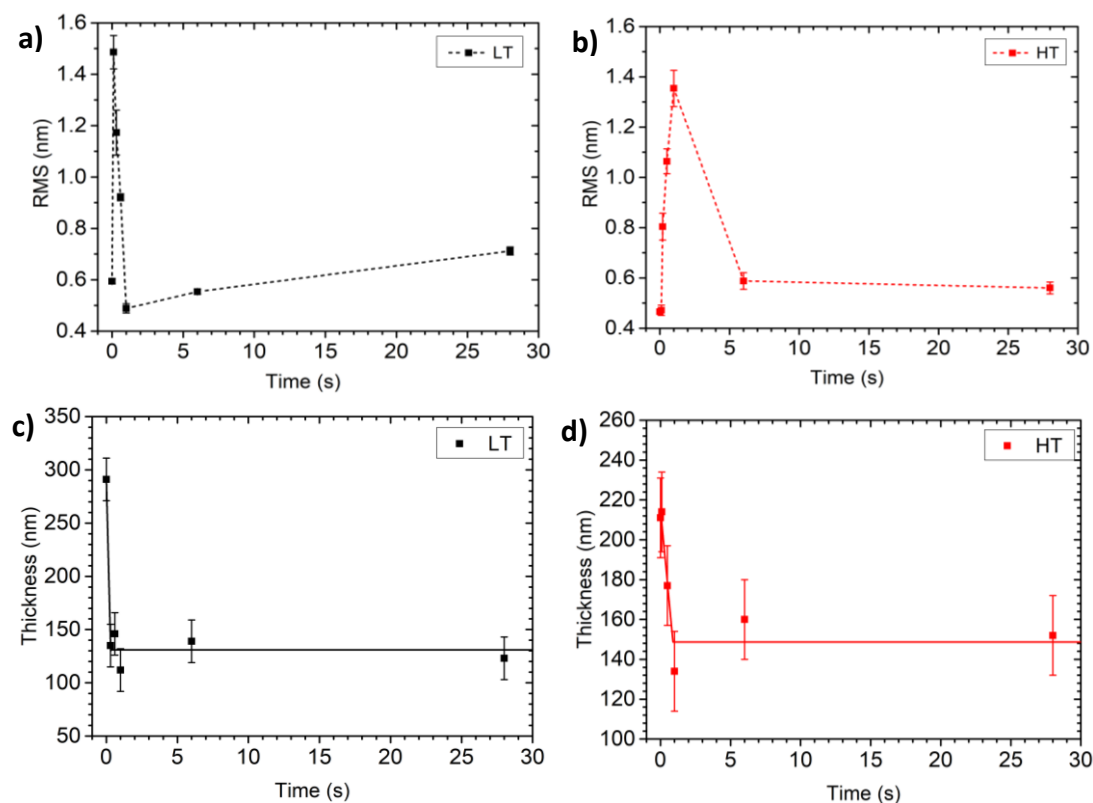


Figure 44. Thickness variation as a function of time for (a) LT (black) and (b) HT (red).

Both the roughness plots show a sharp increase in roughness in the early stages of conversion, followed by a reduction to a value comparable to the initial one.

It should be noticed that the initial values of roughness are based on wet non-crosslinked films and thus they could be easily influenced by instrumental errors. The same consideration is applicable to the thickness measurements, that are performed with a method that strongly relies on the ability of the operator: for this reason, an instrumental error of 20 nm has been considered. In both polymers, a strong reduction in thickness is detected, which reaches its minimum in correspondence of the maximum in the roughness profiles; after this point the thickness remains roughly constant.

The obtained results, in term of thickness, also allow to confirm the previous rough estimations that have been done on the base of the obtained colour by using the interference colour chart (Tab. 6): indeed, the constant thickness value for LT results to be lower than the one of HT.

Finally, it is also interesting to perform a visual comparison among the evolution in surface morphology of the two materials at different curing time (Fig. 45a-h; Fig. 46a-d).

Results

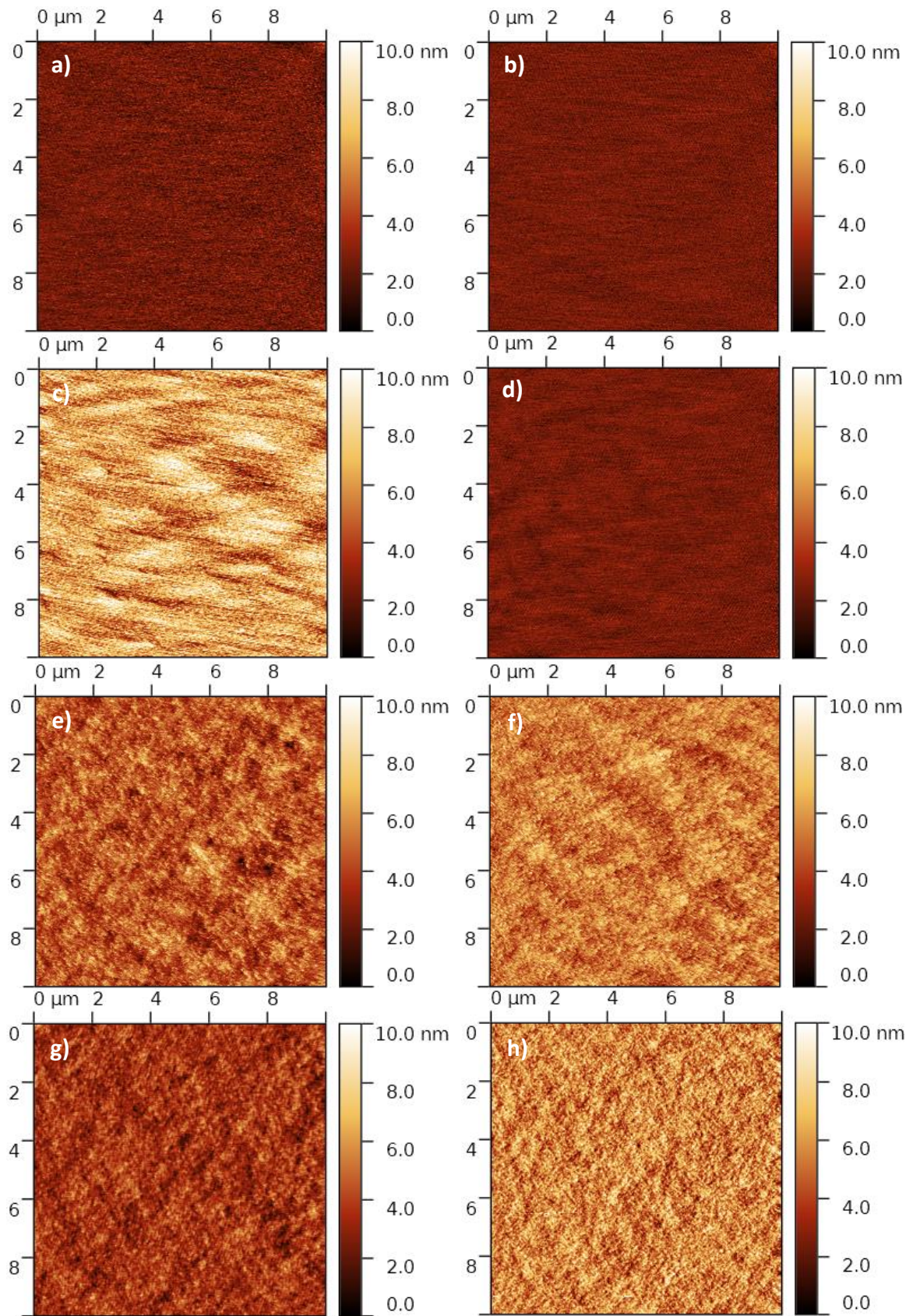


Figure 45. AFM images ($10 \times 10 \mu\text{m}$) which show the evolution in surface morphology with the curing time for the two materials: (a) LT_{6000_0} , (b) HT_{6000_0} , (c) $\text{LT}_{6000_{0.1}}$, (d) $\text{HT}_{6000_{0.1}}$, (e) $\text{LT}_{6000_{0.3}}$, (f) $\text{HT}_{6000_{0.5}}$, (g) $\text{LT}_{6000_{0.6}}$, (h) HT_{6000_1} .

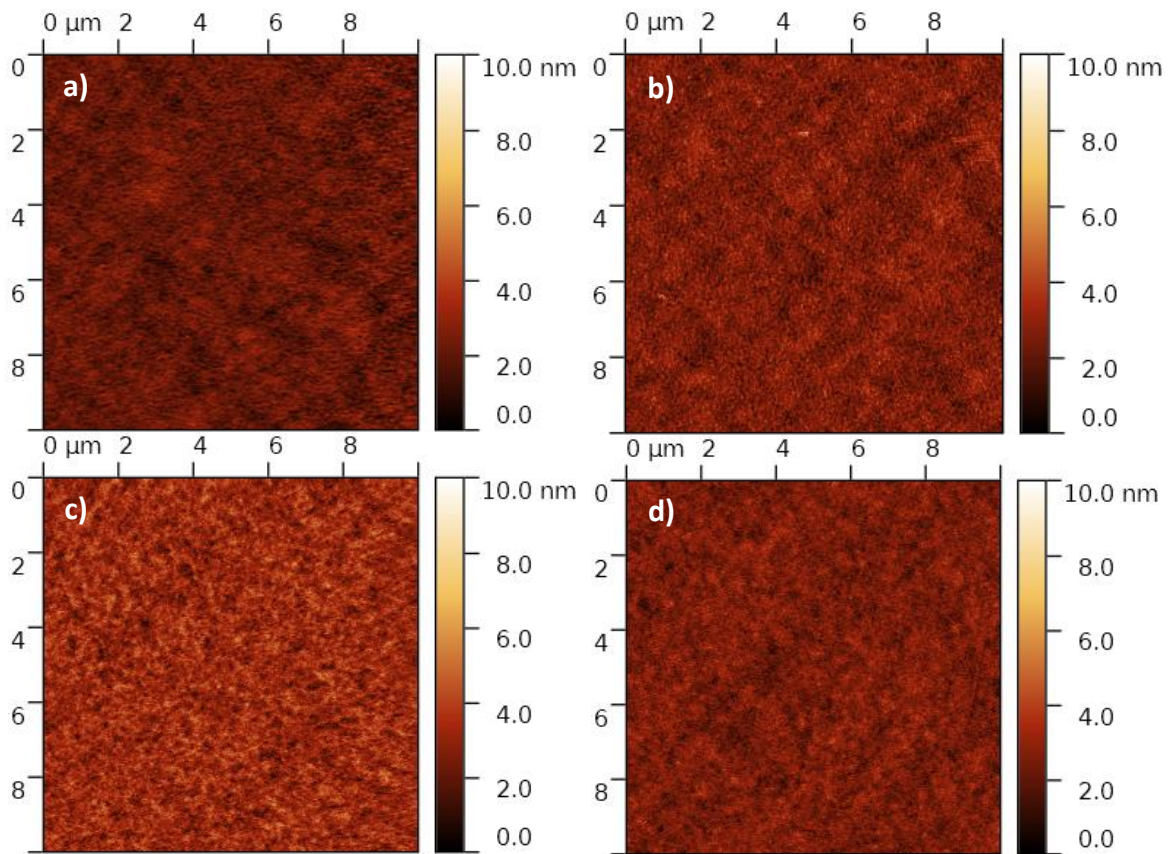


Figure 46. AFM images ($10 \times 10 \mu\text{m}$) which show the evolution in surface morphology with the curing time for the two materials: (a) LT_6000_1, (b) HT_6000_6, (c) LT_6000_28, (d) HT_6000_28.

4.4. Dynamic mechanical analysis

The mechanical properties of a photo-polymerized coating are strictly dependent on the parameters which are selected during the curing procedure, since they will define a change in the homogeneity and degree of crosslinking.

With the aim to understand better both the aspects, DMA tests have been performed. The study involves a first comparison among the mechanical properties of the two fully crosslinked polymers and a subsequent investigation and evaluation of the density of crosslinking.

4.4.1. General overview

From a general point of view, the mechanical properties of the two materials appear to be different because of their different composition. In order to offer a visual and direct comparison among them, the results obtained by DMA are firstly presented in Fig. 47a,b. The curing time and intensity have been selected to achieve the full crosslinking of the two polymers.

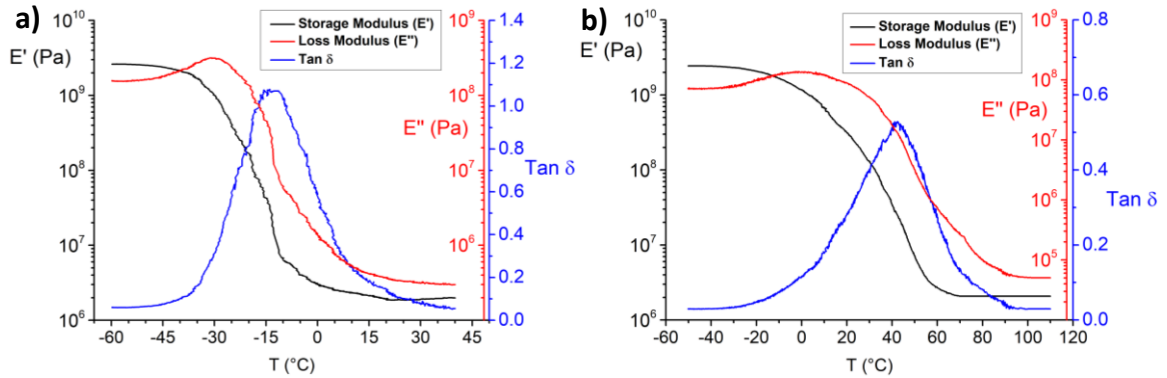


Figure 47. Comparison among the DMA results obtained after exposure to the same dose of radiation (300 mw/cm² for 90s) of (a) LT and (b) HT.

The used curing parameter are shown in Table 10, together with the values of the derived mechanical properties. An evaluation of the crosslinking density can be obtained by exploiting the expression derived by Sarkar *et al.*¹⁰:

$$\rho_c = \frac{E'_{rubbery}}{3k_B T} \quad [12]$$

ID	Resin composition	Curing		E' (MPa)		Tan δ height	Crosslink density (10 ²⁰ /cm ³)
		Time	Intensity	Elastic	Rubbery		
LTdma_90/300	LT + 651 (0.25%)	90 s	300 mW/cm ²	2610	1.98	1.07	1.63
HTdma_90/300	HT + 651 (0.25%)			2430	2.07	0.53	1.46

Table 10. Curing parameters and mechanical properties resulting from DMA analysis.

4.4.2. Density of crosslinking

An effective way to characterize the change in crosslink density inside a photopolymer consists on the analysis of the shape of the dissipation function tan δ (T). The curing intensity and time have been modified in order to understand how the density of crosslinking and its homogeneity are affected (Tab. 11; Fig. 48a-d).

ID	Resin composition	Curing	
		Time	Intensity
LTdma_90/5	LT + 651 (0.25%)	90 s	5 mW/cm ²
LTdma_90/10			10 mW/cm ²
LTdma_90/50			50 mW/cm ²
LTdma_90/300			300 mW/cm ²
HTdma_90/5	HT + 651 (0.25%)		5 mW/cm ²
HTdma_90/10			10 mW/cm ²
HTdma_90/50			50 mW/cm ²
HTdma_90/300			300 mW/cm ²
LTdma_20/10	LT + 651 (0.25%)	20 s	10 mW/cm ²
LTdma_90/10		90 s	
LTdma_180/10		180 s	
HTdma_20/10	HT + 651 (0.25%)	20 s	
HTdma_90/10		90 s	
HTdma_180/10		180 s	

Table 11. List of the analysed samples with the corresponding curing parameters.

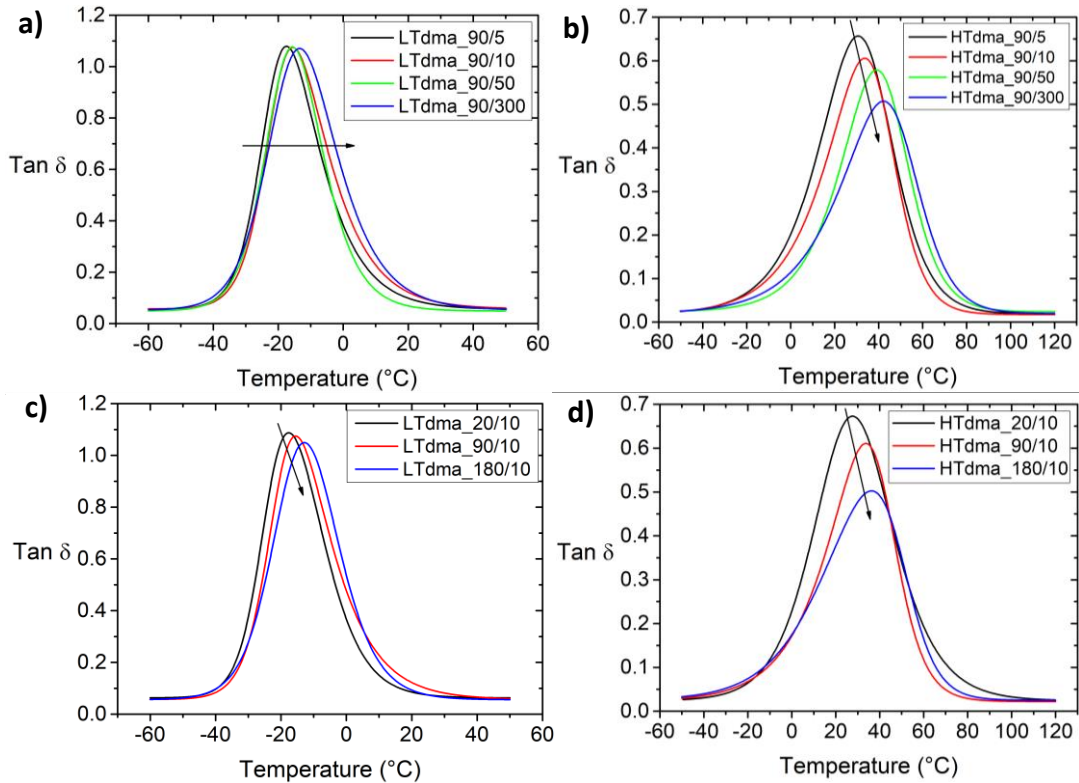


Figure 48. Changes in the $\tan \delta$ vs T plot in case of (a,b) variation in curing intensity and (c,d) variation in curing time; (a,c) refer to the LT monomer mixture, while (b,d) refer to HT.

The above graphs show that increasing times and intensities produce the progressive shift towards higher temperature of the $\tan \delta$ peak, which is accompanied in Fig. 48b-d by a clear decrease in the height of the peak. A non-monotonic change in the width of the peak can also be noticed.

Since it is possible to have an indication over the density of crosslinking by looking at the height of the peak and over the homogeneity of the network by considering its amplitude (Full-Width at Half-Height, FWHH), their values are explicitly reported in Table 12.

ID	Resin composition	Tan δ height	FWHH (°C)
LTdma_90/5	LT + 651 (0.25%)	1.08	22.68
LTdma_90/10		1.08	23.84
LTdma_90/50		1.08	23.15
LTdma_90/300		1.07	26.55
HTdma_90/5	HT + 651 (0.25%)	0.66	42.01
HTdma_90/10		0.61	38.77
HTdma_90/50		0.58	39.32
HTdma_90/300		0.51	44.98
LTdma_20/10	LT + 651 (0.25%)	1.09	24.33
LTdma_90/10		1.08	23.84
LTdma_180/10		1.05	25.99
HTdma_20/10	HT + 651 (0.25%)	0.67	45.46
HTdma_90/10		0.61	38.77
HTdma_180/10		0.50	48.74

Table 12. *Tan δ height and full-width at half-height (FWHH) values derived from DMA measurements.*

The crosslink density can also be evaluated by means of the storage modulus values in correspondence of the rubbery plateau and by using Eq. 12 (Fig. 49a-d; Tab. 13).

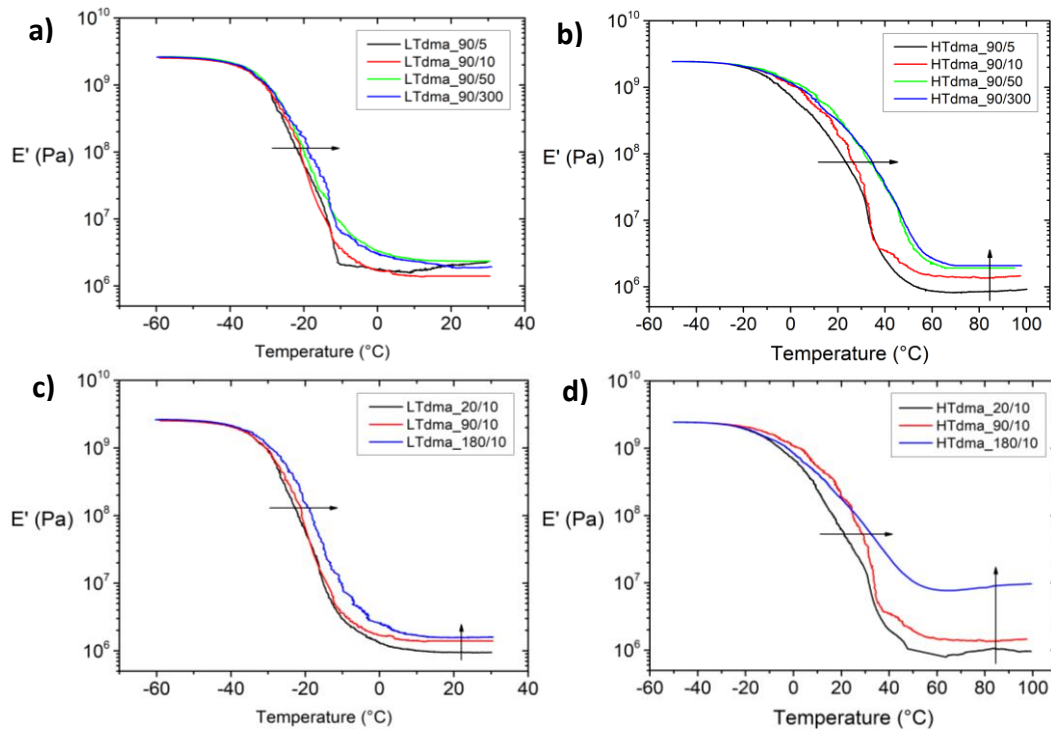


Figure 49. *Changes in the E' vs T plot in case of (a,b) variation in curing intensity and (c,d) variation in curing time; (a,c) refer to the LT monomer mixture, while (b,d) refer to HT.*

ID	Resin composition	Rubbery modulus (MPa)	Crosslink density ($10^{20}/\text{cm}^3$)
LTdma_90/5	LT + 651 (0.25%)	2.02	1.67
LTdma_90/10		1.40	1.19
LTdma_90/50		2.36	1.97
LTdma_90/300		2.06	1.70
HTdma_90/5	HT + 651 (0.25%)	0.88	0.64
HTdma_90/10		1.41	1.02
HTdma_90/50		1.91	1.36
HTdma_90/300		2.07	1.46
LTdma_20/10	LT + 651 (0.25%)	0.94	0.80
LTdma_90/10		1.40	1.19
LTdma_180/10		1.59	1.33
HTdma_20/10	HT + 651 (0.25%)	0.94	0.68
HTdma_90/10		1.41	1.02
HTdma_180/10		7.72	5.60

Table 13. Rubbery modulus and calculated crosslink density values derived from DMA measurements.

From the graphs it can be detected the progressive shift of the storage modulus curve towards higher temperatures when larger curing times or intensities are applied. Moreover, an increase in the value of the modulus in correspondence of the rubbery plateau is clearly visible in Fig. 49b-d.

4.5. Thermal analysis

The thermal analysis has the aim to detect the glass transition temperature of the two polymers or to highlight the existence of secondary transitions. Moreover, the T_g of a photo-polymer is strongly dependent on the selected curing parameters and on the degree of conversion.

Both DMA and DSC have been adopted to follow the changes in glass transition temperature as a function of the curing intensity and time.

4.5.1. Glass transition temperature

The T_g of a polymer can be derived from DMA data by referring to both the peak of $\tan \delta$ or to the peak of the loss modulus $E''(T)$: in the following, the first method will be selected to derive the glass transition temperature.

The values derived from the analysis are reported in Table 14 and presented graphically in Fig. 50a-d.

ID	Resin composition	Glass transition temperature (°C)
LTdma_90/5	LT + 651 (0.25%)	-17.5 ± 1.0
LTdma_90/10		-15.5 ± 1.0
LTdma_90/50		-15.6 ± 1.0
LTdma_90/300		-13.4 ± 1.0
HTdma_90/5	HT + 651 (0.25%)	30.7 ± 2.0
HTdma_90/10		33.9 ± 2.0
HTdma_90/50		39.1 ± 2.0
HTdma_90/300		42.3 ± 2.0
LTdma_20/10	LT + 651 (0.25%)	-17.6 ± 1.0
LTdma_90/10		-15.5 ± 1.0
LTdma_180/10		-12.9 ± 1.0
HTdma_20/10	HT + 651 (0.25%)	27.7 ± 2.0
HTdma_90/10		33.9 ± 2.0
HTdma_180/10		36.3 ± 2.0

Table 14. Glass transition temperature values derived from DMA measurements.

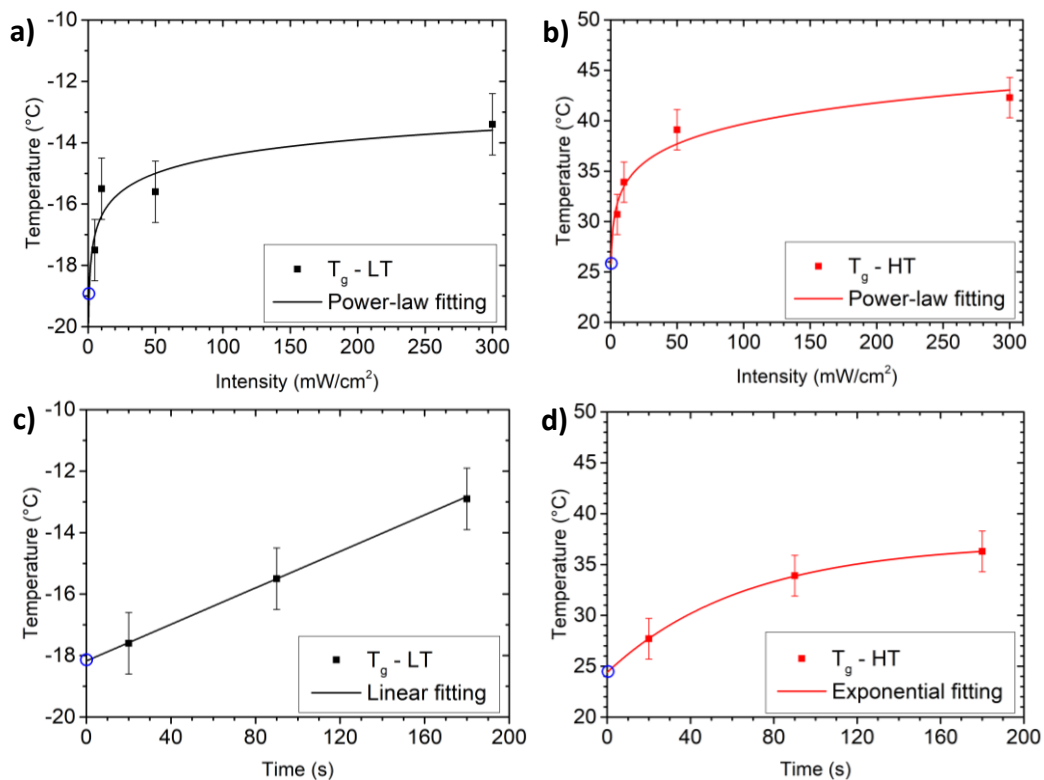


Figure 50. Graphical representation of the change in glass transition temperature as a function of (a,b) curing intensity and (c,d) curing time for both LT (black) and HT (red) polymer. In the graphs, the most proper fitting model is also presented, together with the extrapolated value of T_g at the pristine state.

The graphs show that an increase in the curing intensity produces an increase in the T_g of both the polymers that can be described with a power law fitting. An increase in the curing time also causes the growth of the glass transition temperatures, but the best fitting for the data appears to be different for the two resins: a linear fit suits better LT, while an exponential fit is more adequate for HT.

It can also be noticed for both materials that the extrapolated values for the T_g at the pristine state (curing time and intensity equal to 0) is comparable; furthermore, the glass transition temperature of HT is shown to be greater than the one of LT.

The conclusions derived from DMA can be confirmed by performing DSC tests (Fig. 51a-d).

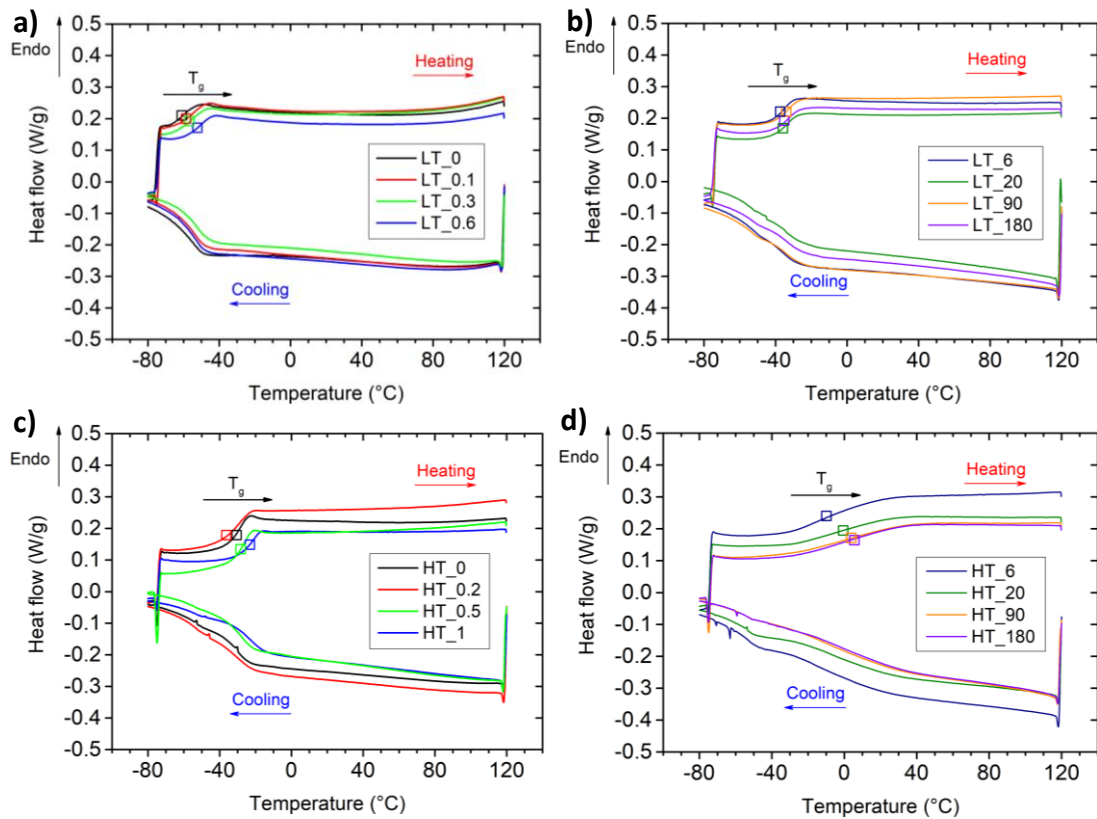


Figure 51. DSC graphs which show the increase in glass transition temperature by increasing the curing time for (a,b) LT and (c,d) HT; (a,c) refer to lower curing time, which are characterized by a localised transition, while (b,d) refer to higher curing time, which have a broader transition. Both the heating (upper curves) and cooling (lower curves) cycles are reported.

Even if the determination of the absolute value of the glass transition temperature is made uncertain by the presence of a wide transition, especially when longer curing times are involved, the T_g values, derived from the analysis of the heating cycle, have been reported in Table 15.

ID	Curing		T_g (°C)	ID	Curing		T_g (°C)
	Time	Intensity			Time	Intensity	
LT_0	0 s	11.4 mW/cm ²	-60.3	HT_0	0 s	11.4 mW/cm ²	-31.0
LT_0.1	0.1 s		-55.8	HT_0.1	0.1 s		-29.1
LT_0.3	0.3 s		-54.8	HT_0.2	0.2 s		-30.8
LT_0.6	0.6 s		-51.3	HT_0.5	0.5 s		-27.9
LT_1	1 s		-46.9	HT_1	1 s		-23.7
LT_6	6 s		-35.7	HT_6	6 s		-7.92
LT_20	20 s		-34.1	HT_20	20 s		-0.89
LT_28	28 s		-33.9	HT_28	28 s		3.09
LT_90	90 s		-33.5	HT_90	90 s		6.60
LT_180	180 s		-33.4	HT_180	180 s		8.93

Table 15. Values for the glass transition temperature (T_g) of the two polymers at different curing time and same light intensity (11.4 mW/cm²).

The trend observed with DMA (Fig. 50c,d) can thus be confirmed by the DSC data, since an exponential increase in T_g is detected when higher curing times are applied (Fig. 52a,b). Particularly interesting is also the correlation between the glass transition temperature and the degree of conversion obtained in correspondence of a certain curing time and intensity: this connection is made possible by the combination of FTIR and DSC data (Fig. 52c,d).

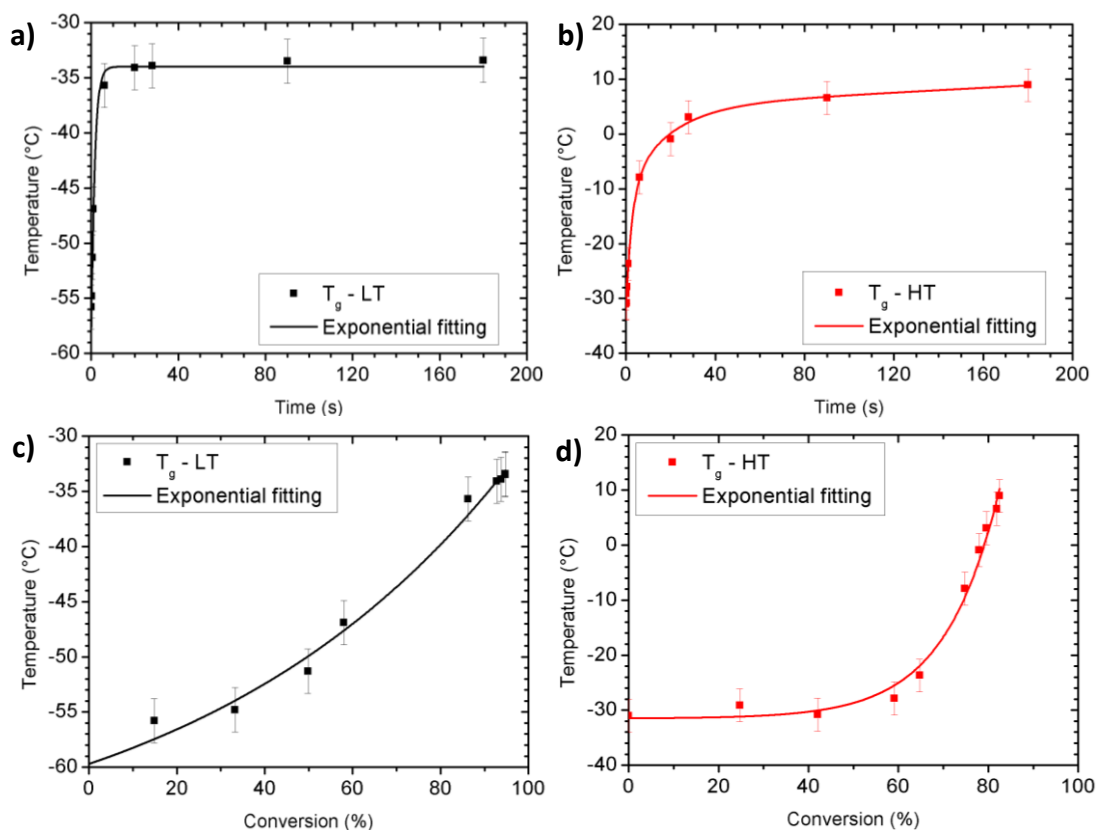


Figure 52. Graphical representation of the change in glass transition temperature as a function of (a,b) curing time and (c,d) percentage of conversion for both LT (black) and HT (red) polymer.

4.6. Scattering experiments

The obtainment of information over the internal structure of the two studied materials becomes possible by using X-Rays to perform advanced scattering experiments.

The use of SAXS allowed to derive average values for the gyration radii of the macromolecules before the polymerization.

In-situ XRR allowed the investigation of the two monomeric mixtures at different instants of polymerization (“intermittent polymerization”): this supplied information about the modifications in roughness, thickness and density during the process, thus permitting to confirm some of the results previously achieved. The data collected have also the important advantage of carrying information about the whole height profile of the analysed coatings.

Finally, by performing *in-situ* GISAXS, it has been possible to follow all the transformations associated to the dimension of the scattering centres directly during the polymerization process.

The use of a UV-Spectrometer also gave confirmations about the attained results.

4.6.1. Radius of gyration

SAXS experiments have been carried out on both the uncured polymers with the aim of characterizing the dimensions of their associated random coils (Fig. 53a). The analysed monomeric mixtures contained no initiator, in order to reduce the probability of activating the polymerization process due to the action of powerful X-Rays. However, the breakage of some C=C double bonds present in the oligomers/monomers remains possible.

The images created on the detector by the scattering experiments (Fig. 53b,c) need to be post-processed to determine a value for the radius of gyration. Firstly, the images have been cut radially by starting from the position of the beamstop shadow, so that a decaying scattering intensity can be determined. Secondly, the data have been averaged over a circular area with the aim to obtain valuable statistics.

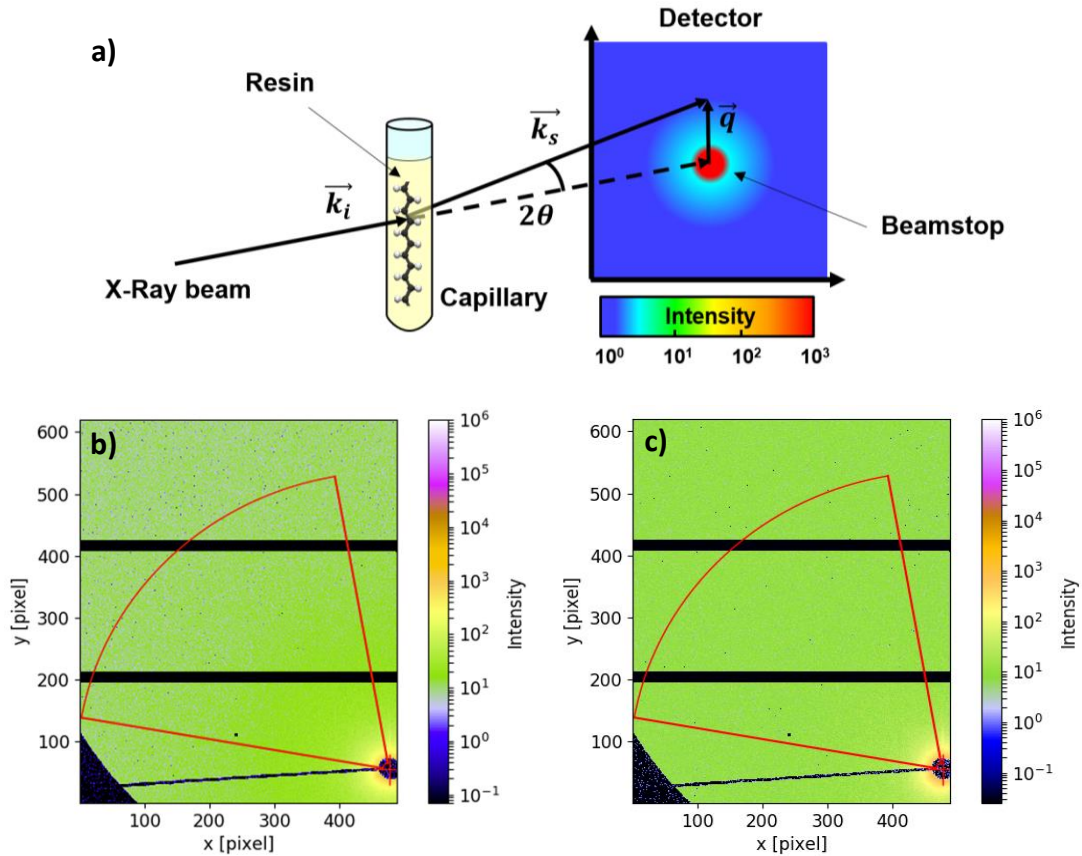


Figure 53. (a) Setup exploited to perform SAXS over the two liquid resins. (b,c) Scattering images obtained by SAXS and circular area considered for the data analysis in case of LT (left) and HT (right).

The derived intensity values can then be plotted as a function of the wavevector transfer q (Fig. 54).

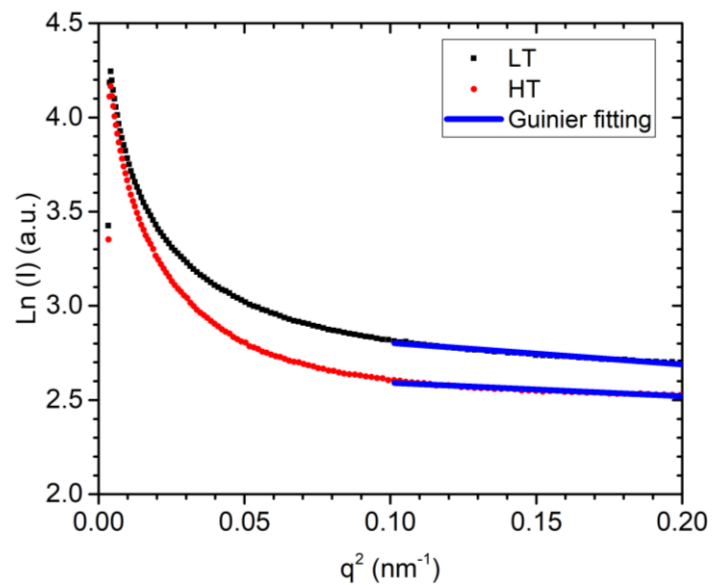


Figure 54. Graph showing the correspondence between the intensity of the scattered signal and the wavevector transfer for (black) LT and (red) HT. The straight lines associated to Guinier fitting are also indicated; the slope of such straight lines allows the calculation of the two gyration radii.

By considering the slope of the curves in the region where it assumes a constant value, it is possible to apply the Guinier analysis according to Eq. 6 and derive a value for the gyration radius associated to the two random coils:

$$Slope_{LT} = -\frac{R_{gLT}}{3} = -0.613 \text{ nm} \qquad Slope_{HT} = -\frac{R_{gHT}}{3} = -0.487 \text{ nm}$$

$$R_{gLT} = 1.84 \text{ nm}$$

$$R_{gHT} = 1.46 \text{ nm}$$

4.6.2. XRR images

The setup used to perform XRR measurements is the same used for *in-situ* GISAXS experiments (Fig. 25,30) with an incident angle α_i which is gradually modified from 0.085° to 1° with the aim to obtain information from different depths inside the material.

The main difference between them is constituted however by the use of a beam-stop in case of GISAXS, which allows to hide the specular beam and avoid signal saturation on the detector; in XRR, instead, such beam-stop is not exploited since the scattering intensity is lower. In fact, also the beam intensity used to perform XRR is much lower, if compared with GISAXS, and this permits the collection of a large number of data without damaging the material.

Due to the necessity to modify the incident angle during the measurement, the obtainment of XRR images during the photopolymerization process can be particularly difficult. For this reason, in the present work an “intermittent photopolymerization” is performed: this expression wants to indicate a photopolymerization process which is interrupted at different instants of conversion and then resumed after collecting the image (Fig. 55). This kind of test is not devoid of possible discrepancies with a real *in-situ* experiment, due to the possible dark polymerization that can occur after switching off the UV lamp; nonetheless, the lack of any external intervention or interaction with the samples makes it possible to derive information over the two materials that can be correlated to the results found with more accessible techniques.

The used lamp intensity to induce the curing is kept fixed to 11.4 mW/cm^2 .

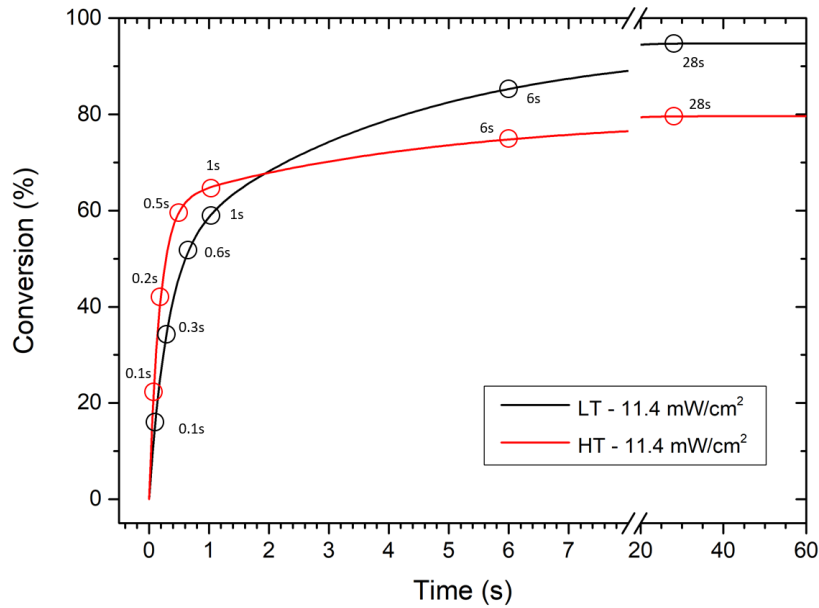


Figure 55. Conversion plot for both LT (black) and HT (red) with an indication of the points in which XRR images are collected.

Since the collection of a good XRR image usually requires the exposition of the material to the X-Ray beam for a long time (~ 40 s), a so-called damage-scan has been carried out: this consists on a control test that allows to estimate the exposure time needed to damage the material. The results obtained showed that both the polymers are not detectably damaged for a time of at least 50 s (Fig. 56a,b) and consequently the collection of XRR images will not be affected by the material deterioration due to X-Rays.

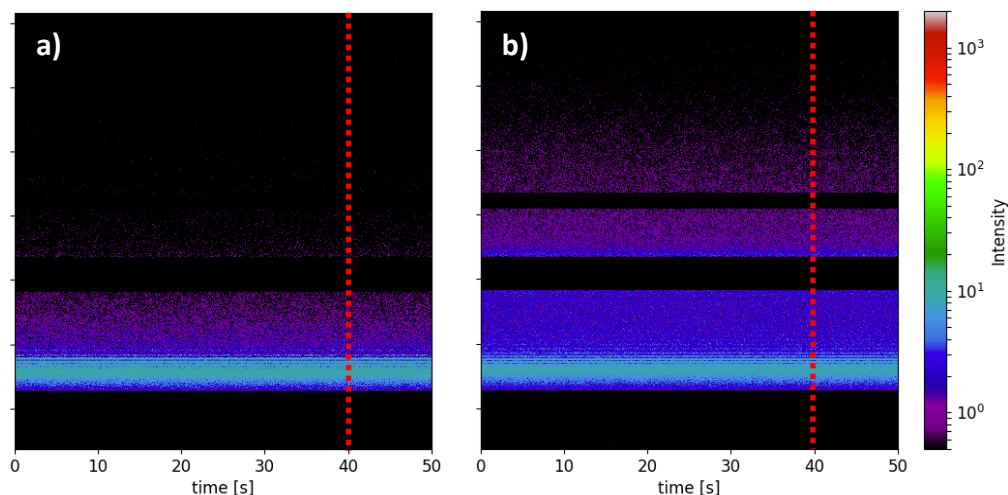


Figure 56. Images showing the variation in signal intensity during the exposition to the X-Ray beam for (a) LT and (b) HT polymer. A constant signal means the absence of material deterioration. The red dotted line indicates the exposure time required to perform the measurement.

An example of the XRR images that are obtained is reported in Fig. 57a-d: when the curing time increases, they show progressive and gradual modifications of the scattering intensity peaks.

In order to derive useful information from the images, it is necessary to consider the variation of q_z in correspondence of the centre of the scattering image: a cut is thus performed along q_z , so that a damping profile can be found (Fig. 58a,b).

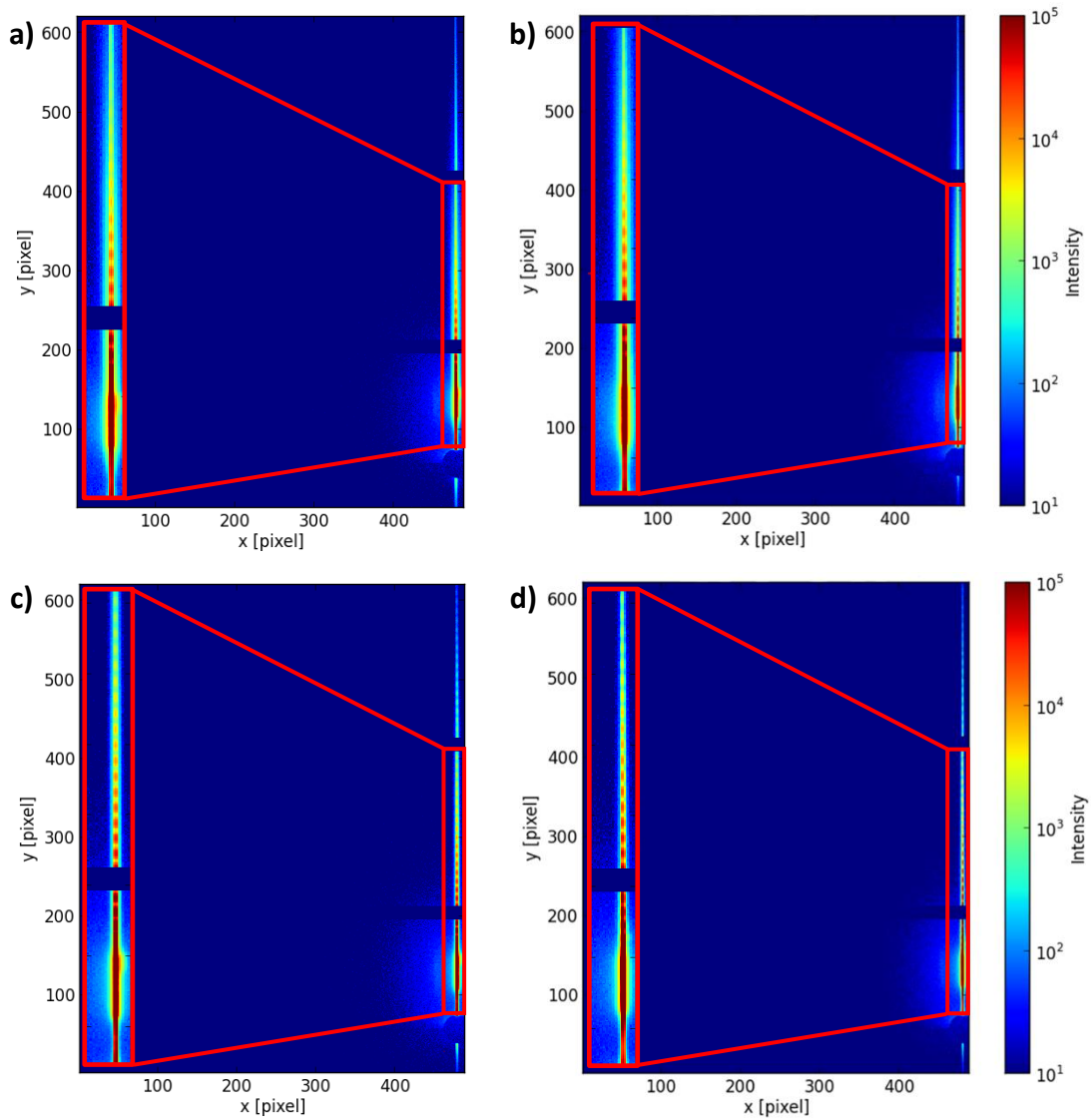


Figure 57. XRR images obtained from the measurements over (a,b) LT_6000 and (c,d) HT_6000; (a,c) refer to the uncured liquid polymer deposited on the substrate, while (b,d) are taken after the polymerization process (curing time: 28 s). In the images it is also reported a zoom over the region of interest.

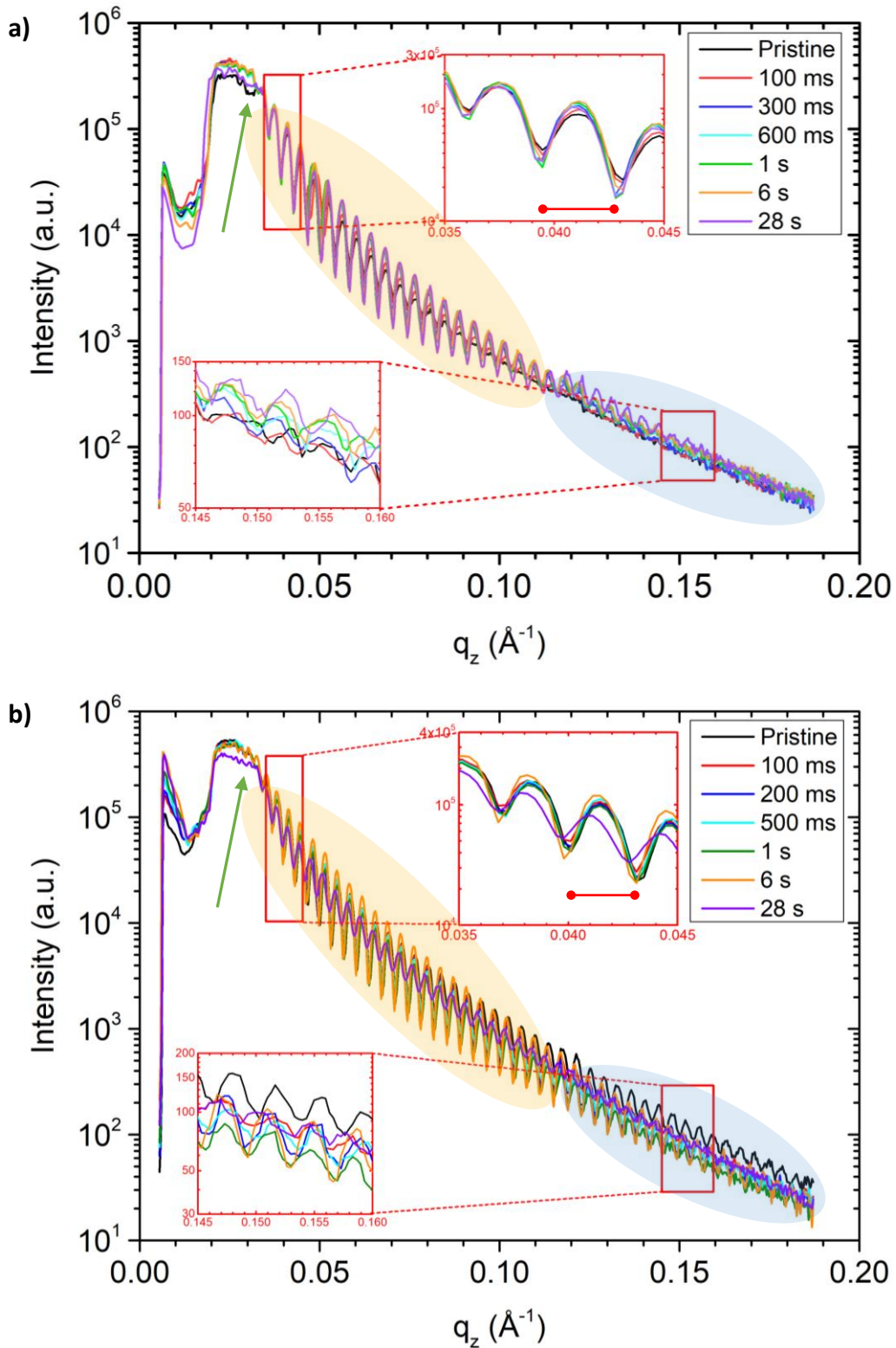


Figure 58. XRR profile for (a) LT and (b) HT polymer at different steps of conversion, obtained by cutting the 2D images along q_z . The graph also presents two insights to show the change in oscillation amplitude at different curing time; the period of oscillation is shown instead to remain constant. The orange area gives information about the air-polymer interface, while the blue area about the polymer-substrate interface; the green arrow shows the region to be considered to evaluate changes in density during the polymerization.

The two profiles shown above carry information over the thickness, roughness and density of the thin coatings, deposited on the substrates, at different steps of the curing process.

According to the theory of XRR, the thickness information is given by the distance between the oscillations, transferred from the reciprocal to the direct space ($d = \frac{2\pi}{\Delta q}$). It has been verified that such distance is invariant at all curing times in both polymers, so that it is possible to conclude that the thickness of the coating is not changing during the photo-polymerization within the range of error of the technique (Tab. 16).

ID	Resin composition	Deposition		Δq (\AA^{-1})	Thickness (nm)
		Ramp	Spinning		
LT_6000	LT + 651 (0.25%) + BA (90%)	-	60 s, 6000 rpm	0.00433 ± 0.00034	145 ± 12
HT_6000	HT + 651 (0.25%) + BA (90%)	-	60 s, 6000 rpm	0.00366 ± 0.00034	172 ± 17

Table 16. Thickness values derived from the distance among oscillations in the XRR images. The parameters selected to obtain the two films are also reported.

The second family of data obtained by XRR is associated to the roughness of the coating, which is inversely proportional to the oscillation amplitude of the intensity: at small wavevector transfer q_z the information can be associated to the air-polymer interface, while at large wavevector transfer to the polymer-substrate interface. In order to better visualise the change in roughness at the air-polymer interface at different curing times, it is possible to plot the reciprocal of the oscillation amplitude (A_0), normalised to an initial arbitrary value (Fig. 59a,b).

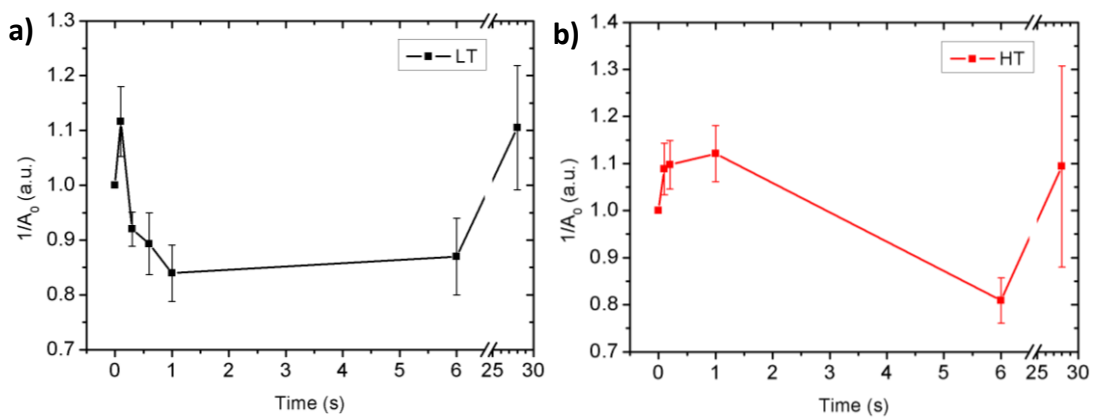


Figure 59. Graphs reporting the reciprocal of the oscillation amplitude, normalised to an arbitrary value of 1, versus the curing time for (a) LT_6000 and (b) HT_6000.

The trends shown above give confirmation of the results obtained by AFM (Fig. 44a,b), with a peak of roughness which is reached in the first stages of conversion. At 28 s both the polymers show an increase in roughness, which is not revealed by the AFM measurements on HT.

Regarding the roughness at the polymer-substrate interface, only qualitative considerations can be done, due to the uncertainty of the signal in this region. It is possible to notice however that LT_6000 shows much smaller changes in the oscillation amplitude at different curing time than HT_6000.

The last information that can be derived is associated to the density of the material at different step of conversion. This data can be derived by looking at the q_z value in correspondence of which the profile starts decaying: this value can be correlated to the critical angle of the material and thus to the coefficient δ , which is directly proportional to the density. From a careful analysis of the profiles, it is possible to assert that the density of LT_6000 is not changing within the range of error of the technique; some possible variation in the density ($\sim 2\%$) have instead been detected for HT_6000 (Fig. 60).

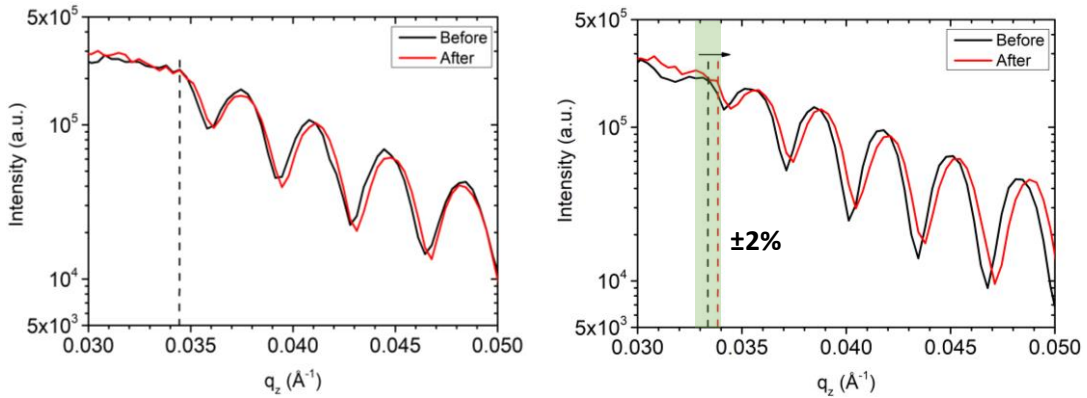


Figure 60. XRR profile for the HT polymer before (black) and after (red) polymerization focused in correspondence of the region where the oscillations are starting. The green region corresponds to a change in critical angle and density in the range of 2%.

The two critical angles, expressed in term of q_z , are:

$$q_{z_{LT}} = 0.0345 \pm 0.0003 \text{ \AA}^{-1}$$

$$q_{z_{HT}} = 0.0333 \pm 0.0003 \text{ \AA}^{-1}$$

Such values can be converted by remembering the relation between q and θ :

$$q_z = \frac{4\pi}{\lambda} \sin \theta \quad [13]$$

$$\theta_{LT} = 0.149 \pm 0.001^\circ$$

$$\theta_{HT} = 0.144 \pm 0.001^\circ$$

These results can be compared with the estimations that have been done previously on a theoretical basis (Tab. 2).

4.6.3. *In-situ* photo-polymerization

The goal to follow *in-situ* and real-time the photo-polymerization of the two polymers has been reached by exploiting GISAXS, which allows to collect data directly during the process.

One of the main issues associated to this technique is however constituted by the very high intensity of the X-Ray beam which is used for the measurement, that can easily degrade the coating after a certain time of exposure or cause the breakage of the double bond, thus favouring the polymerization itself.

A preliminary experiment carried out over coatings with large thickness ($\sim \mu\text{m}$) confirms that the beam actively interacts with the coatings after prolonged exposure (> 5 s), causing thickness reductions that can be explained by induced degradation or polymerization. Nevertheless, this effect is much reduced when very thin coatings are considered: the samples that have been analysed are thus the previously mentioned LT_6000 and HT_6000.

As in case of XRR, a damage-scan for both polymers has been performed to verify the absence of damages during the time required by the measurement (~ 0.1 s): Fig. 61a,b shows, as an example, the results of the damage-scan carried out over LT_6000.

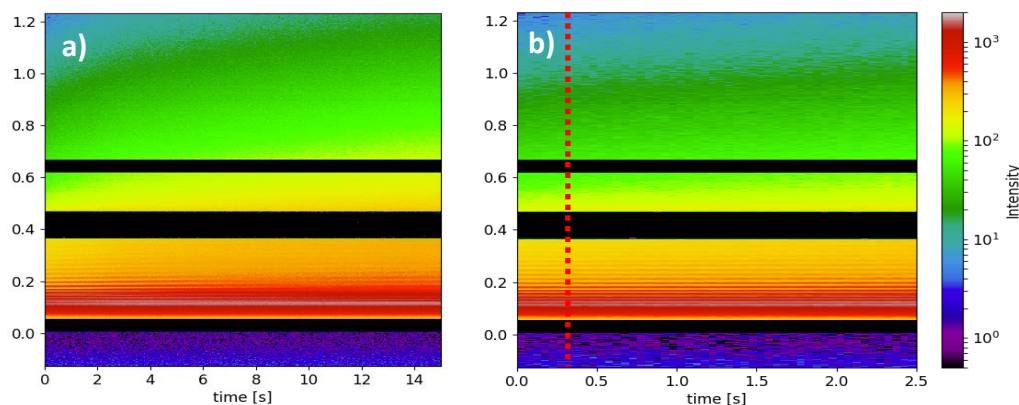


Figure 61. Damage-scan images showing the variation in signal intensity during the exposition of LT_6000 to the X-Ray beam at (a) larger time scale and (b) smaller time scale. It can also be seen that almost no intensity modification is detected in the first 0.3 s.

According to the damage-scans, it is possible to perform the measurements on both polymers without having a detectable interaction with them.

The obtained 2D GISAXS images are reported in Fig. 62a-d.

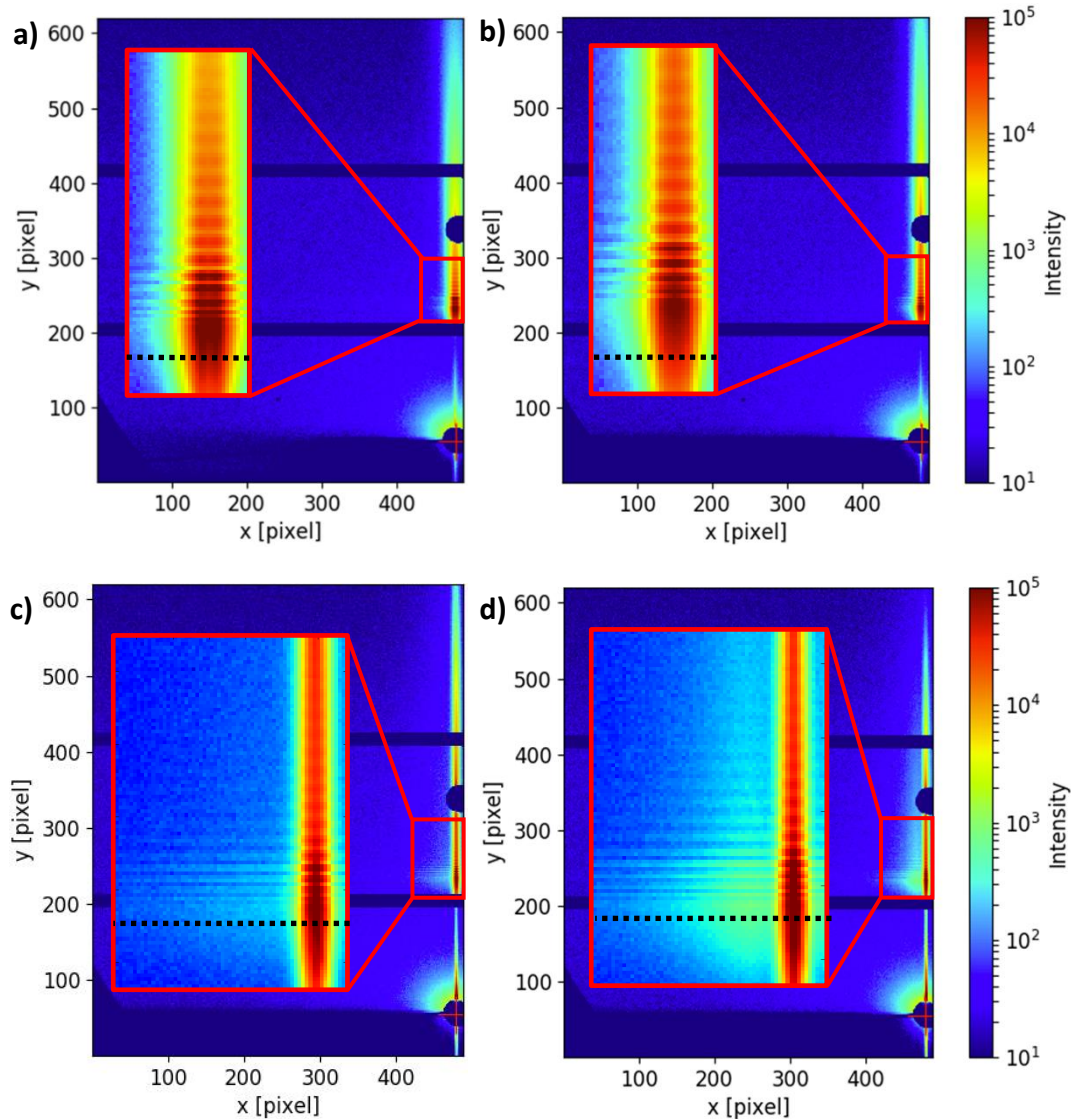


Figure 62. GISAXS images obtained from the measurements over (a,b) LT_6000 and (c,d) HT_6000; (a,c) refer to the uncured liquid polymer deposited on the substrate, while (b,d) are taken after the polymerization process (curing time 1 s). The black dotted lines indicate the regions in which the cuts are performed for the analysis.

The obtained images have been analysed by performing a cut along q_y in correspondence of the Yoneda's peak: this allows to have information about the evolution in dimension of the scattering centres that are responsible for the formation of GISAXS scattering images. The derived profiles are reported in Fig. 63a,b.

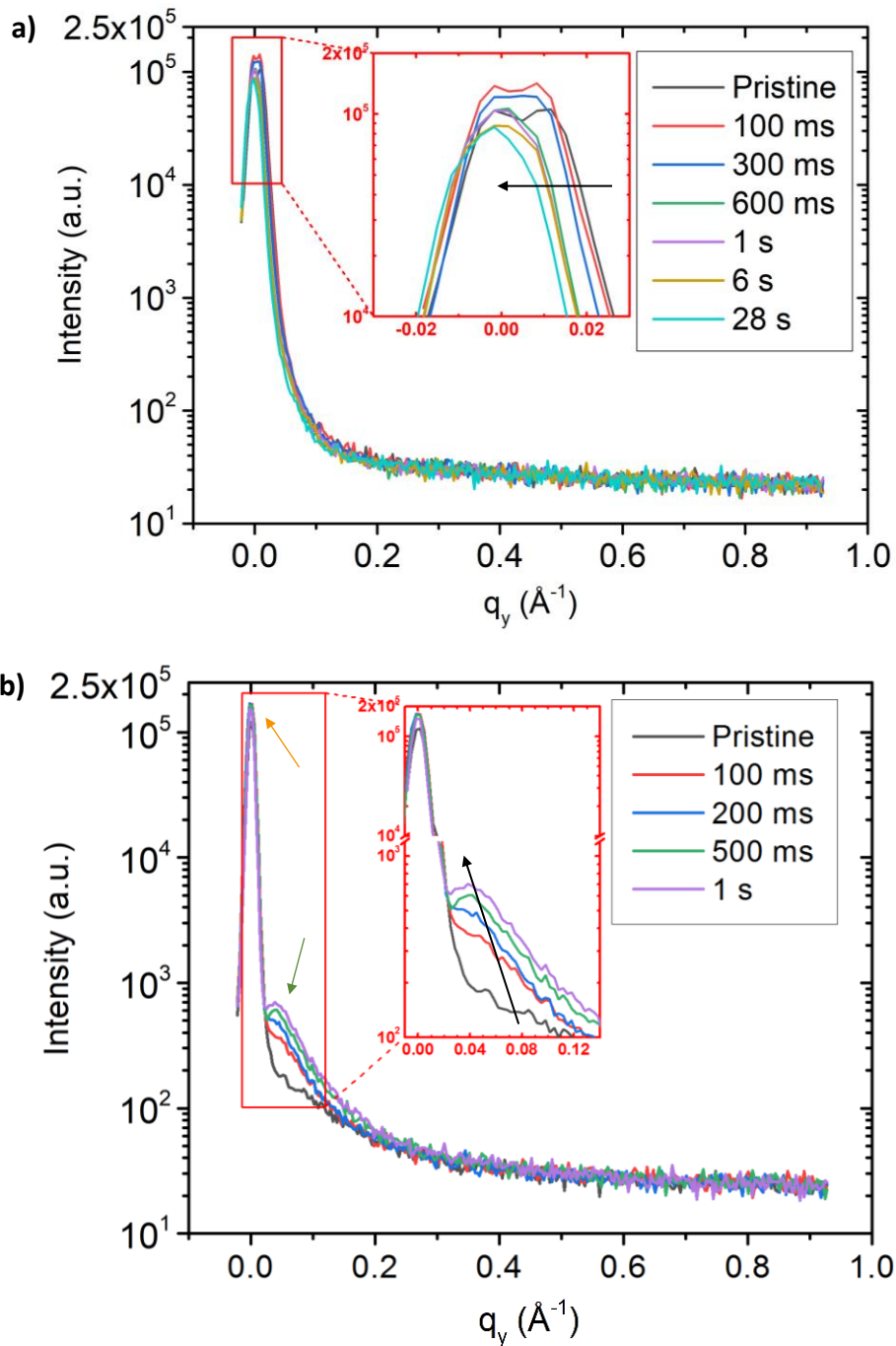


Figure 63. XRR profile for (a) LT and (b) HT polymer at different steps of conversion, obtained by cutting the 2D images along q_y . The orange arrow indicates the position of the main peak ($q_y = 0$), while the green one indicates the second peak. The graphs also present an insight to show the small changes in the position of the second peak: the trend is showed by a black arrow.

In case of both polymer it is possible to notice the presence of two peaks which are progressively merging together as the photo-polymerization time increases: the main peak ($q_y = 0$), associated to the resolution, remains fixed in the same position with almost constant intensity, while the second peak is shifting closer and closer to $q_y = 0$ by increasing its intensity.

This effect, which is well pronounced in case of HT, is much less resolvable in LT: fitting of the profiles has thus been performed only in the first case with the aim to define the exact position of the second peak (Fig. 64).

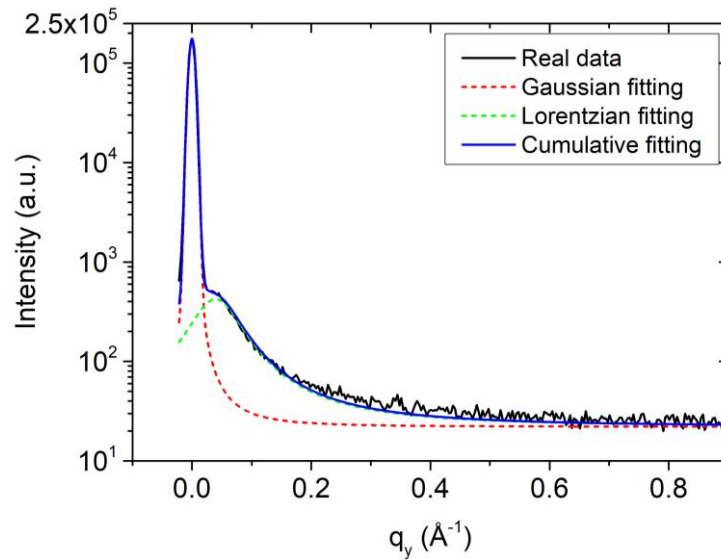


Figure 64. Example of the fitting performed on the profiles derived by the 2D GISAXS images in correspondence of a curing time of 200 ms for the HT polymer. The fitting has been performed by using a Voigt function, that combines Gaussian and Lorentzian distributions.

By plotting the peak position versus the curing time, it is possible to show that the second peak is moving towards the first with an exponential behaviour (Fig. 65a); if this trend is converted from the reciprocal to the direct space, an exponential growth in domain dimension can be derived (Fig. 65b). The term “domain” refers to the existence of scattering centres whose features are not clear yet: some hypothesis about the nature of such domains will be proposed in Chapter 5.

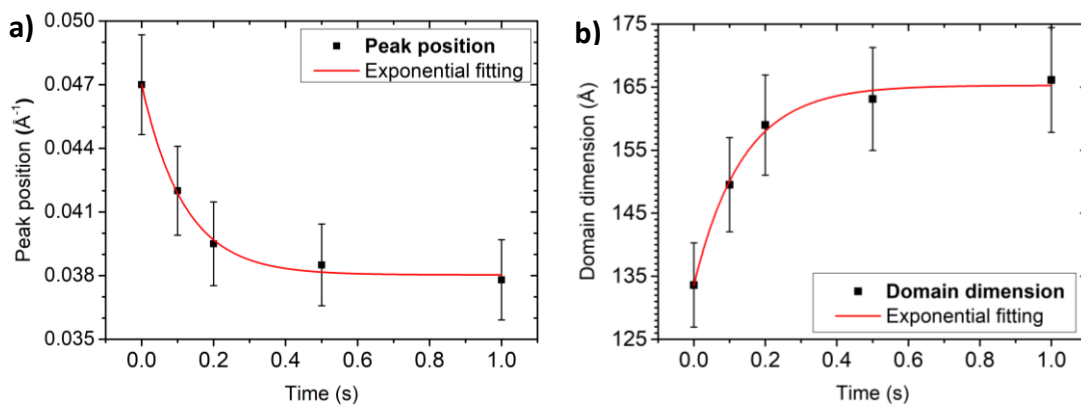


Figure 65. Graphs reporting the evolution at different curing time for HT of (a) the position of the second peak derived by the GISAXS profiles and (b) the domain dimension, obtained by transferring the peak position from the reciprocal to the direct space.

4.6.4. Surface differential reflectance spectroscopy

The *in-situ* experiment performed with GISAXS has been accompanied by the use of a UV-Spectrometer, together with a light source. This technique could eventually permit the obtainment of information over the changes in roughness or thickness of the polymeric films through a modification in intensity or position of the spectra peaks.

Nevertheless, the technique did not supply any relevant information for the present analysis, since no changes in the spectrum have been detected during the photopolymerization: as an example, the changes in reflectance spectrum of HT are reported in Fig. 66.

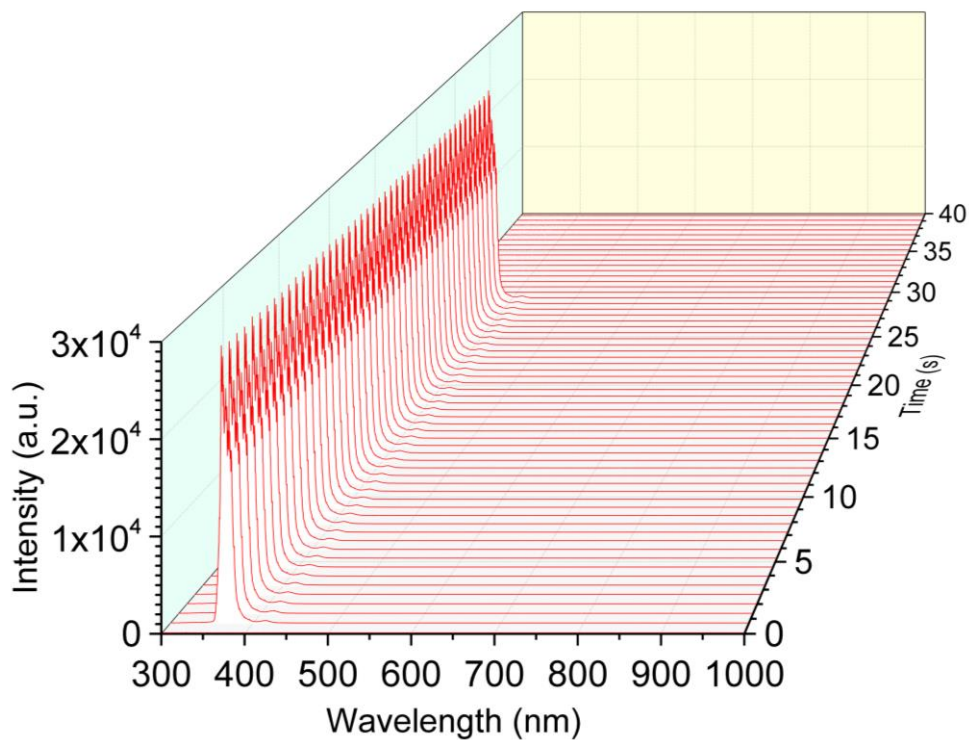


Figure 66. 3D plot which shows the changes in time of the reflectance spectrum of HT_6000, derived by surface differential reflectance spectroscopy.

5. DISCUSSION AND CORRELATIONS

5.1. General features

Although the analysis of the two polymers was not aiming at a mere material characterization, but more at a description of the polymerization process, some general features have also been derived.

In first analysis, it is possible to state that the two analysed resins, with no solvent addition, are stable enough after the deposition: this has been proved by the results reported in Table 4, which show a higher stability of the HT with respect to the LT monomer mixture. Such difference can be associated to the higher quantity of Ethylhexyl acrylate that is present in LT.

Secondly, the thickness analysis produced a clear demonstration of the existence of a logarithmic relation between the viscosity of the liquid mixture and the amount of solvent that is added; furthermore, the extrapolated value for the viscosity at 100% is found to correspond exactly to the viscosity of the used solvent (Fig. 31). It has also been shown theoretically and experimentally (Fig. 32, Tab. 6) that the thickness obtained with the same deposition parameters will always be higher for HT than for LT, due to its higher viscosity. Chemically, the higher viscosity is due to the larger amount of aromatic groups that are present in the HT mixture.

Finally, the FT-IR/RT-IR measurements (Fig. 34-35) permitted to gain information over the change in chemical structure of the materials during their transformation from a series of oligomers to a dense packed network. The most important modification is associated to the disappearance of the C=C groups: although it can be followed by the analysis of many different peaks (1410-1065-990-960-810 cm^{-1}), the most commonly used peak is located at 1636 cm^{-1} . Other important variations are connected with the C=O ester stretching ($\sim 1725 \text{ cm}^{-1}$), whose main peak is shown to decrease in intensity, move to higher wavenumber and then increase again; some associated effects can also be detected in the fingerprint of both the materials (1290 cm^{-1}). A final consideration over the formation of a strong network of hydrogen bonds must be done: thanks to the presence of urethanes groups, the

oligomer itself is supposed to create long-range interactions with other oligomers. The obtained spectra for the two materials (Fig. 33) show however that such interactions are stronger and more widespread in HT than in LT thanks to the broad band at 3300-3500 cm^{-1} , that can be attributed to the hydrogen bonds that are formed both at the uncured liquid- and at the cured solid-state. The different results are related with the presence of DGEBA units in the HT formulation.

5.2. Polymer conversion and gelation

The photo-polymerization of complex systems, as the ones taken into consideration during the current project, implies the synergistic action of a large number of variables which participate to the formation of a dense branched network that is responsible for the properties of the final product.

One of the most influential parameter to be considered resulted to be the curing time, which also constitutes the simplest way to control the degree of conversion achieved at the end of the process. As a matter of fact, a higher curing time produces a higher degree of conversion and consequently modifies the behaviour of the material from liquid- to solid-like.

The overall conversion reaction can be distinguished into two different steps divided by the so-called “gelation” of the network, that corresponds to the moment in which the oligomers are not anymore free to move in the space and are only allowed to create bonds with the nearest monomers. The existence of two different regimes of reaction is shown clearly by almost all the techniques which have been performed and especially by FT-IR: Fig. 38 shows for example the initial strong increase in conversion that is allowed during the first instants of the polymerization thanks to the random reaction of the reactive diluents with any other oligomeric chain present in the liquid mixture, followed by a much slower saturation to a constant value that requires longer times. Such behaviour can also be intended in term of rate of polymerization (Fig. 40), which is shown to be maximum at around 30-40% of conversion, according to what has been found by previous researches⁸. The polymerization rate appears also higher for HT than for LT, which confirm the larger velocity of the first over the second during the first steps of the reaction.

Fig. 38 also shows a delayed change in slope of the conversion curve associated to LT, which means that HT is characterized by a faster gelation than LT; such hypothesis is directly confirmed by a lower maximum degree of conversion that is

achieved after 60 s by the HT mixture: as a matter of fact, the rapid gelation of the network hinders the molecular movements of the oligomeric chains and the diffusion of the reactive diluents, so that some of the double bonds will need more time before being able to react or, in some cases, they will be isolated and unable to participate to the overall conversion.

The different resulting gelation time can be motivated by bearing in mind the chemical composition of the two resins: LT is constituted by a large number of oligomers and by a smaller amount of mono-functional reactive diluents, while HT contains a smaller quantity of long oligomers and a larger amount of mono- and bi-functional reactive diluents. It is thus possible to realise that HT contains a larger average number of reactive end-groups that can be initiated as soon as the process starts, leading to a very fast propagation reaction that delays the rearrangement of the polymeric chains; nevertheless, the large quantity of free volume entrapped in the material is destined to evolve, leading to changes in the material properties that occur after the gelation.

Opposite is instead the behaviour of LT, where the conversion is much more gradual and the gelation requires longer times: this implies that a large part of the movement of the oligomeric chains will be concentrated in the very first instants of the process, when the activated radicals want to react by attacking the acrylic double bonds. The change in material properties will thus be concentrated before the gelation.

The different behaviour of the two materials can also be associated to the quantity of oligomers and reactive diluents which is present in the two cases. After the gelation of LT, the network, mostly composed by oligomeric chains connected together, will be already very dense, so that any kind of movement would be blocked; in HT instead, the gelation involves only half of the constituents, so that the density of the network will be lower and some molecular rearrangement will still be allowed.

This behaviour has been proved by the RT-IR measurements that have been performed (Fig. 39): they show indeed the tendency for HT to increase its conversion degree even at very long time, while the saturation of LT to the maximum value is much more defined. The trend shown in Fig. 39 is completely equivalent to the ones represented in Fig. 38, with the important difference of having a certain delay time, in which the conversion of the material is not occurring.

This effect can be attributed to the specific polymerization conditions which have been used, that imply the possible presence of residual amount of oxygen inside the

resin mixture: the migration of the oxygen out of the liquid is in fact complicated by the higher thickness of the deposited film and by the absence of complete nitrogen purging. The eventual oxygen entrapped in the liquid monomer mixtures is thus acting as an inhibitor for the photo-polymerization until when it is completely consumed: oxygen inhibition is also proved to be particularly effective for the lower light intensities ($< 3 \text{ mW/cm}^2$)⁸.

A further explanation of the different behaviour of the two materials can be found in their different viscosity, which makes the chain movements and the monomer diffusion slower in case of HT.

The thesis of having delayed molecular movements occurring in HT assumes a higher value if the results obtained by other techniques are considered: both AFM (Fig. 44a,b) and XRR (Fig. 59a,b) show for instance that the roughness reaches a maximum in the first stages of the process and, in term of time, this occurs later for HT than for LT. Such increase in roughness can be motivated by the strong and rapid changes that occur initially during the polymerization of the resins, which can determine an inadequate chain distribution and the tendency to form aggregates instead of a smooth film. By giving time to the polymers, the roughness decreases again to a lower value until the degradation of the material starts: this could explain the trend associated to the final increase in roughness.

The same techniques supply also information over the thickness changes occurring during photo-polymerization: AFM (Fig. 44c,d) shows again a late chain rearrangement of HT, demonstrated by the delayed achievement of a constant thickness value. It should be noticed that the final thickness obtained with HT is around 150 nm, against 135 nm achieved by LT: this is explained by the different viscosities of the two mixtures and it is in agreement with the results obtained by XRR (Tab. 16). An important difference is however the lack of thickness variation in case of XRR, which is instead shown by AFM: this is probably due to the resolution of the technique, which is not able to detect the slight modifications occurring in the coatings. Also, the first AFM measurements have been performed on films which are not completely solid and possess a certain liquid percentage, thus making it difficult to have a good thickness evaluation with the method that has been chosen. This consideration can also explain why the initial thickness value of LT detected by AFM results higher than the HT one.

It must be pointed out that AFM and XRR supply similar, but not identical information: as a matter of fact, XRR is much more powerful, since it analyses the

sample through its whole thickness, while AFM only takes into account the considered surface morphology. It is thus possible to obtain qualitative information about the roughness at the polymer-substrate interface (Fig. 58a,b), which results to change more in case of HT than in LT: this difference may be due to a higher shrinkage and consequent de-wetting of the coating from the substrate in case of HT, which is happening because of the faster gelation and retarded chain movements.

Surface differential reflectance spectroscopy has also been performed to obtain information over possible thickness or roughness changes (Fig. 66); nonetheless, the resolution of the technique and the specific conditions of the experiments did not allow to obtain reliable results, so that it is not possible to confirm the occurrence of a thickness or roughness change during the polymerization of thin films.

An alternative way to follow the progressive conversion of the two polymers is to detect the changes in glass transition temperature with time and this is possible by using both DMA (Fig. 50c,d) and DSC (Fig. 52a,b). The obtained results show an exponential increase in time for both polymers: although this trend is very clear by looking at the DSC data, it becomes more difficult to be detected in case of DMA, where the presence of only three experimental points does not allow the definition of a correct behaviour. From a careful comparison of the results it is however possible to conclude that the linear trend revealed in Fig. 50c is not in contrast with what is derived by DSC, but it reproduces a specific region of the curve in which the exponential drift can be approximated by a linear behaviour.

Finally, the difference in the glass transition temperature values derived by the two techniques for the same curing time and intensity should not be intended as a mistake; in fact, the glass transition temperature does not represent by definition an enthalpic characteristic of the material, as instead the melting temperature, but it represents an endothermic entropic thermo-dynamic condition in correspondence of which the free volume starts to increase (during heating) and the polymer dissipates large quantities of energy to rearrange its chains in the space. It follows that such state is firstly a function of the cooling/heating rate, but also of the amount of free volume in the polymer. The first dependence explains why the T_g measured by DSC during heating and cooling is different and also why there are differences among the results obtained by the two techniques, which exploit different heating rates; the second dependence explains instead why the T_g is progressively increasing with

conversion, since the formation of new bonds among the chains will reduce the amount of free volume available.

Lastly, these DSC and DMA measurements also allow to confirm the late chain movements occurring in HT, which is proved by a much slower change in T_g with respect to the one occurring in LT.

To conclude, the reason for the different gelation time of the two polymers can be found by considering the photo-polymerization reaction as the continuous competition of kinetic and of thermo-dynamic sub-reactions, which alternate their actions depending on the capability of the monomers to diffuse inside the monomeric mixture and thus also on its viscosity. The kinetic aspect is thus stronger in HT and lead to a fast gelation and a slower chain reorganisation, while it is weaker in LT, where the entropic rearrangement tends to be predominant and starts together with the conversion.

A complementary parameter which allows to detect the same effects highlighted previously, is the light intensity. In this case, a decrease in the light intensity causes a reduction in the polymerization rate (Fig. 40) and a consequent delay in the gelation of the network, so that the maximum conversion degree is achieved after a longer curing time (Fig. 38); therefore, an equivalent dose of radiation (time \times intensity) is able to produce the same results, in term of conversion. Furthermore, it has been demonstrated that the rate of polymerization is directly proportional to the square root of the UV intensity adopted (Fig. 41): this is true during the first steps of the reaction and before the gelation of the network.

Another important correlation which has been derived regards the possibility to describe with a power-law function the increase in glass transition temperature with the selected light intensity (for the same curing time) (Fig. 50a,b). A power-law function, instead of an exponential one, was chosen to describe this variation thanks to the better data fitting that can be obtained: such decision is however based on a rather limited number of experimental points and consequently it can be subjected to mistakes, due to the similar behaviour of the two functions.

5.3. Development and structure of the network

Despite the use of equivalent doses of radiation can lead to the obtainment of the same degree of conversion, one could expect that the obtained network will be characterized by a different structure depending on the applied rate of polymerization; in practice, a photo-polymerization carried out at low light intensity for longer times, is expected to create a different result with respect to what is obtained by exposing the polymer for shorter time to high light intensities. Another important factor that can determine the obtainment of substantial differences in the final network is the chemical composition of the monomeric mixture.

According to the literature, it is possible to achieve information about the homogeneity and structure of the network by considering the shape of the $\tan \delta$ function and, in particular, the height and width of the peak.

As a general consideration, it is possible to notice that LT is characterized by a much higher and sharper $\tan \delta$ peak with respect to HT (Fig. 47; Tab. 10), which implies a higher homogeneity of the network (narrower width) and a higher dissipation of the material (larger height). Such properties are directly connected with the chemical composition of the material: LT is characterized by large amounts of long oligomers that favour the obtainment of an ordered homogeneous network, whose polymerization can proceed without particular complications. Moreover, according to what discussed in paragraph 5.2, LT consumes all its molecular movement in the very first instants of the reaction and before the gelation: this involves a more accurate distribution of the chains for the following steps of the reaction. HT is instead subjected to a fast gelation and to a subsequent partial rearrangement of the residual reactive diluents in the mixture: this involves the formation of a more heterogeneous network, which is proved by the large obtained peak. Another consequence of the specific behaviour of the two materials is the obtainment of a different density of crosslinking after the obtainment of maximum conversion: in principle, HT is expected to create a greater number of crosslinks because of the higher average number of functionalities; nevertheless, this is not happening because the conversion of the material is not reaching very large extents.

Furthermore, if the same material is subjected to increasing curing times and intensities, the development of the network can be tracked through a decrease in the height of $\tan \delta$ and a tendential broadening of the function (Fig. 48; Tab 12), indicating the progressive polymerization of the material and consequent decrease in the network homogeneity. It should however be pointed out that the width of the

function is non-monotonically increasing with the time and intensity, but shows a minimum in correspondence of the intermediate curing parameters, thus indicating the presence of ideal photo-polymerization conditions which favour the obtainment of a more homogeneous network. By comparing the supplied radiation dose with the obtained width, it is possible to notice that the network homogeneity cannot feel any difference associated to the use of high intensity/low times or low intensity/high times. This is completely true for the lower curing parameters, but doesn't hold when very high light intensities are used: in this case a strong inhomogeneity of the network is detected. Very similar considerations are applicable to the density of crosslinking that is calculated through the storage modulus (Tab. 13): equivalent doses of radiation produce a comparable density, which is progressively increasing with an increase in supplied dose. This appears to be always true, unless very high light intensities are exploited: they result into a much larger density with respect to the same dose applied with larger times and lower intensity. The described behaviour is probably associated to the activation of a larger number of radicals when higher light intensities are involved.

The development of the crosslink network of the material has been followed also by exploiting X-Ray techniques. First of all, SAXS has been used to determine the gyration radius associated to the two resins before the polymerization (Fig. 54), which resulted to be slightly bigger in case of LT with respect to HT, according to the Guinier analysis.

The meaning of the derived gyration radius is not straightforward: since X-Ray techniques are based on scattering events occurring when the radiation interacts with regions characterized by strong variations in electron density, a possible interpretation is to identify the gyration radius with an average dimension of the random coil which is formed by the oligomeric chains contained in the two mixtures; according to this, the presence of a larger quantity of long oligomers in LT makes the random coil bigger than the one formed in case of HT.

An alternative view would be to consider the gyration radius as an indicative dimension of the points of physical/chemical link among the chains.

More generally, it is possible to classify the scattering centres responsible for SAXS as domains, which are supposed to increase their dimensions as soon as the polymerization starts. The domains growing process has been proved by performing *in-situ* GISAXS measurements: in case of both LT and HT the growth of the domains is visible by looking at the reduction in distance between the two obtained

scattering peaks (Fig. 63a,b). By transferring from the reciprocal to the direct space it is also possible to derive, in case of HT, a value for the dimensions of the growing domains (Fig. 65); the transformation has not been performed in case of LT because the distance reduction between the peaks was very small and not accurately resolvable: the instrumental resolution is thus probably the reason why it was impossible to obtain well-resolved peaks. However, even if it is not possible to have a clear evaluation of the domain dimensions in case of LT, it is likely to conclude that the LT-domains are bigger than the HT ones and this confirms the results obtained by SAXS. The shape of the curve obtained for HT (Fig. 65b) also resembles the conversion curve found for the same light intensity (Fig. 38): this is the proof that the two process are connected and directly correlated.

Comparing the results obtained by GISAXS on the uncured resins and the ones obtained by SAXS, similar values are expected, since they are referring to the same kind of domains. Their difference can be explained in first analysis by a wrong fitting process performed on the GISAXS profile at 0 s, where the localisation of the secondary peak results to be very difficult: such peak can be much more shifted to higher values than what has been derived and this implies a strong reduction in the initial domain dimensions. A further explanation can be found by remembering that SAXS measurements have been performed on the uncured monomer mixture only, without the addition of solvent or initiator: this implies slightly different conditions, since the initiator and the solvent can physically interact with the oligomeric chains, causing agglomeration or dispersion and thus modifying the domains shape and dimension.

Although the identification of the detected growing scattering centres with the progressive densification of the network and formation of crosslink points among the chains is at the moment quite difficult, the achieved results *in-situ* are particularly significant and unique, since they offer a way to follow step-by-step the formation of the polymeric crosslinked network at a very low time scale in a controlled environment, without altering the system from outside. Such results have never been obtained in the past or reported in the literature and thus constitute a milestone towards further findings about the formation process of a polymeric network.

Finally, XRR was also used to detect variations in the density of the material during the process that could be connected with a change in the crosslink density: this has been done by considering the change in critical angle (directly dependent on the

density) before and after the photo-polymerization. However, no clear change in density has been detected in case of LT, while only a very slight change can be seen for HT (Fig. 60a,b); it must be noticed that the resolution of the technique, together with the difficulty in the individuation of the starting point of the oscillations, especially for HT, makes it complicated to state if a change in density is occurring or not. It is thus unlikely that such density value could be used as an indication of the crosslink density of the material. A final comparison can be done among the values of the critical angle obtained by XRR and the ones obtained by theoretical computation (Tab. 2): even though they are in the same order of magnitude, the detected values are higher and this could be related with the difficult localisation of the oscillations starting point; moreover, the theoretical computation has been performed by using a value for the density of the oligomer which was purely an indication and by combining the parameters of the different constituents with a simplified rule of mixtures. It follows that the real penetration depth is probably smaller than the calculated one (Fig. 27), but still high enough to have the full penetration of the film when X-Rays are used.

6. CONCLUSIONS AND FUTURE WORKS

6.1. Conclusions

The properties of two thermoset polymers deposited in form of thin coatings have been studied before, during and after the photo-polymerization by using various techniques, which allowed to characterize the materials and their curing process, developing a correlation among the selected curing parameters and the characteristics of the final product.

The most important parameters to be controlled resulted to be the curing time and intensity, together with the composition of the monomeric mixture. All the other parameters have been kept constant in order to obtain simple cause-effect relationships.

According to the obtained results, an increase in curing time has the power to push the reaction ahead leading to an increasing conversion of double bonds, which is accompanied by a series of changes in the molecular chemistry of the material, that are the direct consequences of the development of a crosslinked network. The maximum polymerization rate is found at 30-40% of conversion, in correspondence of which the gelation of the network occurs; after the gelation, the rate of polymerization is forced to decrease because of the reduced movement ability of the dispersed monomers. The change in reaction rate allows the definition of two different regimes.

The polymer conversion is accompanied by a profound modification in the properties of the material, that can be connected with the molecular movements occurring in it. During the first steps of the reaction, a chain rearrangement tends to occur, which is the consequence of a free volume reduction and of the tendency for diffusion of the dispersed monomers. It follows an increase in roughness, which reaches its maximum when the rearrangement of the polymeric chains is occurring, and a decrease in the coating thickness. Immediately after the reorganization, the roughness decreases and the thickness of the coating reaches its minimum constant value.

The curing time has also the effect of increasing the glass transition temperature of the polymer and this occurs with an exponential relationship, that is connected with a reduction in the free volume of the polymer due to the bonds formation.

Also, the conversion of the material is proved to strongly depend on the selected light intensity, which can shorten the time required for the gelation of the network by increasing the rate of polymerization: a root square dependence of the rate of polymerization on the light intensity has been demonstrated. However, by applying the same dose of radiation, the same degree of conversion can be achieved.

An increase in curing intensity is also proved to cause an increase in glass transition temperature with a power-law dependence.

Finally, the resins composition resulted to be crucial in the definition of the gelation time: the presence of a larger number of functional reactive groups determines a higher reaction rate and a shorter gelation time. Such condition hinders the molecular movements and entraps a large amount of free volume inside the polymer; after the gelation the free volume tends to be recovered through a series of slow molecular movements, which are favoured by the presence of many small reactive diluents. This implies the obtainment of a lower maximum conversion, as demonstrated in case of HT. It was also shown that in longer times the conversion of HT tends to increase slowly, while for LT it saturates to a constant value: this effect is associated with the achievement of an equilibrium status, in case of LT, thanks to the molecular movements that occur before the complete gelation of the network. Such conclusions can be derived by the comparison among the obtained trends for the variation in roughness, thickness and T_g .

Another important consequence of having a fast gelation time in HT is the occurrence of roughness changes in correspondence of the interface between the substrate and the coating, which can be explained by the retarded shrinkage that occurs after the gelation and contributes to a possible partial detachment of the coating from the substrate.

The different gelation time of the two polymers can also be attributed to the different viscosity of the resins, which favours or complicates the monomers diffusion and the chain reorganization during the photo-polymerization.

It is thus possible to conclude that the photo-polymerization process can be described as the competition of a kinetic and of a thermo-dynamical sub-reactions, which alternate their action depending on the capability of the monomers to diffuse in the monomeric mixture and of the polymeric chains to rearrange properly.

With the goal of studying the development process of the polymer network, the density of crosslinking has been considered: it is possible to conclude that equivalent doses of radiation are able to produce networks characterized by roughly the same homogeneity and density of crosslinks. This is true unless very high light intensities are used, which activate a large number of radicals, making the process particularly fast and favouring the obtainment of a very heterogeneous network, with a high density of crosslinking. It was also found that the selection of intermediate “ideal” curing parameters in term of time and intensity lead to more homogeneous networks.

Finally, the obtained density of crosslinking and homogeneity of the network are also affected by the chemical composition: the presence of a large quantity of long oligomers, which can rearrange before the gelation of the network, favours the obtainment of more ordered structure, with higher homogeneity. The achievement of a higher final degree of conversion also implies a higher density of crosslinking. Therefore, on one side the presence of a larger average number of acrylate functionalities theoretically favours the formation of bonds among the chains, but on the other side the gelation is reached in an earlier stage and this makes impossible to achieve very high degree of conversion and high density of crosslinking.

The photo-polymerization of the two resins has been followed also *in-situ* and real-time by using more advanced techniques and this allowed to obtain further information about the chemical and physical changes occurring during the photo-polymerization. In particular, GISAXS was performed *in-situ* with the aim to follow the growth in dimensions of the scattering centres contained in the material: the success of such experiment, which have never been reported in literature before, constitutes a milestone towards further findings about the formation process of a polymeric network. As a matter of fact, a growth of the scattering centres from a dimension of few nm to hundreds of nm has been detected and such results are also supported by SAXS measurements: the growth trend can also be put into relation with the conversion trend for the same material, thus confirming the existence of a cause-effect dependence between the two.

In this case, the composition of the monomeric mixture is able to affect the initial dimension of the domains: the presence of a larger amount of long oligomers favours therefore the formation of bigger domains at any step of the process.

Even though a clear understanding about the nature of such “domains” has not been reached in the present research, it can be proposed to identify them with the

polymeric random coils or with the points of physical/chemical link among the chains.

In conclusion, the purpose of the study has been fully reached, since an in-depth characterization of the two materials has been performed, together with an *in-situ* analysis which demonstrated the possibility to follow the photo-polymerization with innovative techniques in order to understand better the features of this complex process.

6.2. Future works

Being the present research a starting point for further analysis, the possible future works can be carried out in different contexts.

First of all, it would be interesting to go deeper in the examination of the RTIR spectra, trying to define in what moment of the polymerization a certain chemical transformation occurs.

Another interesting possibility would be to repeat, by using more accurate techniques, the analysis over the thickness of the coatings at different instants of polymerization: this would allow to confirm the obtained results and to calculate the actual shrinkage of the material.

Further studies can be carried out by using other characterization techniques, such as photo-calorimetry, which can supply complementary information about the residual presence of enthalpy of reaction after a certain curing time. This would allow to recognize with certainty when a material is fully crosslinked, and it would constitute an accurate confirmation of the results obtained by infrared spectroscopy. Moreover, a big part of the future works should concentrate on the synchrotron characterization: GISAXS should be repeated on both the samples, by increasing the sample-beam distance so that the resolution of the technique can be improved, and the domain growth of LT can be seen more clearly. New XRR images can also be collected before, during and after the polymerization, with the aim of verifying the previously obtained results.

Finally, new varying parameters can be integrated in the study, such as the concentration or the type of initiator.

7. ACKNOWLEDGMENT

The results and conclusions obtained in the present work would not have been reached without the continuous support and contribution given by all the people that accompanied me.

First of all, I would like to thank Prof. Mats Johansson, which have been my supervisor at KTH (Kungliga Tekniska Högskolan, Stockholm, Sweden), where the project has been developed: he gave me the chance to move to the city that I have dreamt for years, challenging me with a complex thesis work which required to learn a lot in the field of X-Rays. Mats also taught me not to give up in front of difficulties and especially not to under-evaluate any aspect of the experimental preparation of a sample.

A special mention goes also to Calvin Brett, which has been my direct tutor and supervisor during the whole experimental activity; he helped me in understanding the importance of working in a precise and cleaned manner and also taught that physics and chemistry are only two sides of the same coin and that they can cooperate to reach important results. Calvin has been a teacher, since he was continuously providing me inputs and requiring a lot of efforts from my side, but most of all he was a friend and I could not have wished for another person to follow me during this six-months period.

Thanks to Prof. Stephan Roth, which have been my supervisor at DESY (Deutsches-Elektronen Synchrotron, Hamburg, Germany), since he allowed me to visit twice an internationally renowned synchrotron facility, where I could test my own samples and understand more about the theoretical and experimental characteristics of recently discovered X-Rays techniques.

Thanks to Prof. Gianmarco Griffini, my Italian supervisor and reference person at POLIMI, who accepted to follow me step-by-step during the project even if I was not developing the work at Politecnico di Milano. Thank you for the kindness and availability demonstrated and for all the suggestions given before, during and after the drafting of the present essay.

Thanks to the YT division of Coating and Polymer Technology at KTH, which offered me a stimulating and talkative environment where I could learn more about polymers and their chemistry. Thanks for offering me new ideas about what I could have done and for the patience demonstrated in showing me the working mechanism of all the experimental techniques that I used.

Thanks to Dr. Jogan Jansen and Prof. Rolf van Benthem from DSM, which provided the materials over which the analysis has been performed.

I would like to thank my parents and all my relatives which have been close to me during the whole education path and supported me economically and morally, even and especially when things were going bad.

Finally, but not less important, a big merit should be given to my Italian friends Chiara, Valeria, Federico, Mirko, to my university colleagues Daniele, Umberto, Matteo, Andrea, and to my new Swedish friends, which have always been ready to help and sustain me when I was in need.

Since big results are more easily achievable when many people are supporting your work, I would like to say "*Tack så mycket*" (Thank you, in Swedish) to all who made this Swedish adventure possible.

8. REFERENCES

- (1) Kloosterboer, J. G.; Lijten, G. F. C. M.; Boots, H. M. J. Network Formation by Chain Crosslinking Photopolymerization and Some Applications in Electronics. *Makromol. Chemie. Macromol. Symp.* **1989**, *24* (1), 223–230.
- (2) Crivello, J. V.; Reichmanis, E. Photopolymer Materials and Processes for Advanced Technologies. *Chem. Mater.* **2014**, *26* (1), 533–548.
- (3) Stansbury, J. W. Dimethacrylate Network Formation and Polymer Property Evolution as Determined by the Selection of Monomers and Curing Conditions. *Dent. Mater.* **2012**, *28* (1), 13–22.
- (4) Bowman, C. N.; Kloxin, C. J. Toward an Enhanced Understanding and Implementation of Photopolymerization Reactions. *AIChE J.* **2008**, *54* (11), 275–2795.
- (5) Kloosterboer, J. G.; Lijten, G. F. C. M. Thermal and Mechanical Analysis of a Photopolymerization Process. *Polymer (Guildf)*. **1987**, *28* (7), 1149–1155.
- (6) Priola, A.; Gozzelino, G.; Ferrero, F.; Malucelli, G. Investigation on the Structure-Property Relationships for Films Obtained from UV Curable Coatings. *Prog. Org. Coatings* **1993**, *22* (1–4), 301–314.
- (7) Gorsche, C.; Harikrishna, R.; Baudis, S.; Knaack, P.; Husar, B.; Laeuger, J.; Hoffmann, H.; Liska, R. Real Time-NIR/MIR-Photorheology: A Versatile Tool for the in Situ Characterization of Photopolymerization Reactions. *Anal. Chem.* **2017**, *89* (9), 4958–4968.
- (8) Iedema, P. D.; Schamböck, V.; Boonen, H.; Koskamp, J.; Schellekens, S.; Willemse, R. Photocuring of Di-Acrylate. *Chem. Eng. Sci.* **2018**, *176*, 491–502.
- (9) Taki, K.; Taguchi, T.; Hayashi, R.; Ito, H. Photopolymerization Kinetics of Different Chain Sizes of Bi-Functional Acrylic Monomers Using Real Time FT-IR. *J. Photopolym. Sci. Technol.* **2016**, *29* (1), 133–137.
- (10) Sarkar, S.; Baker, P. J.; Chan, E. P.; Lin-Gibson, S.; Chiang, M. Y.

- M. Quantifying the Sensitivity of the Network Structure and Properties from Simultaneous Measurements during Photopolymerization. *Soft Matter* **2017**, *13* (21), 3975–3983.
- (11) Fouassier, J. P. Photopolymerization Reactions. In *Photoinitiators for Polymer Synthesis*; Wiley-VCH Verlag GmbH & Co. KGaA: Weinheim, Germany, **2012**; pp 41–72.
- (12) Microchem. Silicon Wafers Quartz Wafers Glass Wafers. *Microchem. Prod. data* **2014**.
- (13) Ohm, W.; Rothkirch, A.; Pandit, P.; Körstgens, V.; Müller-Buschbaum, P.; Rojas, R.; Yu, S.; Brett, C. J.; Söderberg, D. L.; Roth, S. V. Morphological Properties of Airbrush Spray-Deposited Enzymatic Cellulose Thin Films. *J. Coatings Technol. Res.* **2018**.
- (14) Yoo, H. J.; Lee, Y. H.; Kwoit, J. Y.; Kim, H. Do. Comparison of the Properties of UV-Cured Polyurethane Acrylates Containing Different Diisocyanates and Low Molecular Weight Diols. *Fibers Polym.* **2001**, *2* (3), 122–128.
- (15) Kim, H. Do; Kang, S. G.; Ha, C. S. Properties of UV-Curable Polyurethane Acrylates for Primary Optical Fiber Coating. *J. Appl. Polym. Sci.* **1992**, *46* (8), 1339–1351.
- (16) Novartis AG. Ciba IRGACURE 651 Product Sheet. *Coating* **2001**, 2–4.
- (17) Sahu, N.; Parija, B.; Panigrahi, S. Fundamental Understanding and Modeling of Spin Coating Process: A Review. *Indian J. Phys.* **2009**, *83* (4), 493–502.
- (18) Hall, D. B.; Underhill, P.; Torkelson, J. M. Spin Coating of Thin and Ultrathin Polymer Films. *Polym. Eng. Sci.* **1998**, *38* (12), 2039–2045.
- (19) Als-Nielsen, J.; McMorrow, D. *Elements of Modern X-Ray Physics*; John Wiley & Sons, Inc.: Hoboken, NJ, USA, **2011**.
- (20) Ehlers, J.; Hepp, K.; Board, E.; Beig, R.; Domcke, W.; Frisch, U.; Hillebrandt, W.; Jaffe, R. L. *Applications of Synchrotron Light to Scattering and Diffraction in Materials and Life Sciences*; Gomez, M., Nogales, A., Garcia-Gutierrez, M. C., Ezquerra, T. A., Eds.; Lecture Notes in Physics; Springer Berlin Heidelberg: Berlin, Heidelberg, **2009**; Vol. 776.
- (21) Smilgies, D.; Busch, P.; Papadakis, C. M.; Posselt, D. Characterization of Polymer Thin Films with Small-angle X-ray Scattering under Grazing Incidence (GISAXS). *Synchrotron Radiat. News* **2002**, *15* (5), 35–42.

- (22) Meyer, A., Institute of Physical Chemistry, U. of H.
<http://www.gisaxs.de>.
- (23) Dosch, H.; Batterman, B. W.; Wack, D. C. Depth-Controlled Grazing-Incidence Diffraction of Synchrotron X Radiation. *Phys. Rev. Lett.* **1986**, *56* (11), 1144–1147.
- (24) Yasaha, M. X-Ray Reflectivity Measurement. *Rigaku J.* **2010**, *26* (2).
- (25) Sørensen, B. E. A Revised Michel-Lévy Interference Colour Chart Based on First-Principles Calculations. *Eur. J. Mineral.* **2013**, *25* (1), 5–10.
- (26) Socrates, G. *Infrared and Raman Characteristic Group Frequencies*; **2004**.